CHALMERS
UNIVERSITY OF TECHNOLOGY

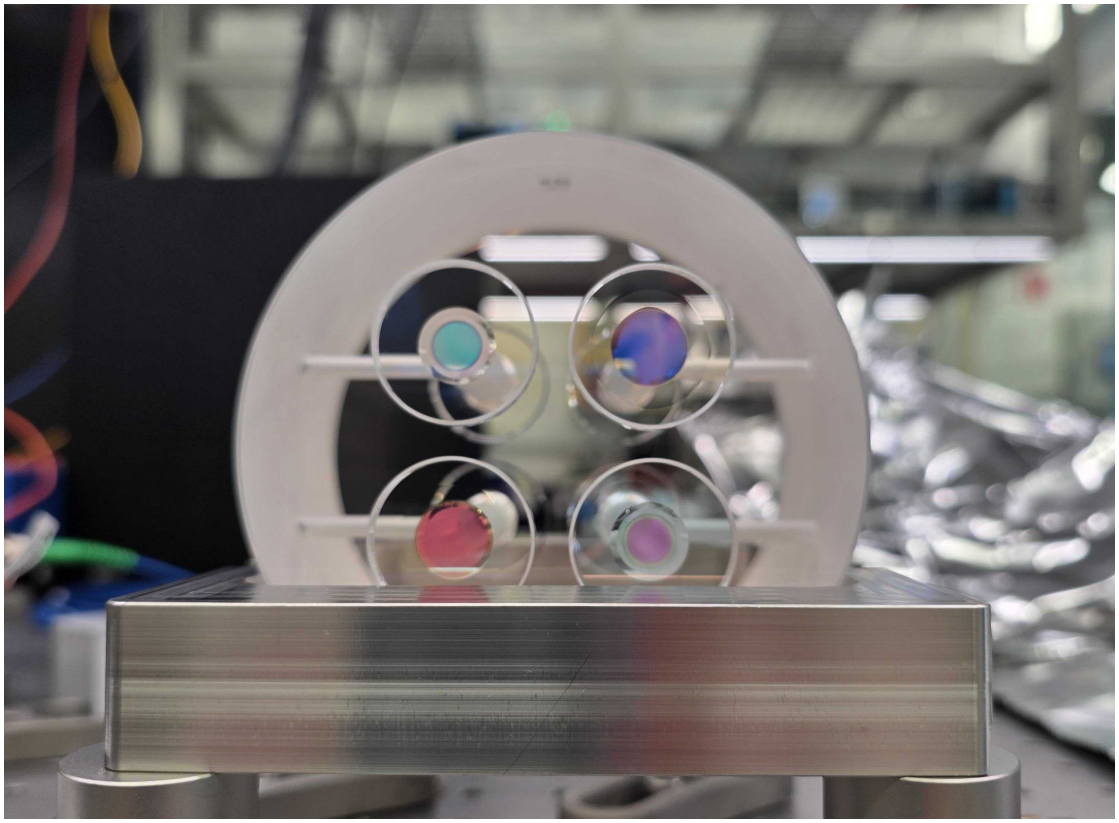

Laser frequency stabilisation onto a high-finesse optical cavity

towards narrow-line laser cooling of 88 strontium

Master's thesis in Nanotechnology

ALEX JERNSTEDT

DEPARTMENT OF MICROTECHNOLOGY AND NANOSCIENCE

CHALMERS UNIVERSITY OF TECHNOLOGY
Göteborg, Sweden 2026
www.chalmers.se

Laser frequency stabilisation onto a high-finesse optical cavity

towards narrow-line laser cooling of 88 strontium

ALEX JERNSTEDT

CHALMERS

Department of Microtechnology and Nanoscience
CHALMERS UNIVERSITY OF TECHNOLOGY
Göteborg, Sweden 2026

Laser frequency stabilisation onto a high-finesse optical cavity
towards narrow-line laser cooling of 88 strontium
ALEX JERNSTEDT

Examiner: Nils Johan Engelsen, Department of Microtechnology and Nanoscience
Supervisor: Sebastian Kock, Department of Microtechnology and Nanoscience

Master's Thesis 2026
Department of Microtechnology and Nanoscience
Chalmers University of Technology
SE-41296 Göteborg
Sweden
Telephone +46 (0)31-772 1000

Cover:
Picture of the 4-bore optical cavity used as an external reference for laser stabilisation.

Abstract

Laser cooling of strontium requires repump lasers to maintain an atom population in states accessible to the cooling cycle. This work presents the development of an experimental setup for frequency stabilisation of two repump lasers at 679 and 707 nm using a high-finesse optical cavity. The method utilises the Pound-Drever-Hall (PDH) technique to produce error signals. Coupling of the 707 nm laser to the cavity is demonstrated with a mode-matching efficiency of 40%. Phase modulation using an electro-optic modulator (EOM) is generated and detected, enabling the production of PDH error signals. While these signals have not yet been used to lock the lasers, the setup provides a foundation for future implementation of cavity-stabilised repump lasers.

Acknowledgements

I'd like to thank Nils J. Engelsen, first of all for your patience, and secondly for the opportunity to learn so much about laser cooling and the practical skills needed to create optical setups. Things might not have ended up working perfectly, but I have learnt a lot of things, and that is something I'm grateful for. I'd also like to thank the group: Sebastian, Alex, Pritwish, Awse, and Yincheng, for your support, ideas, and knowledge. I also thank the people in the periphery of the project: Witlef Wieczorek for our few but meaningful discussions about resonators and cavities, Lars Jönsson for fabricating components necessary for the setup, and everyone who has been passionate and encouraging about my popular science project. Finally, I'd like to thank everyone who has provided Inkscape libraries of figures and open source code. These people are doing a wonderful job for science.

Alex Jernstedt, Göteborg, June 2026

Glossary

ABCD matrices	Matrix formalism used to simulate wave propagation through optical systems.
AC-Stark shift	Shift and splitting of atomic energy levels due to electric field.
Anti-Helmholtz coils	Two identical circular coils through which identical current of opposite sign is run. A component of a MOT.
Astigmatism	The location of the beam waist is different for the two beam axes.
Axial modes	Resonant wave that travels perfectly along the optical axis.
Beam waist	The narrowest diameter of a laser beam.
Bounce number	The number of round trips a photon makes in a cavity before it has a $1/e$ probability of leaving it.
Capture range	A measure of how wide of a A) velocity range atoms can be trapped in, or B) frequency range locking onto an optical cavity is valid.
Chirp cooling	A type of laser cooling. Frequency sweeps quickly to account for loss of velocity and resulting Doppler shift.
Coupling	The interaction between different systems when they are connected.
Decay time	Determines how long photons stay inside a cavity.
Doppler effect	The observed frequency of a wave is dependent on the observer's position relative to the source.
Doppler cooling	Utilises the Doppler effect to trap atoms.
Doppler limit	The theoretical limit for how cold atoms can get through Doppler cooling.
EDT	Electric dipole transitions occur when an atom interacts with a perturbing electric field.
Einstein coefficients	Constants describing atom absorption and emission probabilities.
Ellipticity	When a beam is elliptic, the waist is different along two orthogonal axes. It is also common that the two axes show different divergence.
EOM	Electro-optical modulator. A component that changes as voltage is applied over it.
Equipartition theorem	Relates temperature to energy.
Fabry-Pérot cavity	An optical cavity with two parallel flat mirrors.
Fermi's golden rule	Yields transition rate $\Gamma_{1\to 2} = \frac{2\pi}{\hbar}\lvert\langle 2\rvert H'\lvert 1\rangle\rvert^2 \rho(E_2)$.
Finesse	A measure of the narrowness of the peaks in a specific cavity.
Frequency comb	An optical frequency comb is a type of laser with very precise and equidistant frequency lines. It relates optical frequencies to radio frequencies.
Frustration	When arrays of atoms or molecules compete and prevent bonds from being satisfied, they form networks with highly degenerate ground states.
FSR	Free spectral range. Spacing between two fundamental resonant modes.
Fundamental mode	See *Axial mode*.
FWHM	Full width at half maximum. A measure of linewidth.
GPS	Global positioning system: uses satellites and ground stations to find position.
HC-locking	Hänsch-Couillaud locking is a laser frequency stabilisation technique.
Ising spins	A variable representing the magnetic dipole moment of an atom in a lattice.
Jevon's paradox	When things get more efficient, more energy is used.
Larmor frequency	Angular momentum vector of an atom precesses around external field axis with frequency Ω_L.
LASER	Light emission by stimulated emission of radiation.
Laser cavity	An optical cavity but with a medium that can be excited in it.
Laser cooling	A method where radiation pressure is used to slow down the speed of atoms.

Laser medium	The contents of a laser that are excited and emit light.
Leakage beam	The light that escapes the cavity after light has made round trips inside the cavity.
Linewidth	The spectral width of a resonant mode.
MDT	Magnetic dipole transitions occur when an atom interacts with a magnetic field.
Modes	Specific wave distributions that propagates through space.
Modulation depth	A measure of how much the EOM changes the incoming light.
MOT	Magneto-optical trap. Uses laser cooling and magnetic fields to restrain a sample.
Optical cavity	A structure capable of confining light and causing resonance. A well-known cavity is the *Fabry-Pérot cavity* which is made from two parallel mirrors. Some cavities have other arrangements of mirrors.
Optical mode	A path light can take through an optical medium. Solves the wave equation and satisfies the boundary conditions of the relevant situation.
Optical molasses	A 3D configuration of lasers that traps and cools atoms at its centre.
Optical resonator	See *Optical cavity*.
PDH	The Pound-Drever-Hall stabilisation technique uses a feedback loop to stabilise a laser with an optical cavity.
Photon lifetime	See *Decay time*.
Pockels effect	Change in reflective index of a material due to electric field.
Polarisation	Specifies geometrical orientation of a wave.
Population inversion	When more atoms/molecules are in a higher than lower energy state.
Pumping process	The process that continuously excites the laser medium.
QCD	Quantum chromodynamics is a theory supposing quarks are subject to colour charge.
Quadrupole transitions	A forbidden transition that can occur during interaction with field.
Quark	The currently known smallest constituent of matter.
Rabi frequency	The rate of an atom's oscillation between the ground state and an excited state when the atom is illuminated.
Radiation pressure	The pressure from the force exerted on matter by light.
Rayleigh range	Two times the distance from waist to location where waist has doubled.
Recoil velocity	Velocity gained when atom absorbs or emits a photon.
Saturation intensity	Intensity required to gain significant saturation of some medium.
Sidebands	Frequencies spaced at a set distance from a carrier frequency.
Singlet state	All electrons are paired → S=0.
Stability criterion	$0 \leq g_1 g_2 \leq 1$. Determines if cavity can confine light.
Standing waves	When wavelength is right, a wave reproduces itself in a cavity.
Stimulated emission	Photon interaction can induce excited atom to release a photon with the same energy and phase as the incoming photon.
TEM	Transverse elecromagnetic waves exhibit orthogonal relations between the magnetic and electric fields, as well as the direction of the wave.
Thomas precession	A relativistic correction to the spin of particles.
Transverse mode	A mode in the direction perpendicular to the optical axis.
Triplet state	Two unpaired electrons with parallel spin → S=1.
Vacuum field	Fundamental background state of the universe. A combination of lowest-state energy waves at different frequencies and phases.
Virtual photons	Model the interaction between light and matter. Cannot be observed.
Wave equation	A description of the propagation of waves in space as a function of time.
Wave function	The mathematical description of a quantum state.
Zeeman effect	Splitting of one atomic level into several in the presence of magnetic field.

List of Figures

List of Tables

Contents

1 Introduction

Laser cooling is the most powerful technique currently available to mankind for reducing the motion of atoms and molecules to almost total immobility, which corresponds to temperatures near absolute zero [1]. When samples are this cold, they are in their motional ground state, where their behaviour is governed solely by quantum mechanics. Repeatedly obtaining motional ground states is an important step in ensuring repeatability of atomic physics experiments, and laser cooling is therefore a useful tool in many types of research about quantum systems. However, the applicability of laser cooled strontium is not limited to the world of research and academia; in fact, it is highly promising for current time-keeping through atomic clocks, and has potential within quantum computing.

In this introduction, laser cooling will be briefly explained, followed by some applications laser cooled strontium atoms could have in modern and future technology. There will be a focus on atomic clocks and their application, and on so called hybrid systems, in which ultracold atoms are coupled to small mechanical resonators.

1.1 An introduction to laser cooling

Initially, it might seem counter-intuitive that lasers can be used to cool down nanomechanical systems. After all, lasers contain energy, and are often used in construction and textile industries to cut or melt materials [2, 3]. However, laser cooling can be understood through considering the fact that light has momentum.

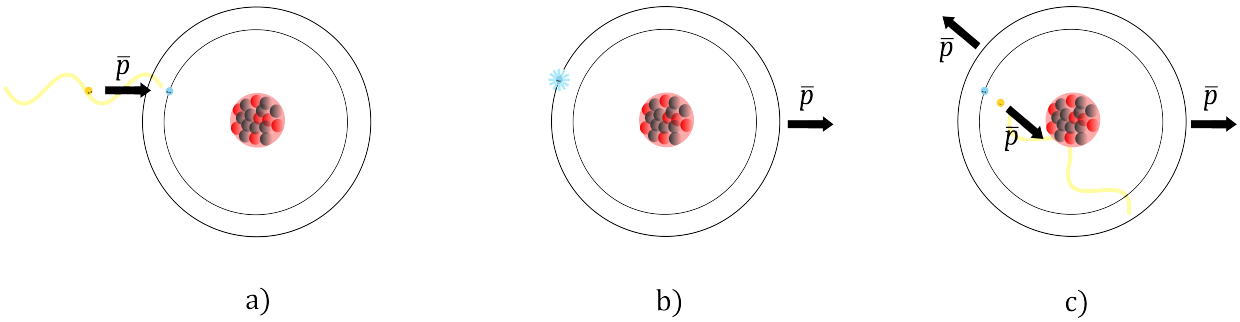

Figure 1.1: a) Incoming light with a wavelength corresponding to an energy gap in the atom hits the atom that is in an initial state $|1\rangle$. b) The atom absorbs the energy and enters a higher energy state $|2\rangle$. The momentum of the photon is conserved and affects the atom's motion. c) The photon is emitted and the atom returns to its initial state. Momentum laws apply to both the atom and the photon. Note that the images show a simplified and inaccurate model of the atom.

Absorption of light can occur when incoming light has a wavelength λ which corresponds to an energy gap $\Delta E = E_2 - E_1 = hc/\lambda$ between a lower energy state E_1 and a higher energy state E_2 in an irradiated atom. Here, h is Planck's constant and c is the speed of light in the relevant medium. A photon with energy ΔE is massless, but it has some momentum $p = E/c$. When the photon is absorbed, this momentum must be conserved. The momentum is transferred to the atom, and the atom is excited to the higher energy state. When the atom later emits the energy from the photon and returns to its lower energy state, the outgoing photon has the same momentum p, but if unaffected by external electromagnetic fields, it is emitted in an arbitrary direction. The atom is given an additional momentum in the direction opposite to the direction in which the photon was emitted.[1]

When an atom is hit by n photons with momentum p coming from the same direction, the net momentum imparted onto the atom is np in the direction of the photons. The atom will also be induced to move with momentum p in n arbitrary directions due to spontaneous emission. If n is large, it can be seen that the net change in momentum due to spontaneous emission tends to zero, under the assumption that the atom isn't influenced by other electromagnetic fields. In figure 1.1, a simplified schematic describes the approximate process of photon absorption and emission. More detailed information about radiation pressure and spontaneous emission can be found in section 2.4.1 and 2.2.3.

1.2 Applications

Laser cooling of strontium atoms has many applications, both in fundamental physics research and for industrial projects on a global scale.

The narrow line transitions of strontium isotopes are extremely precise, and if correctly measured, can provide a new, more exact standard for how humanity measures time [4, 5]. In other words, laser cooling of strontium could lead to better clocks, which would have a direct impact on everything that concerns time and synchronisation of different kinds. GPS, telecommunication and geodesy would improve, and therefore affect the daily lives of all humans on earth who make use of GPS-based navigation and telecommunication services. While atomic clocks with higher precision and the spin-off effects of these are promising fields for the future, this is far from the only application of laser cooled strontium.

An attractive aspect of laser cooling is that once an atom or molecule is properly cooled, it can be found to be in its motional ground state. This holds true no matter when or where the experiment is done. Repeatedly obtaining motional ground states is a requisite for reliable results from atomic experiments. Laser cooling and similar light-mitigated effects on particles can be used to precisely control the position and behaviour of large ensembles of atoms in lattices, allowing for quantum simulations of bulk models [6, 7]. Utilising these techniques can also increase the statistical precision of measurements by reducing thermal noise [8]. On the other side of the spectrum, light can also be used to control individual atoms to study fundamental phenomena such as *frustrated Ising spins* [9].

A more relevant application of laser cooling of strontium atoms to future research in this project are hybrid systems. Ultracold atoms could be used to cool vibration modes of small mechanical resonators, like membranes and cantilevers, without the use of cryogenics [10, 11]. This would facilitate the process of reaching quantum regimes of motion for mechanical resonators. Atoms are sensitive probes of fields and forces, and if coupled to a mechanical resonator, this would theoretically mean the hybrid system would be capable of detecting much weaker signals than the resonator would on its own. Realisation of such a sensor would enable much more exact measurements, which would have applications in all natural science research fields, not just in physics [12].

1.2.1 Optical clocks

Many animals have some sense of time, but humans in particular have reached a point in which knowing the time is crucial to everyday life. The first clocks were based on the movements of the sun and the length of shadows, but other clocks based on for example water or sand flow have also been used in different cultures around the world. A breakthrough in timekeeping was the implementation of pendulum clocks, that enabled many households to keep

time with precision in the span of minutes. Well made pendulum clocks were used in science until the turn of the 19th century. In the early 20th century, other clocks were developed based on electro-mechanical resonators in the form of quartz crystals. By this point in time, scientists had realised that to make a clock, one needs to build a mechanism that somehow utilises the resonance of some structure. That could be the period of a pendulum, the oscillation of a crystal lattice, or the vibration of a loaded spring.[13]

All these options will, however, end up keeping time at a slightly different pace. That is because no two pendulums or crystals will end up being the exact same. Even if they are extremely well made, and seem undistinguishable to the naked eye, as long as they are macroscopic objects, they will be different on a microscopic and nanoscopic level. This will cause clocks to drift, meaning they will move faster or slower than the time they're supposed to keep. The time it takes for a clock to drift differs - for older pendulum clocks, it might take a few days, and for really good ones, it might take years. This is why it's necessary to have a standard time, that can be used as a reference to correct the drift. The rotation of the Earth was used as a standard for time well into the 20th century, before atomic clocks entered the stage [5, 13].

The issue with man-made time-keeping devices is that they are man-made, and therefore differ. Atoms, however, are immaculate. As far as humanity knows, two atoms of the same species and isotope are perfectly identical. That means that if the oscillation of an atom can be used to build a clock, it is possible to measure time based on a mechanism that isn't man-made, and that will remain unaffected by who makes the measurement. A clock based on that could be made extremely precise, and the experiment would be repeatable.

Atomic clocks operate based on the electronic properties of atoms. Atoms can absorb and emit electromagnetic radiation by making transitions between quantised energy levels. If one finds the frequency of light that causes a transition, it is possible to define a second from that.

Optical atomic clocks utilise the light emitted from an ultra-stable laser as an oscillator for the clock. The frequency of this light will be sensitive to surrounding fields and forces, which is why the light is used to sample the electromagnetic resonance of the atomic species of interest, for example caesium or strontium. The signal from the probed atom will act as a control frequency to determine the difference in frequency between the imperfect laser and the atom's fundamental electronic properties. The frequency is measured with a fs *frequency comb*, allowing the signals from the system to be translated into a useful way for humans to measure time [5].

The current way of measuring time is based on caesium, and the second is defined as the duration of 9192631770 periods of the radiation corresponding to the transition between the two hyperfine levels of the ground state of 133 caesium. Currently, the best caesium clocks will only be a second off in 100 million years, but experiments on strontium atoms indicate that even better precision could be obtained with this atomic species [5].

Improving the time standard would lead to more precise measurements of distances and speed. GPS, which is an abbreviation for *Global Positioning System*, is an invention that utilises signals from 24 satellites to determine the position of objects on Earth's surface. Each satellite has an atomic clock onboard, and through knowing the time and their relative distances, they can measure the position of things on Earth down to 1 mm for objects at rest under favourable circumstances. While GPS has revolutionised navigation and facilitated navigation for different types of vehicles, the current system has a few weak points. The current limitations of GPS is its accuracy for moving objects, that could be between 1-10 cm. Furthermore, the accuracy of position measurements is dependent on several satellites operating at once. If a satellite

is inoperable for some reason, the accuracy of position measurements is greatly reduced. A way to increase the accuracy of satellites is to improve the atomic clocks on board. Increasing the accuracy by a factor of 1000 would enable better measurements of the position of moving objects. This could enable sensing of vibrations in the Earth crust, which could mean that earthquakes could be predicted faster. A positioning system that knows the position of a moving object with a mm-level precision would also facilitate the design of self-driving cars that rely on such a system.

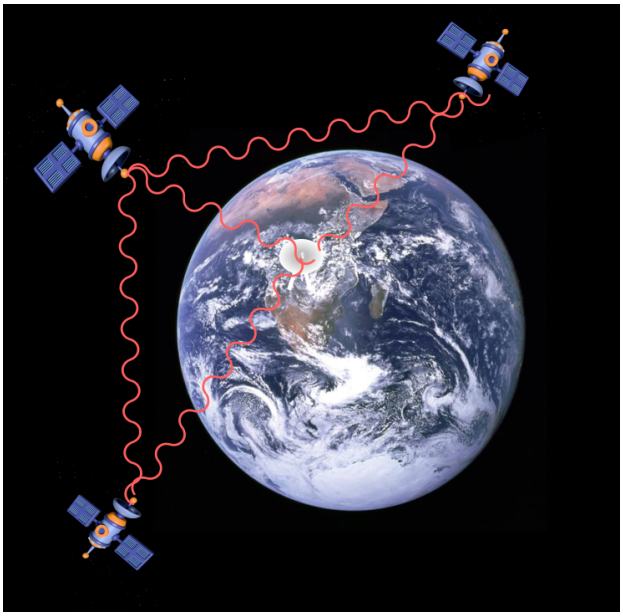

Figure 1.2: An illustration of the principle of GPS. The satellites communicate using radio frequencies, and reference their signals to a stationary ground station. Through determining the time it takes for the signals to reach the other satellites and the ground reference, they can determine distances with centimetre precision. Picture of Earth from NASA (Apollo 17 in 1972) and cartoons of satellites by Julia Eskina.

The signals from GPS satellites are also used to synchronise computer networks and ensure that the internet works properly. It is also a crucial factor in communication by mobile phone. Improving the atomic clocks of the GPS satellites therefore means improving plenty of other things that are connected to timing in some way.

1.2.2 Hybrid systems: coupling laser cooled atoms to microscale structures

Ultracold atoms can be used to cool vibration modes of small mechanical resonators, like membranes and cantilevers, without the use of cryogenics. This field is comparatively young, with the earliest research about larger systems being sympathetically cooled using atomic ions being published around 2008. The interest in it grows due to its possible applications for highly controllable qubits and in sensing technology.

Already in 2008, Offenberg *et al.* published a study in which they used laser cooling to sympathetically cool a protein to less than 1 K [14]. In 2009, Geraci and Kitching investigated mechanical resonators coupled to ultracold atoms trapped in a lattice, with possible applications for two-qubit controlled-NOT gates [11]. These results were followed by further studies coupling ultracold atoms to mechanical oscillators in 2011 [15, 16]. An inverse application of using atoms to cool down mechanical oscillators was done by Kolkowitz *et al.* in 2012, where they

achieved coherent sensing of a mechanical resonator with a single-spin qubit [17]. In 2014, Jöckel *et al.* used ultracold atoms to sympathetically cool the vibrations of a nanomembrane with a mass exceeding that of the atom by 10^{10} [10]. Since then, the groups have investigated other hybrid systems and applications of their research, and new studies have been done [18]. There are still things to be done and discovered in this field before applications can be realised and put out on the market.

1.3 Aim and limitations

The aim of this project was to achieve narrow line laser cooling of Strontium. However, the vacuum chamber necessary to achieve this was not ordered in time and could not arrive within the time-frame granted to the project. The scope of the thesis was forced to be reduced to the stabilisation of a laser pair onto an optical cavity.

2 Theory

To achieve laser cooling, a number of lasers is needed. This section presents the fundamental atomic physics needed to understand the theory behind laser cooling, followed by the practical knowledge about optical cavities and the laser frequency stabilisation technique.

2.1 Atomic physics

Atomic physics concern the physics used to describe and predict the behaviour of atoms. The field is closely tied to quantum theory, and the two sciences evolved together throughout the 20th century. This section describes the selection rules of atoms and the interaction of the atom with a perturbing electric radiation field.

2.1.1 Selection rules

Selection rules are guidelines that can predict transitions between different states and determine which of these transitions are more or less probable. Transitions with high probability are often referred to as allowed, while ones with low probability are referred to as forbidden. There are two main types of transitions, namely *electric dipole transitions* (EDT) and *magnetic dipole transitions* (MDT), but higher order transition types, for electric and magnetic *quadrupoles* (EQT and MQT) and octupoles exist as well. The general characteristics of these transitions are summarised in table 1.

Quantum number	**EDT**	**MDT**	**EQT**	**MQT**
Δl	± 1	0	$0, \pm 2$	$0, \pm 2$
Δm_l	$0, \pm 1$	$0, \pm 1$	$0, \pm 1, \pm 2$	$0, \pm 1, \pm 2$
Δm_s	0	0	0	0

Table 1: Selection rules for EDT, MDT, EQT and MQT. The changes occur to the orbital angular momentum quantum number l and the magnetic quantum number m_l. The magnetic quantum number for spin m_s remains unaffected by electric and magnetic dipole and quadrupole transitions.

These selection rules can be found through introducing electromagnetic effects to quantum systems. The change to the angular momentum quantum number follows as a natural consequence to the conservation of angular momentum during an exchange. Since photons are particles with spin 1, their angular momentum is also 1, which means a photon can either add or remove this angular momentum from the atom. The spin quantum number doesn't change because the photon's interaction with the system doesn't affect the electron's spin directly.

The wavefunction solutions to the Schrödinger equation for eigenstates of the atom are standing waves [1]. When a transition occurs, the wavefunction must change, but the eigenstates and wavefunction are also affected by fields. A particle interacting with an oscillating electric field

$$\mathbf{E}(t) = |\mathbf{E}_0| \mathrm{Re}(e^{-i\omega t} \hat{\mathbf{e}}_{\mathrm{rad}}) \tag{1}$$

can be found to cause a perturbation to the time-dependent Hamiltonian of the particle. This Hamiltonian is described by a perturbation $\hat{H}' = e\mathbf{r} \cdot \mathbf{E}$. The interaction with radiation stimulates transitions from $|1\rangle$ to $|2\rangle$ with a rate γ proportional to the square of the matrix element

of the perturbation. This γ follows directly from *Fermi's golden rule* concerning the rate of transitions in oscillating fields.

$$\gamma \propto |e\mathbf{E}_0|^2 \left| \int \psi_2^*(\mathbf{r}\cdot\hat{\mathbf{e}}_{\text{rad}})\psi_1 d^3\mathbf{r} \right|^2 = |e\mathbf{E}_0|^2 |\langle 2|\mathbf{r}\cdot\hat{\mathbf{e}}_{\text{rad}}|1\rangle|^2 \tag{2}$$

The dipole matrix element $\langle 2|\mathbf{r}\cdot\hat{\mathbf{e}}_{\text{rad}}|1\rangle$ in equation 2 can be written as a product of the radial integral $D_{12} = D_{21}$ and the angular integral I_{ang} as $\langle 2|\mathbf{r}\cdot\hat{\mathbf{e}}_{\text{rad}}|1\rangle = D_{12} I_{\text{ang}}$. While D_{12} is typically non-zero, I_{ang} is typically always zero unless strict criteria are fulfilled [1]. The selection rules can be found by investigating the angular integral and its criteria. To calculate I_{ang}, the unit vector $\hat{\mathbf{r}}$ is expressed using spherical harmonic functions

$$\hat{\mathbf{r}} \propto Y_{1,-1}\frac{\hat{\mathbf{e}}_x - i\hat{\mathbf{e}}_y}{\sqrt{2}} + Y_{1,0}\hat{\mathbf{e}}_z + Y_{1,1}\frac{-\hat{\mathbf{e}}_x + i\hat{\mathbf{e}}_y}{\sqrt{2}}, \tag{3}$$

while the polarisation vector $\hat{\mathbf{e}}_{\text{rad}}$ is expressed in similar terms as

$$\hat{\mathbf{e}}_{\text{rad}} = A_{\sigma-}\frac{\hat{\mathbf{e}}_x - i\hat{\mathbf{e}}_y}{\sqrt{2}} + A_\pi\hat{\mathbf{e}}_z + A_{\sigma+}\left(-\frac{\hat{\mathbf{e}}_x + i\hat{\mathbf{e}}_y}{\sqrt{2}}\right). \tag{4}$$

This leads to

$$\hat{\mathbf{r}}\cdot\hat{\mathbf{e}}_{\text{rad}} = A_{\sigma-}Y_{1,-1} + A_z Y_{1,0} + A_{\sigma+}Y_{1,1}, \tag{5}$$

which simplifies evaluation of the angular integral. It can be found that for π-transitions, the system has a cylindrical symmetry, which means that the value of the angular integral is unchanged when a rotation by an angle ϕ_0 occurs about the z-axis.

$$I^\pi_{\text{ang}} = e^{i(m_1-m_2)\phi_0} I^\pi_{\text{ang}} \tag{6}$$

Equation 6 is satisfied if I^π_{ang} is zero or if $m_1 = m_2$. The electric field component in the xy-plane causes σ-transitions. This yields that $I^{\sigma+}_{\text{ang}} = 0$ unless $m_1 - m_2 + 1 = 0$, and likewise, $I^{\sigma-}_{\text{ang}} = 0$ unless $m_1 - m_2 - 1 = 0$. As a consequence, the change to the magnetic quantum number is $\Delta m_l = \pm 1$, while unpolarised light or a system without a defined quantisation axis will yield $\Delta m_l = 0, \pm 1$.

Many particles, notably electrons, possess some intrinsic charge, which, as far as is possible to understand today, is a constant property of the particle and equal for all electrons. If a particle with charge q is subjected to an electromagnetic field with components $\mathbf{E}$ and $\mathbf{B}$, these charges will be subjected to a force $\mathbf{F} = q(\mathbf{E} + (\mathbf{v}\times\mathbf{B})/c)$. The forces acting upon electrons in atoms will give rise to new changes and phenomena. When charges move in closed loops, they generate a magnetic dipole moment $\vec{\mu}$[19]. By classical physics, the magnetic dipole moment and the angular momentum can be shown to be related by

$$\vec{\mu} = \frac{q}{2mc}\mathbf{L}. \tag{7}$$

However, particles like electrons are not points, and applying classical physics to them can be lacking. Therefore, $\vec{\mu}$ is redefined as a quantum mechanical operator for some particle with known spin J. Since J is parallel to $\mathbf{L}$, the new magnetic dipole moment is defined as

$$\vec{\mu} = g\frac{e}{2mc}\mathbf{J}, \tag{8}$$

where e is the elemental charge, and g is a measure of the deviation of the actual magnetic moment from the fundamental electric properties of an electron. Typically, the g-factor is defined to be able to take on both positive and negative values, while the fundamental charge, e, is defined to be positive [19].

With these new concepts introduced, it is now possible to study the Schrödinger equation for a particle with magnetic dipole moment $\vec{\mu}$. It is perturbed by a Hamiltonian $\hat{H}_\mu$ from an external magnetic field acting upon the magnetic dipole moment is $\hat{H}_{\text{Tot}} = \hat{H}_0 + \hat{H}_\mu = \hat{H}_0 - \vec{\mu}\cdot\mathbf{B}$ [19]. While $\hat{H}_0$ commutes with $\mathbf{J}$, the same cannot be said for the perturbed Hamiltonian. If the quantisation axis is chosen to be along the magnetic field, however, it still holds that $[\hat{H}_0 + \hat{H}_\mu, \hat{J}_z] = 0$, which means that the wavefunction and energy of the particle will remain unaffected when the particle rotates about the z-axis, but not if it would rotate about other axes. The result of this is that $\mathbf{J}$ is no longer conserved, and the previously $2J+1$-fold degenerate energy levels are removed.

2.1.2 Fine structure

The atomic energy levels have small splittings, or fine structure, that is caused by relativistic effects. At the start of the last section, a one-electron atom was studied with respect to its radial and angular wavefunctions. However, electrons also possess an intrinsic property called spin. Spin affects the energy levels of an atom through something called spin-orbit interaction. An electron moving through an electric field $\mathbf{E}$ experiences an effective magnetic field $\mathbf{B}$ given by 9.

$$\mathbf{B} = -\frac{1}{c^2}\mathbf{v}\times\mathbf{E} \tag{9}$$

By rewriting the electric field on its potential energy form, the relevant Hamiltonian $\hat{H}_\mu$ can be deduced according to

$$\begin{aligned} \mathbf{E} &= \frac{1}{e}\frac{\partial V}{\partial r}\mathbf{r} \\ \implies \mathbf{B} &= \frac{1}{m_e c^2}\left(\frac{1}{er}\frac{\partial V}{\partial r}\right)\mathbf{r}\times m_e\mathbf{v} = \frac{\hbar}{m_e c^2}\left(\frac{1}{er}\frac{\partial V}{\partial r}\right)\mathbf{l} \\ \implies \hat{H}_\mu &= -\vec{\mu}\cdot\mathbf{B} = g_s\mu_B\mathbf{s}\cdot\frac{\hbar}{m_e c^2}\left(\frac{1}{er}\frac{\partial V}{\partial r}\right)\mathbf{l}. \end{aligned} \tag{10}$$

In the last row of system 10, the factor g_s is analogous to the factor found in equation 8, and is approximately equal to 2. However, this theoretical measure results in energy splittings that deviate from the practical ones by a factor of two. This discrepancy stems from relativistic effects and is called *Thomas precession*. To account for this error, g_s is substituted with $g_s - 1$, resulting in a spin-orbit interaction Hamiltonian equal to

$$\hat{H}_{\text{spin-orbit}} = (g_s - 1)\frac{\hbar^2}{2m_e^2 c^2}\left(\frac{1}{r}\frac{\partial V}{\partial r}\right)\mathbf{s}\cdot\mathbf{l}. \tag{11}$$

The potential can be set to the Coulomb potential. The total angular momentum is the sum of the orbital and the spin angular momenta, and the total angular momentum must be conserved for a system without any external torque acting on it. Since $\mathbf{j} = \mathbf{l} + \mathbf{s}$, it follows that $2\mathbf{s}\cdot\mathbf{l} = \mathbf{s}\cdot(\mathbf{j}-\mathbf{s}) + (\mathbf{j}-\mathbf{l})\cdot\mathbf{l} = \mathbf{j}\cdot(\mathbf{l}+\mathbf{s}) - \mathbf{s}^2 - \mathbf{l}^2 = \mathbf{j}^2 - \mathbf{s}^2 - \mathbf{l}^2$. This means that the expectation value can be expressed in terms of the expectation values for each independent momentum. This yields the expectation value

$$\langle \mathbf{s}\cdot\mathbf{l}\rangle = \frac{1}{2}[j(j+1) - l(l+1) - s(s+1)], \tag{12}$$

that follows from normal energy level operations. The fine structure energy shifts are proportional to this expectation value. In the case of hydrogen, there is only one electron, that can either have a positive or negative half-integer spin. This means that for each l, the total angular momentum quantum number j is $l \pm \frac{1}{2}$.

2.1.3 The Rabi two-level problem

The time-dependent Schrödinger equation for an atom unaffected by external fields is given by

$$\hat{H}_0\Psi(\vec{r},t) = i\hbar\frac{\partial}{\partial t}\Psi(\vec{r},t). \tag{13}$$

If the atom interacts with an external radiation field, the addition to this equation can be said to be $\hat{H}_1(t)$. This, in turn, affects the entirety system, that can now be described by

$$[\hat{H}_0 + \hat{H}_1(t)]\Psi(\vec{r},t) = i\hbar\frac{\partial}{\partial t}\Psi(\vec{r},t). \tag{14}$$

If the wavefunction $\Psi(\vec{r},t)$ is given by the solution on the form $\sum_k c_k\psi_k(\vec{r})\exp(-i\omega_k t)$, equation 14 can be multiplied by the complex conjugate of the spatial wavefunction, $\psi^*(\vec{r})$. Integrating over spatial coordinates will then yield

$$i\hbar\frac{d}{dt}c_j(t) = \sum_k c_k(t)\hat{H}_{1,jk}(t)e^{i\omega_{jk}t}, \tag{15}$$

where $\hat{H}_{1,jk} = \langle\psi_j|\hat{H}_1|\psi_k\rangle$ and $\omega_{jk} = \omega_j - \omega_k$. While this equation is physically correct, it is impossible to solve without approximations. In laser cooling, when narrow-band laser excitation of atoms is used, it is common to use a model that was also used by Rabi. He limited the expression on the right hand side in equation 15 to comprise only two terms: the ground state and excited state connected to it by the frequency of the laser [20].

In the presence of an electric field $\vec{E}(\vec{r},t) = E_0\cos(kz-\omega_t t)\hat{e}$, where $\hat{e}$ is the unit polarisation vector, the perturbing Hamiltonian between two states becomes $\hat{H}_{1,21} = \hbar\Omega_R\cos(kz-\omega_t t)$. This introduces the *Rabi frequency*, Ω_R, which is defined as

$$\Omega_R = -\frac{eE_0}{\hbar}\langle 2|r|1\rangle. \tag{16}$$

Note that different literature define the Rabi frequency in different ways, depending on previous assumptions of the interfering Hamiltonian. In Foot's *Atomic Physics* (2005), for example,

the oscillating electric field is defined as $\hat{H}' = e\mathbf{r} \cdot \mathbf{E}_0 \cos(\omega t)$ for an induced electric dipole $-e\mathbf{r}$ [1]. This definition yields a Rabi frequency

$$\Omega_R = \frac{eE_0}{\hbar} \langle 1|r|2\rangle, \tag{17}$$

but it is to be treated the same as the expression in 16.

As the atom is subjected to an electric field, its wavefunction is also affected. Physically, this is expressed as light shifts with energies corresponding to $\hbar(-\delta \mp \sqrt{\Omega_R^2 + \delta^2})/2$ from the unperturbed states with energies E_2 and E_1. Here, δ represents some frequency that tunes the frequency in such a way that increasing $|\delta|$ increases the frequency of the total oscillation, while also reducing the amplitude [20].

2.1.4 Atomic structure of ^{88}Sr

Strontium is an alkali metal with atomic number 38. It comes in four naturally occurring isotopes, of which the relevant one has 50 neutrons. From this point on, this isotope will be referred to as Sr^{88}. Its mass is 87.9056 mass units and it has zero spin. It has two valence electrons [21].

The valence electrons have spin that can be symmetric or anti-symmetric. The symmetric state is called a *triplet state*, whereas the anti-symmetric alignment is referred to as a *singlet state*. For strontium, the triplet state has a tendency to decay into the singlet state. This transition does not preserve the total spin quantum number, making it a forbidden transition. In strontium, however, this can occur due to spin-orbit coupling, where spin and spatial components of the wavefunction couple and allow the transition to happen at the expense of allowed singlet-singlet transitions. Singlet-singlet transitions occur at time scales in the nanosecond regime, while singlet-triplet transitions range between microseconds to seconds. The electronic structure of strontium can be found in figure 2.1, with notable transitions from the ground state $^1S_0$ to $^1P_1$ and the forbidden transition from $^1S_0$ to $^3P_1$ [5].

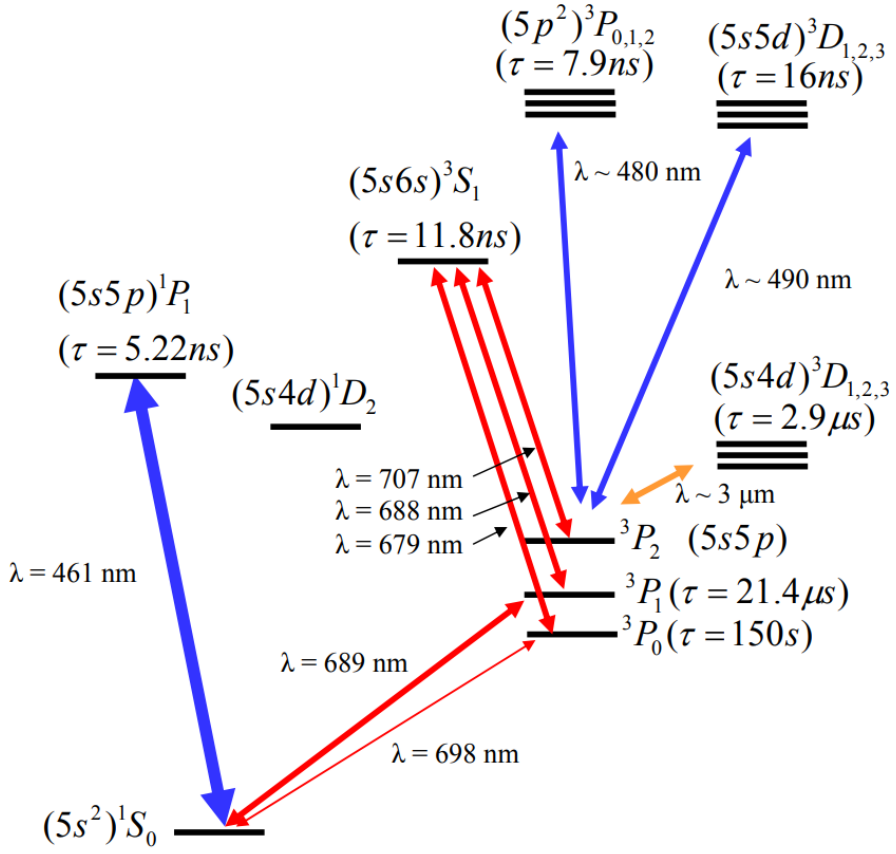

Figure 2.1: Atomic structure of strontium (not to scale). Image retrieved from page 20 in *High Precision Spectroscopy of Strontium in an Optical Lattice: Towards a New Standard for Frequency and Time* by M.M. Boyd (2007) [5].

2.2 Electromagnetic theory

This work is centred on the theory of light and its interactions with matter. A fundamental knowledge about electromagnetic theory is assumed, but to provide a chance to refresh such knowledge, these fundamentals are briefly presented here. This section provides a brief summary of Maxwell's equations and the wave equation that solves these equations, an introduction to the photon as a concept, and finally a more thorough walkthrough of spontaneous and stimulated emission.

2.2.1 Light in the classical sense

Classically, light is seen as a wave in the form of electromagnetic radiation, which is comprised of the electric field and the magnetic field. Often, these are described by the electric field intensity **E** and the magnetic flux density **B**. The former is directly related to the charge density ρ by equation 18, while the latter is more closely related to the movement of charges through space.

As a wave, the light can be described by wave equations. The wave equation is derived from Maxwell's equations, that supply a mathematical description of electromagnetic radiation. Maxwell's equations in free space are given by equations 18-21 below.

$$\nabla \cdot \mathbf{E} = \frac{\rho}{\varepsilon_0} \tag{18}$$

$$\nabla \cdot \mathbf{B} = 0 \tag{19}$$

$$\nabla \times \mathbf{E} = -\frac{\partial \mathbf{B}}{\partial t} \tag{20}$$

$$\nabla \times \mathbf{B} = \mu_0 \left(\mathbf{J} + \varepsilon_0 \frac{\partial \mathbf{E}}{\partial t} \right) \tag{21}$$

In these equations, ε_0 and μ_0 are the permittivity and permeability of vacuum. Both of these parameters depend on the media in which the fields propagate, and affect the fields. The vector **J** is the current density. [22]

From these equations, it is possible to find the *wave function*, that relates the evolution of the **E**-field and **B**-field in space to their evolution in time. A full derivation of the wave function in free space is found in appendix A.1. Given some wave vector **k**, the wave equation in free space can be found to be

$$\mathbf{E}(\mathbf{r}, t) = \mathbf{E_0} e^{i(\mathbf{k}\cdot\mathbf{r} - \omega t)}. \tag{22}$$

Alternately, equation 22 can be written as $\nabla^2 \mathbf{E} + k^2 \mathbf{E} = 0$, where k is equal to $\omega\sqrt{\mu_0 \varepsilon_0}$. When a field propagates through a medium in which the charge density and current density cannot be assumed to be zero, the solution to the wave equation changes. The permeability and permittivity change from μ_0 and ε_0 to $\mu = \mu_r \mu_0$ and $\varepsilon = \varepsilon_r \varepsilon_0$, where μ_r and ε_r are the relative permeability and permittivity of the specific material.

A wave described by 22 can be seen as a superposition of monochromatic waves in a space of the same dimensions as **r** and **k**. When waves interact with optical components, like lenses, mirrors, and wave plates, the composition of the total **E**-field is relevant. Materials in the wave's path can have patterns and structures that show preference to which kind of wave is let through. Therefore, the *polarisation* of a wave has relevance to optical experiments.

Any plane wave propagating in a direction z can be divided into two orthogonal components, that take z as an argument but shows fluctuations in the plane orthogonal to the propagation path. The plane can be substituted with two orthogonal directions x and y, yielding a final **E**-field as given by equation 23.

$$\begin{aligned} \mathbf{E}(z, t) &= \hat{\mathbf{x}} E_x(z, t) + \hat{\mathbf{y}} E_y(z, t) \\ &= \hat{\mathbf{x}} E_{x0} \cdot \cos(\omega t - k_x z + \varphi_x) + \hat{\mathbf{y}} E_{y0} \cdot \cos(\omega t - k_y z + \varphi_y) \end{aligned} \tag{23}$$

In the equation, φ is a phase factor, that determines the position of wave maxima and minima relative to a set point. In Gaussian optics, the equations simplify due to assumptions about polarisation and homogeneity of propagation media.

2.2.2 Quantum theory of light

The approximation of light as a wave works well on the macroscopic scale, but it cannot fully explain all of the phenomena concerning light-matter interaction that have been observed [23, 24]. It has been shown that light also shows quantised behaviour, which supports the existence of the photon; a discrete package of light that lacks mass and electric charge and has a

spin of one. While photons are often referred to as particles, it is important to note that they are more accurately described as diffuse energy packets with some energy E, proportional to some frequency ω by a constant $\hbar = h/2\pi$. Here, h is Planck's constant, that has a value of around $h \approx 6.62607 \cdot 10^{-34}\text{m}^2\text{kg/s}$ [21]. Since the description of photons as discrete particles is problematic [23], they are sometimes referred to as *virtual photons*. The idea of virtual photons is to illustrate the interactions between charged particles and the electromagnetic field via harmonic oscillators, where each of these oscillators can be thought of as a photon. Using these harmonic oscillators, the entirety of the electromagnetic field can be expressed as an operator

$$\hat{\mathbf{E}}(\mathbf{r}, t) = \sum_k \mathbf{E}_k \hat{a}_k e^{-i\omega_k t} + \mathbf{E}_k^* \hat{a}_k^\dagger e^{i\omega_k t}. \tag{24}$$

In equation 24, $\hat{a}_k$ and $\hat{a}_k^\dagger$ are the annihilation and creation operators for field mode k.

An atom's dipole moment can be expressed in terms of the wavefunctions of states $|i\rangle$ and $|j\rangle$ as $e\langle j|\hat{\mathbf{r}}|i\rangle$, where $\hat{\mathbf{r}}$ is the position operator. This relation describes the overlap between the initial and the final state and gives a measure for the coupling strength between the atom and the electromagnetic field. This is an introduction to *stimulated emission*, which will be further investigated in the next subsection. [23]

2.2.3 Spontaneous and stimulated emission

To mathematically represent the interaction between light and matter, it is useful to use so called *Einstein coefficients*. For an introduction to Einstein coefficients, see appendix A.2. In the context of atomic transitions, there are three such coefficients of interest: the spontaneous emission coefficient A_{ij} describing the decay from an excited state $|i\rangle$ to a lower energy state $|j\rangle$, the stimulated emission coefficient B_{ij} and the absorption coefficient B_{ji}. These coefficients can be considered system-specific probabilities for transitions between different states.

Stimulated emission occurs when an atom in an excited state interacts with radiation, something that was expounded on in detail in subsection 2.1.1. The interaction Hamiltonian was then seen as a perturbation $\hat{H}' = e\mathbf{r} \cdot \mathbf{E}$, and using this Hamiltonian, the rate of the stimulated emission process P_{ij} from $|i\rangle$ to $|j\rangle$ can be found to be

$$\frac{dP_{ij}}{dt} = B_{ij}\rho(\omega)|\langle i|e\hat{\mathbf{r}} \cdot \mathbf{E}|\mathbf{j}\rangle|^2, \tag{25}$$

where $\rho(\omega)$ is the energy density of the incoming electromagnetic field at frequency ω. Note the similarity with equation 2.

Quantum mechanics predict fluctuations in the electromagnetic field at all frequencies, and when this field, often referred to as the *vacuum field*, couples to an atom, it can induce the atom to release a photon in an arbitrary direction. The rate of decay of a population of atoms in an excited state $|i\rangle$ to $|j\rangle$ is equal to the constant Einstein coefficient for spontaneous emission, A_{ij}. The rate does not depend on the external radiation, and instead is an intrinsic property of the atom and its current state [24, 25].

2.3 Light coupling with optical cavities

An optical cavity is a type of resonator, usually consisting of two mirrors between which light can be trapped. As light propagates back and forth through an optical cavity, it forms modes with specific resonance frequencies [26]. This can cause amplification of the light intensity. This is used in lasers. A common optical cavity is the *Fabry-Pérot cavity*, that consists of two plane-parallel mirrors [27]. Cavities can also be built from other types of lenses, for example concave and convex lenses. In any optical cavity, the field inside it should satisfy Maxwell's equations (18-21). In vacuum, the solution can be expressed as a travelling wave as found in equation 22. In a simple case. the electric field can be assumed to be

$$E(z,t) = Ae^{i(kz-\omega t)} + Be^{-i(kz-\omega t)}, \tag{26}$$

which represents a superposition of an incident and reflected wave, whose ratios are governed by the coefficients A and B. In a cavity with bounds at zero and some distance L, the electric field must satisfy the boundary conditions at these locations. For perfectly reflecting mirrors, the electric field must be zero at the two interfaces. This leads to *standing waves* in the cavity, where only certain frequencies of the light are found to satisfy the boundary conditions. These solutions are *modes* of the electric field, and can, in this simplified case, be found to be

$$E(z,t) = \mathrm{Re}\left[\sum_n E_n e^{i(k_n z-\omega_n t)}\right], \tag{27}$$

where E_n is the amplitude associated with the n^{th} resonant mode, $k_n = n\pi/L$ satisfies the boundary conditions of the cavity with length L for the n^{th} mode, and $\omega_n = cn\pi/L$ is the corresponding frequency.

During the stabilisation of a laser onto a cavity, one specific wavelength is needed. Therefore, the relevant modes will be close together in frequency domain. For frequencies so close to each other, the reflectivity and transmissivity of the two mirrors can be assumed to be independent of frequency within the range of interest. These constants are set to be r_1, r_2, t_1 and t_2. Each mirror is also characterised by some loss coefficient l_1 and l_2. Using these coefficients, the electric field after the first mirror as a result of incoming radiation E_0 becomes

$$E_{i,0} = t_1 E_0.$$

After one round trip, the field at the same spot is

$$E_{i,1} = t_1 E_0 r_1 r_2 e^{2ikL}.$$

Following the same logic, the electric field after N round trips becomes

$$E_{i,N} = t_1 E_0 (r_1 r_2)^N e^{2NikL}.$$

Assuming light keeps entering the cavity, the total electric field inside the optical cavity adds up to form a geometrical series,

$$E_i = t_1 E_0 \sum_{n=0}^{N} (r_1 r_2)^n e^{2nikL}, \tag{28}$$

which for a large number of round trips N can be approximated to

$$E_i \approx t_1 E_0 \sum_{n=0}^{\infty} (r_1 r_2)^n e^{2nikL} = \frac{t_1}{1 - r_1 r_2 e^{2ikL}} E_0. \tag{29}$$

The transmitted field can be found to be

$$E_t = \frac{t_1 t_2 e^{ikL}}{1 - r_1 r_2 e^{2ikL}} E_0. \tag{30}$$

The total losses of the cavity are given by $L_{\text{TOT}} = 2 - r_1^2 - r_2^2$, from which it is possible to find the *bounce number* b, which is defined as the number of times a photon travels back and forth through the cavity before the probability of it escaping the cavity is more than $1/e$. Mathematically, b is given by

$$b = \frac{1}{L_{\text{TOT}}}, \tag{31}$$

which corresponds to a larger number for better cavities. A related quantity is the *cavity decay time*, which is a frequency-independent property given by b/FSR. Here, the *free spectral range* (FSR) is introduced, which describes the spacing between fundamental modes for a cavity. It is defined as $c/2L$. In real cavities, the resonant frequencies are not perfect delta functions, spaced by the FSR. Instead, the cavity transfer function yields peaks with a finite *linewidth*. The linewidth is given by

$$\Delta f_{\text{FWHM}} = \frac{\text{FSR}}{\mathcal{F}}, \tag{32}$$

where $\mathcal{F}$ is the *finesse*, which is a property of cavities. The abbreviation FWHM is short for *full width at half maximum* and is commonly used during the characterisation of both beams and spectra. The finesse is determined by the quality of the mirrors and their alignment, and can for a pair of perfectly aligned mirrors be defined as

$$\mathcal{F} = \frac{\pi \sqrt{r_1 r_2}}{1 - r_1 r_2}, \tag{33}$$

where r_1 and r_2 are the reflectivities of the mirrors, that are set to be equal to $\sqrt{R}$ from here on. In the upcoming parts of the text, the coupling of a Gaussian beam with an optical cavity will be treated in further detail. In 2.3.4, there will also be an introduction to lasers, followed by a look at the electrooptical modulator in 2.3.5, and some more theory behind the experimental setup.

2.3.1 Propagation of Gaussian beams

When electromagnetic waves enter a waveguide or cavity, they can exhibit different behaviours. Different types of waves will act differently in the same type of media. Generally, waves are referred to as belonging to one of three classes: *transverse electromagnetic* (TEM), *transverse magnetic* (TM), or *transverse electric* (TE). TEM waves have no electric or magnetic field components in the direction of propagation, while TM and TE waves have longitudinal electric field components and magnetic field components, respectively [22].

In 2.2.1, the wave equation for light was presented as a solution to Maxwell's equations. Assuming that the electric field function can be separated into a time-dependent part and a part only dependent on position, the scalar wave equation $\tilde{E}(x,y,z)$ solves $\nabla^2\tilde{E}+k^2\tilde{E}=0$ for

$$\tilde{E}(x,y,z)=\tilde{u}(x,y,z)e^{-ikz}. \tag{34}$$

In fibres that only support the propagation of Gaussian modes, the light coming out at the end of the fibre can be assumed to be Gaussian as well. The $\tilde{u}$-function for a Gaussian wave propagating in $\hat{\mathbf{z}}$ is given by the expression found in 35 [27].

$$\tilde{u}(x,y,z)=\frac{1}{z-z_0}e^{-ik\frac{(x-x_0)^2+(y-y_0)^2}{2(z-z_0)}} \tag{35}$$

Here, x_0, y_0, z_0 are coordinates for the source of the wave, and x, y, z are the coordinates for the position of the observer. This function does not accurately describe a real physical beam, and to overcome this, a complex number can be introduced to the equation. The real value z_0 is replaced by a complex value equal to $z_0-\tilde{q}_0$. Equation 35 is now rewritten as

$$\begin{aligned}\tilde{u}(x,y,z)&=\frac{1}{z-z_0+\tilde{q}_0}e^{-ik\frac{(x-x_0)^2+(y-y_0)^2}{2(z-z_0+\tilde{q}_0)}}\\&=\frac{1}{\tilde{q}(z)}e^{-ik\frac{(x-x_0)^2+(y-y_0)^2}{2\tilde{q}(z)}}\end{aligned} \tag{36}$$

where $\tilde{q}(z)=z-z_0+\tilde{q}_0$ can be thought of as a complex radius of curvature of a spherical wave at point z. The function $\tilde{u}$ is sometimes referred to as the *spatial envelope* of the field, and in equation 36, the Gaussian shape is adjusted with a factor $\tilde{q}_0$, which allows for a better approximation of a beam with a space-dependent divergence. The value z_0 is also called the *beam waist*, and is defined as the point at which the beam is most tightly focused.

Assuming that waves come in Gaussian packages is useful, since the Gaussian solves Maxwell's equations while also taking the diverging behaviour real beams have into account. Many optical components are built to optimise transmission when the incoming beam is Gaussian and *circular*, which means that the cross section of the beam in the plane orthogonal to the propagation axis is a circle. Two common defects of laser beams are *ellipticity* and *astigmatism*. While a circular beam is circular, and elliptical beam can be thought of as being comprised of two beams whose waists are in the same place but that diverge at different speeds. In an astigmatic beam, the waist for the two beams can be at different positions in z and have different divergences.

Gaussian waves are treated further, then in combination with an optical cavity, in subsection 2.3.2.

When light propagates through a system of optical components, like mirrors, lenses, and even air, it experiences some change to its spatial distribution. Some optical components require an incoming beam of a certain size, and to know what the size of a beam is at a certain point, so called *ABCD-matrices*, can be used to determine the shape of a beam at any point in an optical setup. ABCD-matrices are 2×2 complex matrices, that take a position z and deflection angle θ as arguments, where z and θ are measured from a known and constant optical axis.

ABCD-matrices are useful when studying the propagation of Gaussian beams. To easily predict the behaviour of a Gaussian beam, it is common to define a complex beam parameter

$$q_{in} = z_{in} + iz_R \tag{37}$$

that results in an output parameter

$$q_{out} = \frac{Aq_{in} + B}{Cq_{in} + D}. \tag{38}$$

The real and complex components of q_{out} can be analysed to find the properties of the beam. This is relevant for evaluating the divergence and ellipticity of the beam, for example.

2.3.2 Resonant modes

To achieve resonance in an optical cavity, that is, to obtain the standing wave solutions of the system, the waves must reproduce themselves after every round trip between the mirrors of the cavity.

There are both longitudinal modes and transverse modes, whose intensity pattern across the cross section of the beam changes along the cavity. The resonant modes of a cavity are determined by the cavity's length and the properties of the mirrors at each side of the cavity.

In real cavities, Gaussian beam modes must reproduce both their phase and curvature at every round trip. For a cavity of length L with two mirrors having a radius of curvature equal to R_1 and R_2 respectively, stable resonant modes will only be achieved if the beam inside the cavity propagates in such a way that the beam converges. If the beam diverges more with every reflection between the mirrors, it will eventually propagate outside the cavity, which is undesirable. The *stability criterion* for an optical cavity is given by inequality 39 below [27].

$$0 \leq \left(1 - \frac{L}{R_1}\right)\left(1 - \frac{L}{R_2}\right) \leq 1 \tag{39}$$

From 39, it is possible to find the stability parameters g, also known as resonator g parameters, for each mirror, defined as $g = 1 - L/R$ [27].

For a two-mirror cavity, the resonance frequencies can be found to be

$$f_{qmn} = \mathrm{FSR}\left(q + \frac{m+n+1}{\pi}\arccos(\sqrt{g_1 g_2})\right), \tag{40}$$

where the FSR is the free spectral range defined as $c/2L$ [27]. The modes related to q are occasionally called *axial modes* whereas the mn-modes are referred to as *transverse modes*. The axial modes are spaced by the FSR while the transverse modes are spaced by $\mathrm{FSR}\cdot\arccos(\sqrt{g_1 g_2})/\pi$. The intensity of the transverse modes in a near-planar cavity decreases with higher order modes. This is because higher order modes extend further from the optical axis, generating higher losses for these modes. The modes for a modelled near planar cavity can be found in figure 3.6 in subsection 3.2.4.

2.3.3 Beam waist

A Gaussian beam can be focused to a spot size, but even if light is collected and collimated to a small, focused point, it will not be infinitely small. Instead, the cross section of this spot will have some diameter w_0. This w_0 is also known as the beam waist. To maximise transmission of light from an optical fibre to the optical cavity used for stabilisation of the laser frequency, the light from the laser should be collimated to have the same beam waist as the beam waist of the resonant modes of the cavity where the light beam enters the cavity.

Using the g-parameters, the *Rayleigh range* z_R can be found to be

$$z_R^2 = \frac{g_1 g_2 (1 - g_1 g_2)}{(g_1 + g_2 - 2 g_1 g_2)^2} L^2. \tag{41}$$

The beam waist, as well as the spot sizes w_1 and w_2 at the ends to the resonator, can be found in expression 42-44 below.

$$w_0^2 = \frac{L\lambda}{\pi} \sqrt{\frac{g_1 g_2 (1 - g_1 g_2)}{(g_1 + g_2 - 2 g_1 g_2)^2}} \tag{42}$$

$$w_1^2 = \frac{L\lambda}{\pi} \sqrt{\frac{g_2}{g_1 (1 - g_1 g_2)}} \tag{43}$$

$$w_2^2 = \frac{L\lambda}{\pi} \sqrt{\frac{g_1}{g_2 (1 - g_1 g_2)}} \tag{44}$$

2.3.4 An introduction to lasers

LASER stands for *Light Amplification by Stimulated Emission of Radiation*, but due to its prevalence in both research and industry, it is more commonly known as simply a laser. A typical laser emits coherent radiation at some frequency in the ultraviolet, visible, or infrared spectrum of light. Lasers use stimulated emission to produce a coherent beam. [27]

A laser consists of three essential components: a *laser medium*, *pumping process* and *optical feedback elements* [27]. The optical feedback elements are often referred to as a *laser cavity*. A simplified sketch of the laser can be found in figure is found in figure 2.2.

The laser medium contains an assortment of atoms or molecules that have electronic properties that are favourable for a specific experiment. Different materials have different electronic properties, which in turn will have an impact on the behaviour of the emitted light [28]. The laser medium can be a solid phase, like ruby, which largely consists of aluminium, chromium, and oxygen. It can also be a liquid dye or a gas, as is the case for He-Ne lasers.

The pumping process is some process that excites the atoms or molecules in the laser medium to a higher energy state. This process needs to supply energy to the system, which can be done by supplying light or charges. The goal of this process is to excite the medium so that more atoms are in a higher energy state than in a lower energy state. In other words, the gain of energy must be higher than losses in the cavity. When this happens, a so called *population inversion* is achieved. A population inversion, that is, when the number density of atoms in a higher energy state exceeds that of the atoms in a lower state, is necessary for the laser to function. A mathematical description of this state can be found in appendix A.6.1. [29, 30]

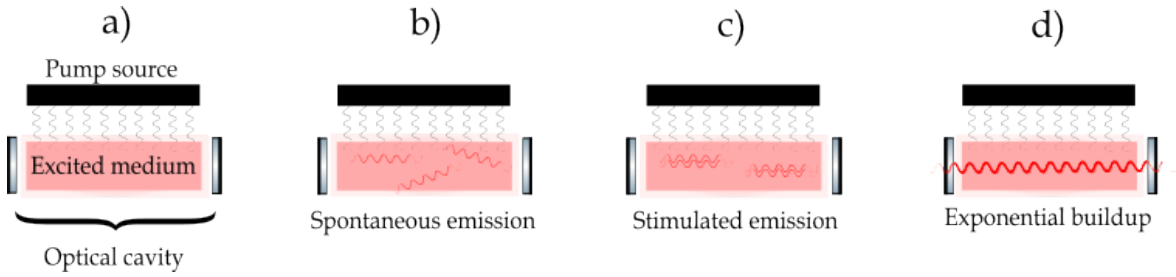

Figure 2.2: The underlying function of a laser. a) The laser consists of a laser medium in an optical cavity, or resonator, that is excited by a pump source. b) Spontaneous emission occurs in random directions. c) The light emitted along the axis of the cavity have a longer lifetime in the cavity and a higher probability of causing stimulated emission. d) The laser builds up exponentially due to stimulated emission, and the leakage field escaping the laser is eventually large enough to be of use as a coherent, in-phase beam.

The laser medium is located inside a cavity, in which the emitted light circulates and amplifies throughout the medium. Meanwhile, the medium is continuously pumped, which means that eventually, the losses of photons will be equal to the gain of photons. The spontaneous emission occurs in a random direction, and eventually, there will be a photon propagating orthogonally to the mirror surfaces of the cavity. Unless a photon propagates perpendicular to the mirrors of the optical cavity, it will propagate outside the bounds of the cavity, and that light will be lost. Only the photons travelling parallel to the optical axis will continue to propagate back and forth, and continue to cause stimulated emission. Since each case of stimulated emission results in double the number of photons with the same phase, the increase of coherent radiation is exponential.[30]

The amount of light builds up and a fraction of it is emitted outside the cavity as laser light. The cavity also serves to preserve some longitudinal and transverse optical modes. Which modes are preserved depend on the length of the cavity and the laser medium. Only wavelengths that achieve constructive interference as they pass from mirror to mirror will be preserved. The resonance criterion is often simplified as

$$n\lambda = 2L, \tag{45}$$

where n is an integer, λ is the wavelength of light in the medium, and L is the length of the cavity. However, more complex systems also include effects stemming from imperfections in physical systems.

This ensures that even if the laser medium can emit radiation of different wavelengths, only one of those wavelengths is preserved.

2.3.5 Electrooptic modulator

An *electrooptic modulator* (EOM) is an optical component whose refractive index changes in response to an applied external electric field, in something called the *Pockels effect*. When the refractive index in the EOM changes, the light inside it will propagate at a different speed, causing a net phase shift. This can be used to change, that is, modulate, the amplitude, frequency, or polarisation of light.

The Pockels effect is a phenomenon some crystals exhibit in the presence of an electric fiels, in which the refractive index changes. Refractive index is tied to the crystal's polarisability **P**,

which is related to **E** by equation 46, where $\overline{\overline{\chi}}$ is the electric susceptibility tensor.

$$\mathbf{P} = \varepsilon_0 \overline{\overline{\chi}} \mathbf{E} \tag{46}$$

The refractive index in an isotropic medium is related to the electric susceptibility by $n^2 = 1+\chi$. When an electric field is applied to a non-centrosymmetric crystal, there can be microscopic ionic displacements or distortions or shifts in the electron density inside the material. Since crystals have periodic structure, a *lattice*, the effects accumulate and form a cohesive change to the material in a predictable way. This makes it possible to calculate the change in refractive index for a specific material.

The change in refractive index in an EOM based on a trigonal crystal with 3m symmetry can be found in equation 47, in which n is the refractive index of the crystal, r is the electro-optic coefficient specific to the material, and $E = |\mathbf{E}|$, where **E** is the applied electric field.

$$\Delta n = -\frac{1}{2} n^3 r E \tag{47}$$

By applying a voltage V across a crystal axis of length d, the refractive index is changed, causing a phase shift $\Delta\phi$ that can be found in equation 48.

$$\begin{aligned} \Delta\phi &= \frac{2\pi L}{\lambda}\Delta n \\ &= \frac{2\pi L}{\lambda}\left(-\frac{1}{2} n^3 r \frac{V(t)}{d}\right) \\ &= -\frac{\pi n^3 r L}{\lambda d} V_0 \cos\omega_m t \end{aligned} \tag{48}$$

In equation 48, L is the length of the crystal along the axis of propagation and λ is the wavelength of light. A sinusoidal voltage $V(t) = V_0\cos(\omega_0 t)$ can also be expressed as a sine wave, with its point of origin shifted by $\pi/2$ radians.

2.3.6 The Pound-Drever-Hall technique

The Pound-Drever-Hall (PDH) technique is a way of stabilising laser frequencies. In this technique, a laser is locked onto an optical cavity, traditionally a Fabry-Pérot cavity, in which the light is allowed to propagate back and forth. In short, it can be said that the output signal from the Fabry-Pérot cavity is detected and fed back to the laser, modulating the laser frequency in turn [31, 32]. The basic layout for an experiment using the PDH method can be found in figure 2.3.

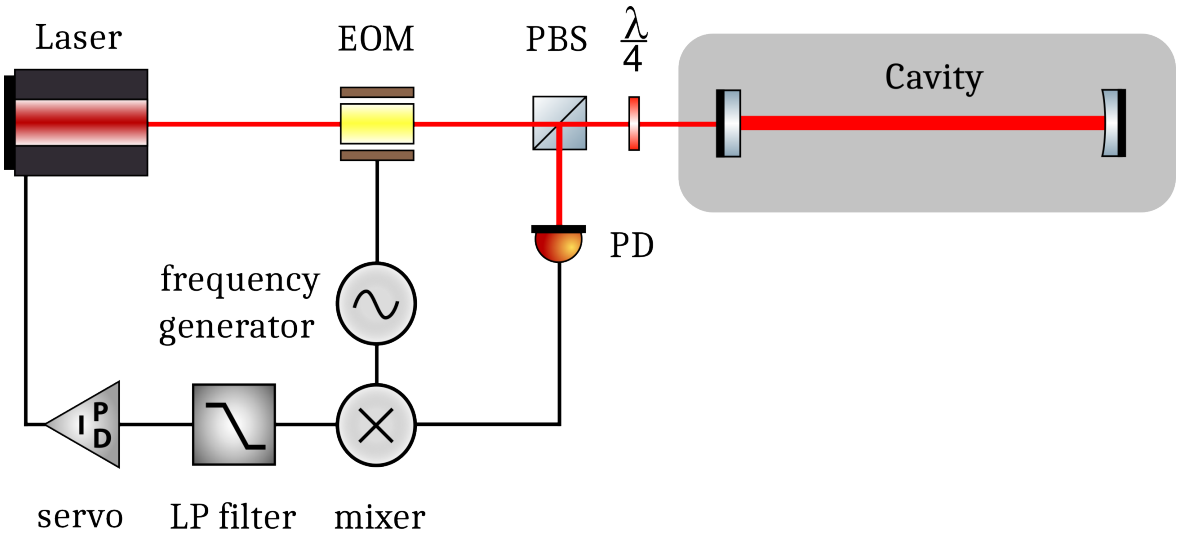

Figure 2.3: A basic PDH setup for laser stabilisation. The light is modulated in the EOM and enters the optical cavity, where it forms stable modes. The signal coming out of the optical cavity is reflected into a photodetector. The signal from the photodetector is mixed with the frequency used to modulate the EOM. The mixed signal is fed through a PID servo before it controls the laser frequency. In a lab situation, more components would typically be used.

The path of the light, as well as the function of the different components of the PDH setup, can be expressed and understood using physical formulae for the shape of the light. To understand what happens in the cavity, the electric field can be studied just outside the cavity. The incident electric field E_{in}, that enters the cavity, can be written as

$$E_{in} = E_0 e^{i\omega t}, \tag{49}$$

while the electric field that is reflected and measured at the same point as E_{in} can be set to $E_r = E_1 e^{i\omega t}$. It is important to note that both E_0 and E_1 are complex, which ensures that phase shifts are accounted for. Using this, the reflection coefficient as a function of frequency, $F(\omega)$, can be defined as the ratio of E_r and E_{in}.

$$F(\omega) = \frac{E_r}{E_{in}} = \frac{r(e^{i\omega/\Delta f} - 1)}{1 - r^2 e^{i\omega/\Delta f}} \tag{50}$$

Equation 50 describes $F(\omega)$ for a symmetric cavity without losses, in which r is the amplitude reflection coefficient of the mirrors, and $\Delta f = c/2L$. The detected electric field coming from the cavity is not just comprised of the immediately reflected electric field, but also of a so called *leakage beam*, which is light that escapes the standing wave inside of the cavity. This is the interesting part of the field. When the light approaches resonance, the intensity of these two components of the electric field is almost identical. They can still be told apart due to their difference in phase. When the frequency approaches resonance, the leakage beam is exactly 180°out of phase with the reflected beam, which causes destructive interference, resulting in a global minimum of detected incoming light. This makes sure that the resonance frequency can be known. However, as the frequency of the laser naturally shifts about the resonance frequency it isn't possible to tell from the reflected signal alone if the laser is above or below the resonance frequency, which makes it difficult to adjust the laser frequency in the right

direction. To account for this, the incoming light is modulated so that sidebands with a known phase relation to the resonance frequency are created.

These sidebands are made by applying a sinusoidal voltage over the EOM in the experiment, as seen in figure 2.3, it is possible to achieve a predictable and periodic variation in phase shift. The phase modulated incoming electric field in expression 49 is therefore updated to the expression found in 51. By applying the Jacobi-Anger rule for Bessel functions to the exponential of the sine and omitting higher order ns, it's possible to find expression 53. Alternately, a similar expression can be found in 54 through using a small-angle approximation. This results in *sidebands* at $\omega \pm \omega_m$ [31].

$$E_{in} = E_0 e^{i(\omega t + \beta \sin \omega_m t)} \tag{51}$$

$$= E_0 e^{i\omega t} \sum_{n=-\infty}^{\infty} J_n(\beta) e^{in\omega_m} \tag{52}$$

$$\approx E_0 \left[J_0(\beta) + J_1(\beta) e^{i\omega_m t} - J_1(\beta) e^{-i\omega_m t} \right] e^{i\omega t} \tag{53}$$

$$\approx E_0 \left[1 \quad + \quad \frac{\beta}{2} e^{i\omega_m t} \quad - \quad \frac{\beta}{2} e^{-i\omega_m t} \right] e^{i\omega t} \tag{54}$$

Here, β is the *modulation depth*, a measure of how much the signal is modulated. It can now be found that the incoming field to the cavity after passing through the EOM is in fact no longer monochromatic, but rather characterised by a carrier frequency ω and several other fields of decreasing intensity for higher values of n at frequencies $\omega \pm n\omega_m$.

The power P_0 of the reflected wave can now be found to be a sum of the power from the reflected carrier frequency and the sidebands. It holds that $P_0 \approx P_c + 2P_s$, where P_c and P_s are given by the expressions below.

$$P_c = J_0^2(\beta) P_0 \tag{55}$$

$$P_s = J_1^2(\beta) P_0 \tag{56}$$

Considering now the reflection coefficient function $F(\omega)$, the reflected power can be found to be $P_0 |F(\omega)|^2$, which varies over time as

$$P_{\text{ref}}(\omega + \omega_m \beta \cos \omega_m t) \approx P_{\text{ref}}(\omega) + P_0 \frac{d|F(\omega)|^2}{d\omega} \omega_m \beta \cos \omega_m t. \tag{57}$$

When the signal from the reflected light is mixed with the modulation frequency ω_m, all terms from the signal that do not vary as $\cos \omega_m t$ will be filtered out, and the error signal will be

$$\epsilon = P_0 \frac{d|F(\omega)|^2}{d\omega} \omega_m \beta \approx 2\sqrt{P_c P_s} \frac{d|F(\omega)|^2}{d\omega} \omega_m. \tag{58}$$

The error signal given by equation 58 can be plotted for $F(\omega)$ as given in equation 50. When the modulation frequency fulfils $\omega_m \gg \text{FSR}/\mathcal{F}$, the error signal becomes purely imaginary, and can instead be found to be

$$\epsilon = -P_0\beta \,\mathrm{Im}\left[F(\omega)F^*(\omega+\Omega) - F^*(\omega)F(\omega-\Omega)\right] \tag{59}$$

if it is assumed that $P_0\beta = 2\sqrt{P_c P_s}$. Graphs simulating the reflected signal and the error signal for the cavity in this experiment can be found in 3.10, with additional notes in appendix B.3.

2.3.7 Other laser frequency locking techniques

The lasers used for the experiment are tunable, which increases the chances of tuning the frequency of the laser to a value closer to the target transition than for a laser which isn't tunable. However, a tunable laser requires a reference of some sort to operate at the desired frequency and not drift across a range of frequencies. The optical resonator, often in the form of a cavity, offers a reliable way to stabilise a laser. A cavity can support several wavelengths of radiation, and a property of cavities is that these resonance frequencies, that are an intrinsic property of it, are uniformly distributed across the radiation spectrum [33]. In this experiment, PDH locking is used to reference the laser frequency to the stable cavity, but there are other frequency locking techniques that use cavities. The most famous after PDH-locking is likely Hänsch-Couillaud (HC) locking. Instead of looking at phase differences, HC locking studies the frequency-dependent polarisation changes in the reflected light. It doesn't require modulation via an EOM and it has a wide *capture range*, that is, the maximum frequency deviation from the cavity resonance frequency where the error signal is effective for stabilising the laser frequency is large. The largest advantage of HC locking is the simplicity of the setup, as it does not require RF modulation or any of the drivers needed to drive the EOM [34]. However, PDH locking is more sensitive and generally produces less noise.

2.4 Laser cooling

Laser cooling is, as expected from the name, the technique of using laser light to cool down atoms, particles, or other small objects. It reduces the motional degrees of freedom of its target through momentum transfer by photons. Understanding laser cooling from the foundations is largely dependent on understanding lasers, which was introduced in subsection 2.3.4. Below, the principles of laser cooling are described in detail, with a focus on *Doppler cooling* in subsection 2.4.1 and *optical molasses* in subsection 2.4.2. Finally, the *magneto-optical trap* (MOT), which is necessary to achieve laser cooling in a controlled environment, is introduced.

2.4.1 Radiation pressure and Doppler cooling

The idea that light has momentum and can exert a force on matter might not be obvious; after all, photons have no mass. However, light has energy, and the momentum of a photon is characterised by its energy divided by its speed. The force light exerts on an area of matter is often called *radiation pressure*.[20]

Radiation pressure is a measure of the force light can have on matter. Radiation with intensity I exerts a force $F_{\mathrm{rad}} = d\vec{p}_{\mathrm{rad}}/dt$ on an area A according to equation 60, where c is the speed of light [1].

$$F_{\mathrm{rad}} = \frac{d\vec{p}_{\mathrm{rad}}}{dt} = \frac{IA}{c} \tag{60}$$

The force F_{rad} will be imparted onto an ensemble of atoms with a certain probability. To account for this, the area A found in equation 60 can be exchanged with an absorption cross section $\sigma_{\text{abs}}(\omega)$ that depends on the frequency of the incoming wave. While the expression $F = \sigma_{\text{abs}} I/c$ can be used to describe the force exerted on a particle, the force can also be expressed in terms of photons. When an atom absorbs a photon and releases it due to spontaneous emission, the photon will be given a new direction. This can be seen as a scattering process, and it is common to express the force as a scattering force equal to the photon momentum times the scattering rate. This expression becomes

$$F_{\text{scattering}} = \hbar \frac{\omega}{c} R_{\text{scattering}}. \tag{61}$$

The constant R describes the scattering rate, and is equal to

$$R_{\text{scattering}} = \frac{\Gamma}{2} \frac{\Omega_R^2/2}{\delta^2 + \Omega_R^2/2 + \Gamma^2/4}, \tag{62}$$

where Γ can be seen as a damping coefficient, Ω_R is the Rabi frequency as defined in equation 16, and $\delta = \omega_L - \omega_A$ is the detuning of the laser's frequency from the atomic resonance frequency. A relevant description of the scattering force is also given in terms of intensity. The Rabi frequency is related to the intensity by

$$\frac{I}{I_{\text{sat}}} = 2\frac{\Omega_R^2}{\Gamma^2}, \tag{63}$$

where I_{sat} is the *saturation intensity*, which in turn is given by

$$I_{\text{sat}} = \frac{\pi}{3} \frac{hc}{\lambda^3 \tau}, \tag{64}$$

where $\tau = 1/\Gamma$ is the *lifetime for radiative broadening*, and is a system-specific value because of the dependency on the constant Γ. Inserting equation 63 into equation 62 yields the full expression for F

$$F_{\text{scattering}} = \hbar \frac{\omega}{c} \frac{\Gamma}{2} \frac{I/I_{\text{sat}}}{1 + I/I_{\text{sat}} + 4\delta^2/\Gamma^2}. \tag{65}$$

The maximum acceleration for an atom with mass M therefore becomes

$$a_{\text{max}} = \frac{F_{\text{scattering, } I\to\infty}}{M} = \frac{\hbar\omega}{c} \frac{\Gamma}{2M}. \tag{66}$$

The acceleration can also be related to the lifetime τ of the excited atomic state by the *recoil velocity* v_r as

$$a_{\text{max}} = \frac{v_r}{2\tau}. \tag{67}$$

The recoil velocity can be thought of as a change to the atom's velocity when it interacts with a photon with some specific frequency.

Now consider that when an atom moves in relation to a light source, it will experience the frequency of the beam as being higher than it actually is if it moves against it, and lower than the actual frequency is if it moves away from the source. This is the *Doppler effect. Doppler cooling* is the most common laser cooling technique, and utilises the Doppler effect to manifest preferential absorption of radiation in certain directions, which ensures the movement of the laser cooled matter can be controlled. In this setup, the laser's frequency ω_L is slightly lower than a transition frequency for the atom, ω_A. This means that for atoms at rest, excitation does not occur. However, when the atom moves towards the light, the atom experiences a blue-shift towards its electron transition, and absorbs the photon.[35, 36]

As the atoms absorb light, they will successively slow down. This means that the relative frequency between the atom and the slowing beam will decrease with time. To account for the change in relative frequency, it is customary to sweep the slowing beam over a range of frequencies in a short timespan, taking the Doppler effect into account. This sweep process is often referred to as *chirp cooling*.

While the atoms leaving the oven are cooled in one direction by the initial slowing beam, they have movement in all three dimensions, which means they must be cooled in all three dimensions to reduce their temperature. This is the idea behind the next subsection: *optical molasses*.

2.4.2 Optical molasses

When two lasers of the same frequency ω_L are applied from opposite directions, the atom will come to a rest between them, since the atom will absorb preferentially from the laser it is moving towards due to the Doppler effect. When pairs of lasers are applied this way in three directions, a trap is created for an atom. This technique has been named *optical molasses*, and although it can slow atoms down considerably, it requires the atoms to be relatively slow to ensure their enclosure by the three sets of lasers. Therefore, it is common practice to precool an atom beam by a counter-propagating beam before subjecting the atoms to three-dimensional laser cooling, as was described in the previous subsection [37].

In optical molasses, pairs of lasers are used to confine the movement of atom gases. An atom moving with velocity v along a laser pair axis, trapped between two laser beams with frequency ω_L is subjected to a total force

$$\begin{aligned} F_{\text{molasses}} &= F_{\text{scattering}}(\omega_L - \omega_A - \omega v/c) - F_{\text{scattering}}(\omega_L - \omega_A + \omega v/c) \\ &\approx \left(F_{\text{scattering}}(\omega_L - \omega_A) - \frac{\omega v}{c}\frac{\partial F}{\partial \omega}\right) - \left(F_{\text{scattering}}(\omega_L - \omega_A) + \frac{\omega v}{c}\frac{\partial F}{\partial \omega}\right) \\ &\approx -2\frac{\partial F}{\partial \omega}\frac{\omega v}{c}. \end{aligned} \tag{68}$$

This holds approximately true for low velocities for the laser cooled particles, such that $\omega v/c \ll \Gamma$. This force acts upon the particles in a manner not unlike forces associated with damping. As can be seen from the final expression in 68, the force is dependent on the velocity of the particle, and through differentiation of equation 65, the damping coefficient $\alpha = 2\omega/c \cdot \partial F/\partial \omega$ can be found to be

$$\alpha = 2\frac{\omega}{c}\frac{\partial F}{\partial \omega} = 4\hbar\left(\frac{\omega}{c}\right)^2 \frac{I}{I_{\text{sat}}}\frac{-2\delta/\Gamma}{\left(1+(2\delta/\Gamma)^2\right)^2} \tag{69}$$

$$= 2\hbar\left(\frac{\omega}{c}\right)^2 \frac{\partial R_{\text{scattering}}}{\partial \omega} = 2\hbar\left(\frac{\omega}{c}\right)^2 \frac{-2\delta}{\delta^2+\Gamma^2/4} R_{\text{scattering}} \tag{70}$$

where $I/I_{\text{sat}} \ll 1$ has been neglected from the denominator. Assuming now that cooling occurs in all three dimensions, it follows that the kinetic energy $E_T = \frac{1}{2}M(v_x^2 + v_y^2 + v_z^2)$ decreases in time as $-2\alpha E_T/M$ because

$$\begin{aligned}\frac{d}{dt}\left(\frac{1}{2}M\vec{v}^2\right) &= \frac{1}{2}M\frac{d}{dt}\vec{v}^2 = M\vec{v}\frac{d\vec{v}}{dt} \\ &= \vec{v}F_{\text{molasses}} \\ &= -\alpha\vec{v}^2,\end{aligned} \tag{71}$$

where $\vec{v}^2 = \vec{v}\cdot\vec{v} = v_x^2 + v_y^2 + v_z^2$.

In theory, the lowest attainable temperature for optical molasses is given by the *Doppler limit*. This is found through considering that during emission, the atom receives a kick in an arbitrary direction, causing it to move around in a random walk in three dimensions. By the *equipartition theorem*, kinetic energy and temperature is related by

$$\frac{1}{2}M\langle v^2\rangle = \frac{1}{2}k_B T, \tag{72}$$

where the mean square velocity spread $\langle v^2\rangle$ in an optical molasses is given by

$$\langle v^2\rangle = -\frac{\hbar^2\Gamma}{M}\frac{\omega^2}{c^2}\frac{I}{I_{\text{sat}}}\frac{1}{\alpha}\frac{1}{1+2\delta/\Gamma}. \tag{73}$$

When α from equation 70 is inserted into equation 73, the relationship between velocity and temperature can be derived to be

$$\begin{aligned}k_B T &= M\langle v^2\rangle \\ &= -\hbar^2\Gamma\frac{\omega^2}{c^2}\frac{I}{I_{\text{sat}}}\frac{1}{1+2\delta/\Gamma}\left(4\hbar\left(\frac{\omega}{c}\right)^2\frac{I}{I_{\text{sat}}}\frac{-2\delta/\Gamma}{\left(1+(2\delta/\Gamma)^2\right)^2}\right)^{-1} \\ &= \frac{\hbar}{2}\frac{\Gamma^2/4+\delta^2}{\delta}.\end{aligned} \tag{74}$$

A minimum is observed when $\delta = \omega - \omega_A = \Gamma/2$, which causes equation 74 to simplify to

$$k_B T_D = \frac{\hbar\Gamma}{2} \tag{75}$$

where T_D is the previously mentioned *Doppler limit*. A curious thing is that in laser cooling experiments, the detected temperature in the chamber could on multiple occasions be detected to be far below the Doppler limit. This cooling mechanism is related to something other than the scattering forces. This will be further discussed in subsection 2.4.5, after a brief introduction to some underlying theory about the *Zeeman effect*.

2.4.3 The Zeeman effect

Charges in motion are affected by magnetic fields. When a magnetic field is applied over an atom, the electrons are affected, which leads to a shift in the atom's energy levels. This effect is also known as the *Zeeman effect*. [1]

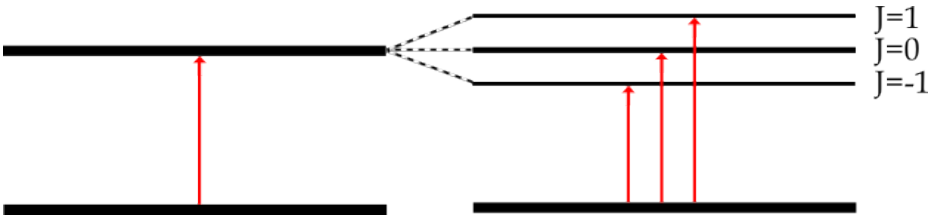

Figure 2.4: Zeeman splitting of atomic sub-levels. When the atom is perturbed by a magnetic field, it slightly shifts the resonances of the atom.

The Zeeman effect can be observed when atomic spectra are measured in the presence of an external magnetic field. To formalise the concept, an atom is considered as a harmonic oscillator in the presence of the magnetic field. The restoring force on an electron is the same for displacements in all directions, and the oscillator can be assumed to have the same resonant frequency ω_0 in all spatial directions in the absence of a magnetic field. When the field $\mathbf{B}$ is applied, the equation of motion for an electron with charge $-e$ and position $\mathbf{r}$ is

$$m_e \frac{d\dot{\mathbf{r}}}{dt} = -m_e\omega_0^2\mathbf{r} - e\dot{\mathbf{r}} \times \mathbf{B}. \tag{76}$$

If $\mathbf{B}$ is applied along one axis, e.g. $\mathbf{B} = B\hat{\mathbf{z}}$, where $\hat{\mathbf{z}}$ is the unit vector on one of three orthogonal axes in three dimensional space, equation 76 reduces to the expression seen in 77.

$$\begin{aligned} m_e\ddot{\mathbf{r}} &= -m_e\omega_0^2\mathbf{r} - eB\dot{\mathbf{r}} \times \hat{\mathbf{z}} \\ \implies \quad \ddot{\mathbf{r}} + \frac{eB}{m_e}\dot{\mathbf{r}} \times \hat{\mathbf{z}} + \omega_0^2\mathbf{r} &= 0 \end{aligned} \tag{77}$$

From equation 77, it is reasonable to define the *Larmor frequency* $\Omega_L = eB/2m_e$, that is often used when the motion of particles in electromagnetic fields is studied. If $\mathbf{r}$ is set to be

$$\mathbf{r} = \mathrm{Re}\left(\begin{bmatrix} x \\ y \\ z \end{bmatrix} \exp(-i\omega t) \right), \tag{78}$$

then equation 77 can be written in matrix form as

$$\begin{bmatrix} \omega_0^2 & -2i\omega\Omega_L & 0 \\ 2i\omega\Omega_L & \omega_0^2 & 0 \\ 0 & 0 & \omega_0^2 \end{bmatrix} \begin{bmatrix} x \\ y \\ z \end{bmatrix} = \omega^2 \begin{bmatrix} x \\ y \\ z \end{bmatrix}. \tag{79}$$

The eigenvalues ω^2 can be found to satisfy

$$\left(\omega^4 - (2\omega_0^2 + 4\Omega_L^2)\omega^2 + \omega_0^4\right)(\omega^2 - \omega_0^2) = 0. \tag{80}$$

It is evident that $\omega = \omega_0$ is a solution. For optical transitions, $\Omega_L \ll \omega_0$, which means that it is possible to define an interval about the resonance frequency with frequencies that are close to the resonance frequency, located at $\omega = \omega_0 \pm \Omega_L$. This results in the three eigenvectors seen in 81.

$$\begin{aligned}
\mathbf{r}_- &= \begin{bmatrix} \cos(\omega_0 - \Omega_L)t \\ -\sin(\omega_0 - \Omega_L)t \\ 0 \end{bmatrix} \\
\mathbf{r}_0 &= \begin{bmatrix} 0 \\ 0 \\ \cos(\omega_0 t) \end{bmatrix} \\
\mathbf{r}_+ &= \begin{bmatrix} \cos(\omega_0 + \Omega_L)t \\ \sin(\omega_0 + \Omega_L)t \\ 0 \end{bmatrix}
\end{aligned} \tag{81}$$

From 81, it can be seen that a magnetic field applied along $\hat{\mathbf{z}}$ does not affect the motion of an electron along that particular axis, but that an effect from it can be seen in the xy-plane about the resonance frequency. This effect causes circular motion in the plane, with frequencies shifted up or down from the resonance frequency by the Larmor frequency. This can be observed as a splitting of the oscillation into three separate oscillations, which can be detected during measurements.

2.4.4 Magneto-optical traps

A magneto-optical trap (MOT) is a device that uses both magnetic fields and radiation fields to trap atoms. It typically consists of first an optical molasses where the lasers in each laser pair have opposite handedness, and second, a pair of identical coils through which current of opposite direction runs. This type of setup is called *anti-Helmholtz coils*, and at the centre of the coils, the magnetic field is zero. The centre overlaps the centre of the beams. Together, the forces from the optical molasses and the magnetic field can trap atoms in larger numbers than a molasses can on its own.

In the previous section, the Zeeman effect was introduced as a phenomenon which shifts the energy levels of an atom. The Zeeman displacement of a sublevel n in an atom with the magnetic moment μ is given by $n\mu B$ for some magnetic field with amplitude B at the atom's location. When the magnetic field is applied to atoms, the atoms will experience a shift in their resonance frequencies, as was described in section 2.4.3. This means that equation 68 can be rewritten while taking the Zeeman effect into account.

$$\begin{aligned}
F_{\text{MOT}} &= F^{\sigma+}_{\text{scattering}}(\omega_L - (\omega_A + \beta z) - \omega_L v/c) - F^{\sigma-}_{\text{scattering}}(\omega_L - (\omega_A - \beta z) + \omega_L v/c) \\
&\approx -2\frac{\partial F}{\partial \omega}\frac{\omega v}{c} + 2\frac{\partial F}{\partial \omega_A}\beta z \\
&= -2\frac{\partial F}{\partial \omega}\left(\frac{\omega_L v}{c} + \beta z\right) \\
&= -\alpha v - \frac{\alpha\beta c}{\omega_L} z
\end{aligned} \tag{82}$$

Here, an atom is assumed to have a resonance at $\omega_A \pm \beta z$ for the $\Delta M_J = \pm 1$ transition at position z. The constant β is to be regarded as a relation between distance and frequency and has

units $s^{-1}m^{-1}$.

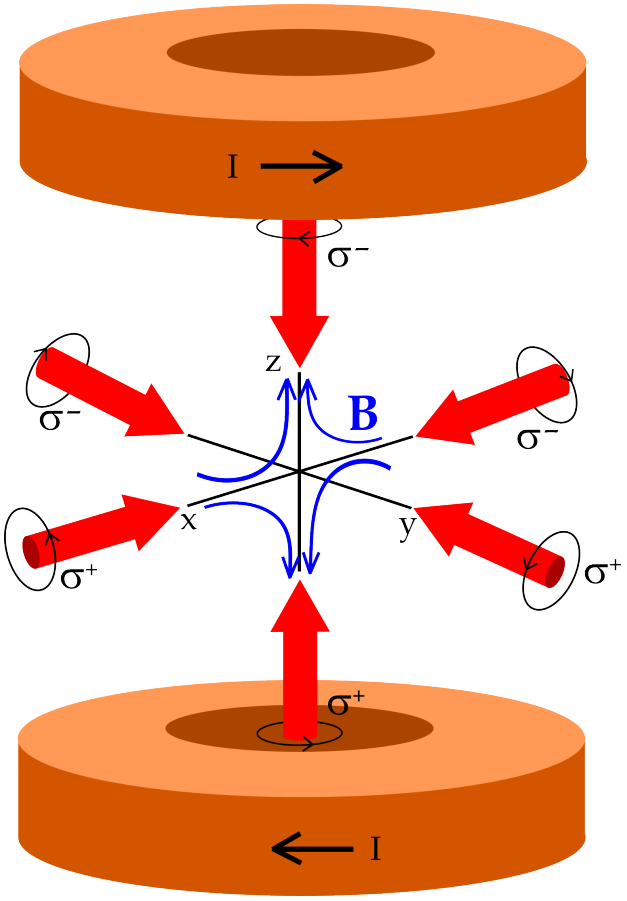

Figure 2.5: A magneto-optical trap (MOT) typically consists of an optical molasses and a pair of anti-Helmholtz coils - two identical coils with current running in opposite directions to each other. The resulting magnetic field is zero at the centre of the trap, and linear close to zero. The magnetic gradient exerts a position-dependent force on the atoms trapped by the optical molasses that pushes the atoms towards the centre of the trap. Each laser pair consists of one laser with circularly polarised light with a right-handed polarisation, and one with a left-handed polarisation. The σ^+ light is sometimes referred to as the light that excites the σ^+-transitions, which correspond to the $\Delta M_J = +1$ state; the σ^- light follows the same conventions.

2.4.5 Sub-Doppler cooling and the Sisyphus effect

In a MOT, the atoms move in standing waves produced by the three pairs of lasers. The polarisation of two lasers forming a pair is set to be orthogonal in such a way that they have opposite handedness if they are circularly polarised or have linear polarisations in $\hat{\mathbf{x}}$ and $\hat{\mathbf{y}}$ respectively. Consider the case where the light is linearly polarised along $\hat{\mathbf{x}}$ and $\hat{\mathbf{y}}$. The resulting polarisation then depends on the phase difference between the two waves and varies with position along the beam axis.

Consider an atom with ground state angular momentum of $J = 1/2$ with two Zeeman sublevels $|j = \frac{1}{2}, m = +\frac{1}{2}\rangle$ and $|j = \frac{1}{2}, m = -\frac{1}{2}\rangle$. The atom's excited state has angular momentum $J' = 3/2$ with its own Zeeman sublevels. The allowed electric dipole transitions follow from table 1, where it is found that $\Delta m = 0, \pm 1$. The spatially dependent polarisation corresponds to different values of Δm such that $\Delta m = +1 \rightarrow \sigma^+$, $\Delta m = -1 \rightarrow \sigma^-$, and $\Delta m = 0 \rightarrow \pi$ (linear). In previous sections, the light-induced perturbation to the atom's Hamiltonian was introduced

along with the Rabi frequencies, that vary with position. Since the polarisation changes along the beam axes, the coupling strength to different Δm-transitions also vary spatially. The *optical potential* for the atom is given by the *AC Stark shift*

$$U_m(z) = \hbar \frac{|\Omega_R(\omega, z)|^2}{4\delta} \tag{83}$$

where $U_m(z)$ is the spatially dependent optical potential for sublevel m. Since the Rabi frequency depends on polarisation, which depends on z, the potential for the two sublevels is not equal. An atom in $|j = \frac{1}{2}, m = +\frac{1}{2}\rangle$ experiences a force $F(z) = -dU_{+1/2}(z)/dz$, which means that as the atom moves, it will experience a periodic force and climb potential hills, which decreases the kinetic energy of the atom as it is converted into potential energy. At positions where the atom is near to the top of its potential, it couples strongly to light, and scattering is maximised. The atom is excited from $|j = \frac{1}{2}, m = +\frac{1}{2}\rangle$ to $|j = \frac{3}{2}\rangle$, but when it returns to the ground state, it will go to $|j = \frac{1}{2}, m = -\frac{1}{2}\rangle$, which has less energy than the initial state. The energy difference between the two levels is lost as light and decreases the total kinetic energy of the atom.

3 Method

This section describes the experimental setup designed and implemented during the thesis. It starts with an overview of the experimental setup in section 3.1, followed by details about the laser systems, the EOMs, and the optical cavity in section 3.2.1. In 3.2.5, a succinct guide to aligning lasers onto an optical cavity can be found.

3.1 Experimental overview

The idea for the experiment is to generate gaseous strontium through heating the substance in an oven. Then, the atoms will pass through a Zeeman slower for first stage cooling, whereupon they will go into a magneto-optical trap (MOT) for confinement and coupling to small resonators.

An optical cavity is used as a reference to keep the lasers used in the experiment stable. This text focuses on the stabilisation of the two repump lasers at 679 and 707 nm.

3.1.1 The role of the repump lasers

When a ^{88}Sr beam is cooled, the atoms can fall into finer states that are not affected by the main cooling beam at 461 nm. For ^{88}Sr these states are the $^3P_2$ and $^3P_0$ states, both of which have a long lifetime (see figure 2.1). If many atoms are trapped in these states, less useable atoms will enter the science chamber. Therefore, the atoms are excited to the $^3S_1$ state, from where they can go to the $^3P_1$ state that strongly decays to the $^1S_0$ ground state, from where the atoms can be affected by the 461 nm cooling beam.

3.1.2 Experimental setup

The optical setups for the 707 nm and 679 nm lasers (DL pro series, Toptica) can be found in figure 3.1. The two experiments are nearly identical. The laser light passes through a half waveplate (quartz with AR/AR at 707 or 679 nm, Eksma Optics). The role of this waveplate is to control how much light enters the cavity and how much goes to the science chamber. The light diffracts in a polarising beam splitter (PBS202, Thorlabs) where the horizontally polarised light travels towards the science chamber to act as repump lasers, while the vertically polarised light travels towards the cavity. The light passes through two convex lenses (N-BK7, B-coated, Thorlabs), of which the first has a focal length of 100 mm and the second has a focal length of 30 mm for the 707 nm laser. They are spaced approximately 140 mm apart to achieve a collimated beam. For the 679 nm laser, the first lens has a focal length of 200 mm and the second has a focal length of 30 mm. They are spaced 233 mm apart. The fine tuning of the distance between the lenses is done through minimising the size of the laser spot at a point approximately 2.5 m from the first lens. The light enters an EOM (TWP2M2-NIR+W, Qubig) and the EOM is angled to maximise transmission. The light is then coupled into FC/APC polarising-maintaining single-mode (PMSM) fibre from SQS Vláknová Optika using two mirrors (BB1-E02, B-coating, Thorlabs) on kinematic Polaris mounts. The collimator (60FC-SF-4-A7.5-01,Schäfter+Kirchoff) has adjustable collimation and coupling is maximised to around 65% for the 707 nm laser and 45% for the 679 nm laser at the time of writing.

On the other side of the fibre, the light exits through a different collimator with fixed collimation (F240APC-B, Thorlabs). The beam waist of the exiting beam could be decided between 0.84 and 3.4 mm from Thorlabs' assortment of fixed collimators, and the actual beam waist of

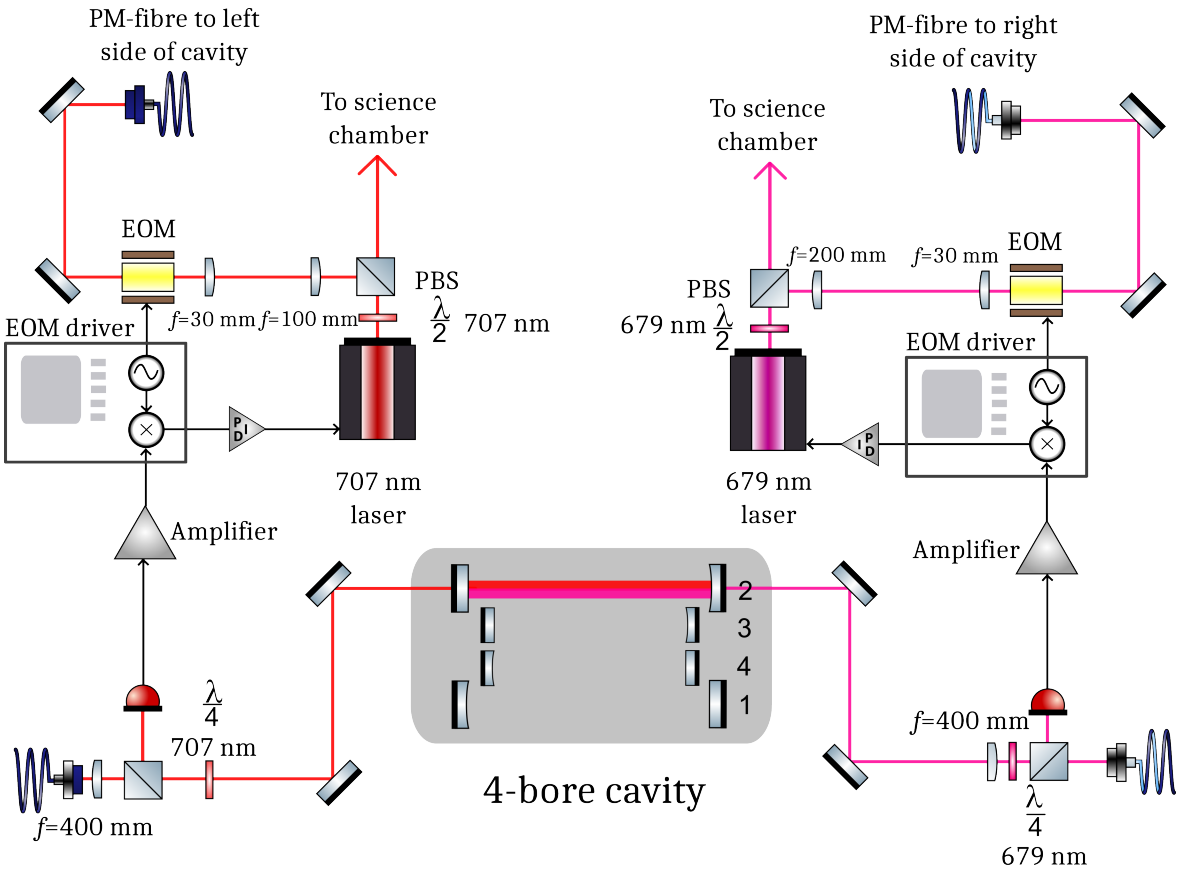

Figure 3.1: A sketch of the experimental setup. The laser light splits into vertically and horizontally polarised light. The vertically polarised light travels through a telescope lens setup, through an EOM, and into a polarisation-maintaining single mode optical fibre. On the other end of the fibre, the light travels through a lens that focuses the light down to its beam waist at the entry point of the cavity. The light is phase shifted by a fourth of a wavelength on its way to the cavity, where it is reflected, and is phase shifted another fourth of a wavelength when it propagates back. It refracts in the PBS and is detected in a photodetector. The signal is amplified and sent to a mixer in the EOM driver. The signal is mixed with the EOM driving frequency and that signal is sent to a servo. The signal from the servo is fed back to the laser and regulates the frequency of the laser.

the chosen collimator, with a theoretical waist of 1.5 mm was measured by camera to be 2.2 mm around 10 mm from the collimator. The real beam waist and the beam divergence differed somewhat from the specifications, and a 400 mm lens was judged to be the optimal lens to make the beam approach a beam waist matching with that of the optical cavity. A camera is used to measure a $1/e^2$ beam waist of around 230-260 µm over a range of 200 mm, which is sufficiently close to the optimal beam waist of 210 µm and also yields a long enough range for the light to propagate in a collimated manner through the cavity. The calculations for the optimal beam waist for the cavity can be found later, in subsection 3.2.3. The beam waist is also found by camera to be around 460 mm from the lens rather than exactly 400 mm from the lens, but the range between 350 and 550 mm is within 260 µm.

The collimators are placed around 450 ± 7 mm from the cavity housing, and the lens is placed 400 ± 7 mm from the cavity housing. The cavity placed inside the housing is guessed to be between 30 and 50 mm from the opening in the cavity housing. The light travels through a PBS, but since the fibre is polarisation maintaining, the fibre has been turned so that a maximum amount of power travels straight through the PBS as horizontally polarised. This light travels

through a quarter-wave ($\lambda/4$) plate (quartz AR/AR at appropriate wavelength, Eksma Optics) of the appropriate material and coating for the wavelength, and is then coupled into the cavity via two mirrors.

Light reflecting off the cavity back-propagates through the setup, but the combined phase-shift from the two passes through the $\lambda/4$-plate introduces a total phase shift of $\lambda/2$, that is, π radians. The $\lambda/4$-plate is rotated to deliver the desired amount of light to the biased photodiode (DET10A2, 200-1100 nm, Thorlabs).

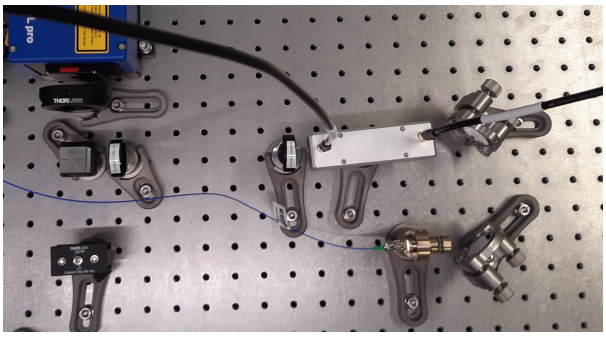

(a) The EOM side of the setup.

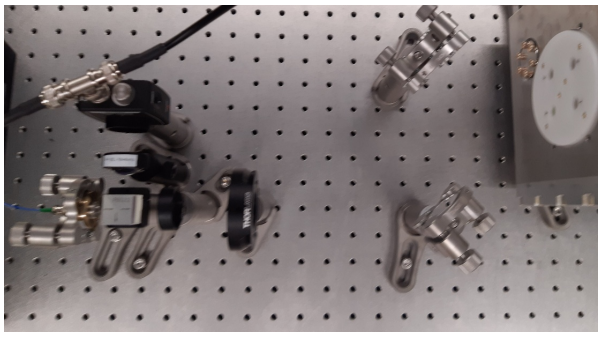

(b) The cavity side of the setup.

Figure 3.2: Pictures of the PDH setup. a) The 707 nm laser, with the telescope setup and EOM before the light is directed into a PMSM fibre. b) The beam leaving the fibre, propagating through a PBS, a 400 mm lens, and $\lambda/2$-plate before reflecting off the cavity and propagating back through the system to be reflected into the photodiode. Compare to figure 3.1.

3.1.3 Electronics

The electronics used to drive the different components are found here. The lasers are operated through a DLC pro from Toptica. The set current is between 32-45 mA for the 707 nm laser and 45-59 mA for the 679 nm laser, but the usual operating values are around 33 mA for the 707 nm laser and 50 mA for the 679 nm laser to reduce the risk for injuries.

The EOMs are driven by Q-drivers from Qubig (QDG10A3+SOL), where the RF power is set to 37.5 dBm, the modulation fequency is 0.75 GHz, and the settings for phase shift, satellite peak frequency, and modulation depth are tweaked to achieve the clearest possible signal. The EOM is also connected to an RF attenuator that can handle 40 dBm.

To observe the signal leaving the cavity, an oscilloscope is used (MXO 4 Series, Rohde & Schwarz). This oscilloscope is also used to sweep a voltage across the piezo inside the laser slowly enough to allow the cavity to respond to the changes in frequency of the incoming wave. The sweeping rate is set to be smaller than the square of the cavity linewidth as defined in equation 32. The linewidth is found to be between 21-75 kHz for a cavity with a finesse between 20000 and 70000, which means the sweeping rate must be slower than approximately 0.46 GHz/s for a cavity of high finesse. If the photodetector detects two fundamental modes, it is known that these are spaced by 1.5 GHz. For the sweep rate to be around 0.46 GHz/s, the distance between two peaks in time domain must be approximately 3.26 s. The distance between the peaks in time domain is measured to have a dependency on frequency and applied voltage which is approximately proportional to $1/fV_{pp}$, meaning that the distance between the peaks increases when the applied voltage and frequency is applied. The sweep settings are set to $f = 55$mHz and $V_{pp} = 1.4$ V, which ensures that the time it takes to sweep one FSR is 4.1 ± 0.1 s, corresponding to a sweep rate of 1.5 GHz/4 s $\approx$ 0.4 GHz/s.

3.2 Optical cavity

The optical cavity is central in the experiment. In this section, the details of the cavity are specified, and the assembly of the cavity housing is described. The technical details and parameters for the cavity are used to calculate the necessary parameters in subsections 3.2.3 and 3.2.4. Finally, a guide to aligning a laser onto an optical cavity is presented in subsection 3.2.5.

3.2.1 Optical cavity specifications

The cavity is a custom made optical cavity in glass with four cylindrical bore holes. On one end of each bore hole, there is a mirror with two plane surfaces. The first side is super polished, and the second side is covered with anti-reflective coating. On the other end of each bore hole, there is a concave/plano mirror that is super polished on the concave side and has anti-reflective coating on its planar side. The concave side of the mirror has a radius of curvature equal to 500 mm. The mirrors are made from ultra-low-expanding (ULE) glass and have a thermal expansion zero crossing temperature in the range 25-40°C. The space between the mirrors is left empty and lossless once the cavity is placed under vacuum. Each mirror is 1 inch, or approximately 25.4 mm, in diameter, and 0.25 inch, or approximately 6.35 mm thick. The cavity itself is 100 mm in diameter and 100 mm long. It is made from the same ULE glass as the mirrors.

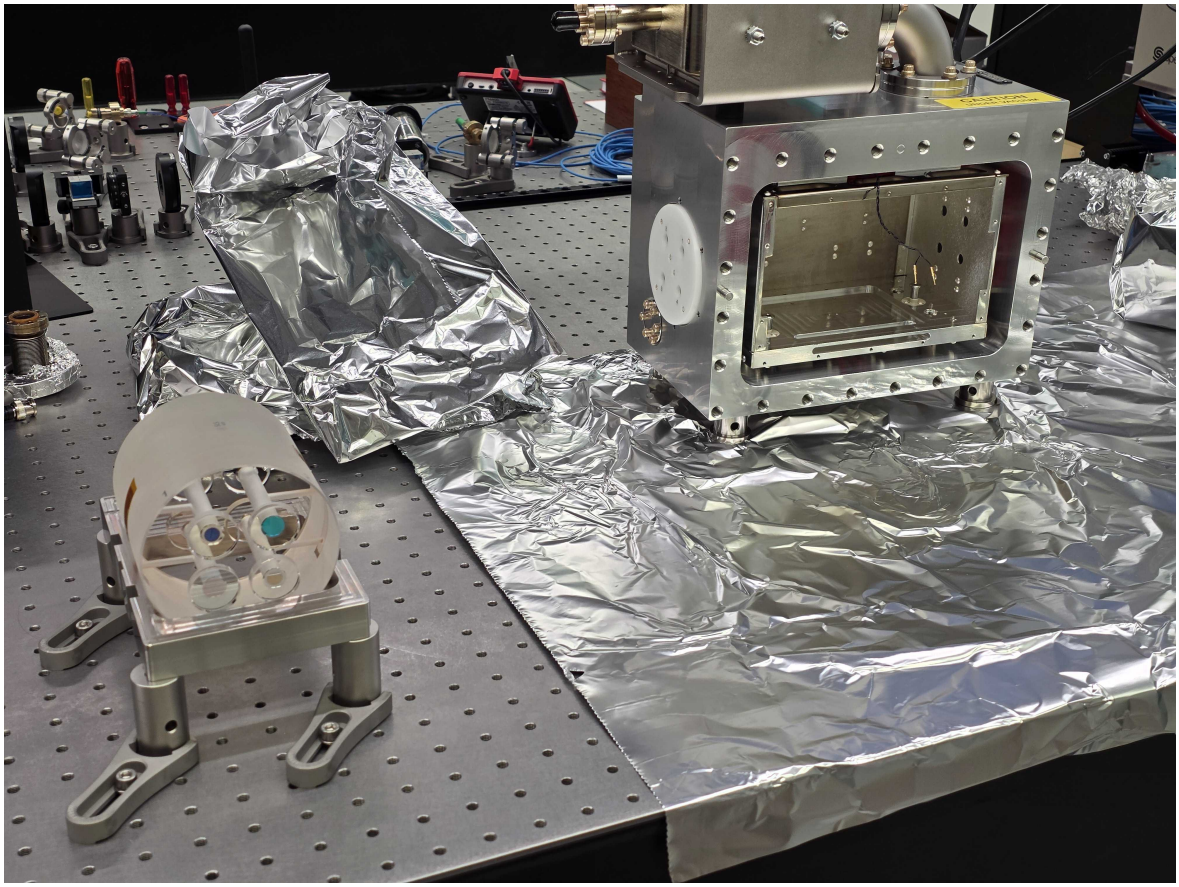

Figure 3.3: The cavity (left) and housing (right) during assembly.

The cavity specifications can be found in table 2. The table specifies the finesse of each bore hole along with its operating wavelength range.

Bore	Wavelength [nm]	Finesse
1	671-707	20000-70000
2	671-707	20000-70000
3	515,813	5000-15000
4	1550	300000-600000

Table 2: Finesse and operating wavelength range for each bore of the optical cavity.

3.2.2 Assembly of cavity housing

The assembly of the cavity housing was mostly governed by the manual supplied by Stable Laser Systems, the manufacturers of the cavity housing. The front panel of the housing is attached to the chamber with 24 screws. The first step is to remove these screws and detach the front from the chamber. Within the outer housing, there is a second chamber, into which the cavity is placed. Four heating blocks, connected with plastic-clad electrical cables, are attached to the front of the inner chamber. To remove the front of the inner chamber, two of these wires need to be detached by loosening two screws at the centre of the inner chamber front. Inside the inner chamber is a block on which the optical cavity rests. It was removed from the chamber and placed on four clean optical posts, so that the cavity could be placed in it. Four rubber balls were placed in the mounting block prior to loading the cavity. The cavity was aligned to be horizontal by eye, resting upon the rubber balls. The mounting block and cavity assembly was put back into the cavity housing and attached to the three pillars it rests upon by screws. The fronts of the inner and outer housings were put back on, following the same procedure as the dismantling of vacuum housing. The screws on the front of the outer housing are torqued to 10 ft-lbs. A technical sketch of the cavity housing's dimensions can be found in figure 3.4.

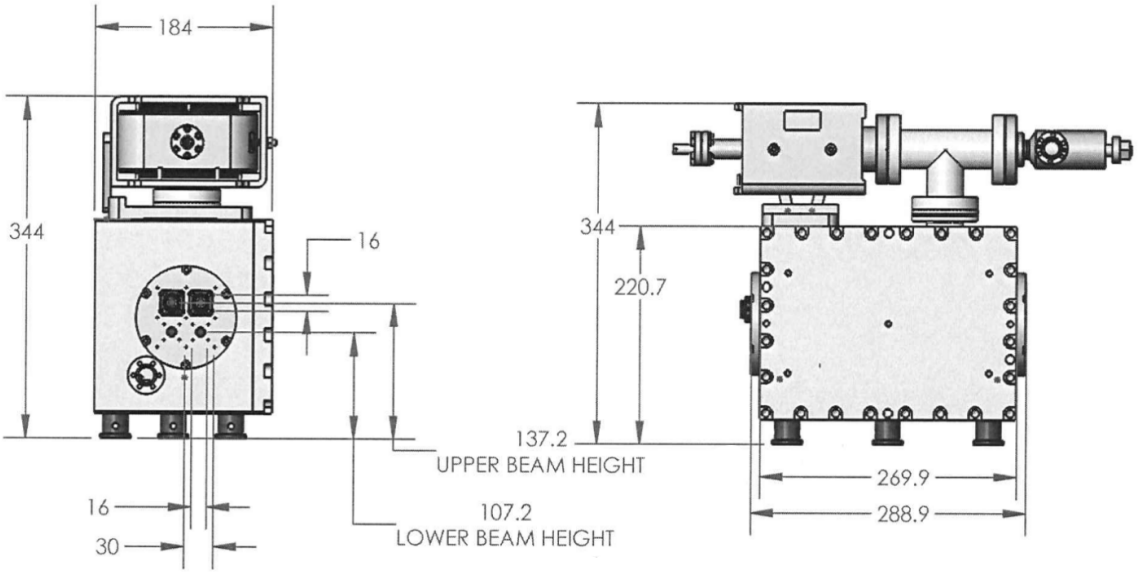

Figure 3.4: Technical sketch of the optical cavity housing used to keep the optical cavity stable and under vacuum. Numbers are given in mm. Sketch taken from housing manual.

3.2.3 Beam waists

To optimise transmission into and resonance in the cavity, it was necessary to collimate the laser beams entering the cavity so they matched the beam waist of the cavity. The cavity specifications can be found in section 3.2.1. One of the mirrors is planar on both sides and the other is concave on the side facing the cavity and planar at the one outside it. The cavity length is $L = 100$ mm. The first lens can be seen as having an infinite radius of curvature, meaning its stability factor $g_1 = 1 - L/\infty = 1$, while the concave mirror has a radius of curvature equal to $R = 500$ mm. This yields a second $g_2 = 1 - L/R = 1 - 100/500 = 0.8$, meaning $0 \leq g_1 g_2 \leq 1$, and the resonator is stable. This can also be seen in the graph found in figure 3.5.

The smallest spot size in this system is found at the plane mirror, which, from equations 43 and 44, yields

$$w_1^2 = \frac{L\lambda}{\pi}\sqrt{\frac{g_2}{1-g_2}}, \qquad w_2^2 = \frac{L\lambda}{\pi}\sqrt{\frac{1}{g_2(1-g_2)}}. \tag{84}$$

The values for w_1 and w_2 vary with wavelength. At 679 nm, $w_1 \approx 0.208$mm, and $w_2 \approx 0.232$mm. At 707 nm, $w_1 \approx 0.212$mm and $w_2 \approx 0.237$mm. To mode match and thereby achieve maximum transmission into the optical cavity, the laser beam was manipulated using lenses.

To achieve a small enough waist within a large enough distance, some mathematics were done. *ABCD*-matrices can be used to do this and was done in Python, but the open-source simulation software, Mode-Matching Optimisation THing (MOTH) by Ian Macmillan, that agrees with calculated results was used for its simplicity and versatility to compare different types of setups in a visual manner and determine which setup would be better for this specific experiment. Once the fixed collimator had arrived, and its waist and divergence angle larger than the natural divergence of a Gaussian beam could be measured, the beam in the MOTH was manipulated to simulate the light leaving the collimator. It was then possible to determine that the 400 mm lens would yield a small enough waist in theory, although when experimentally measured, it yielded a slightly larger waist than calculated.

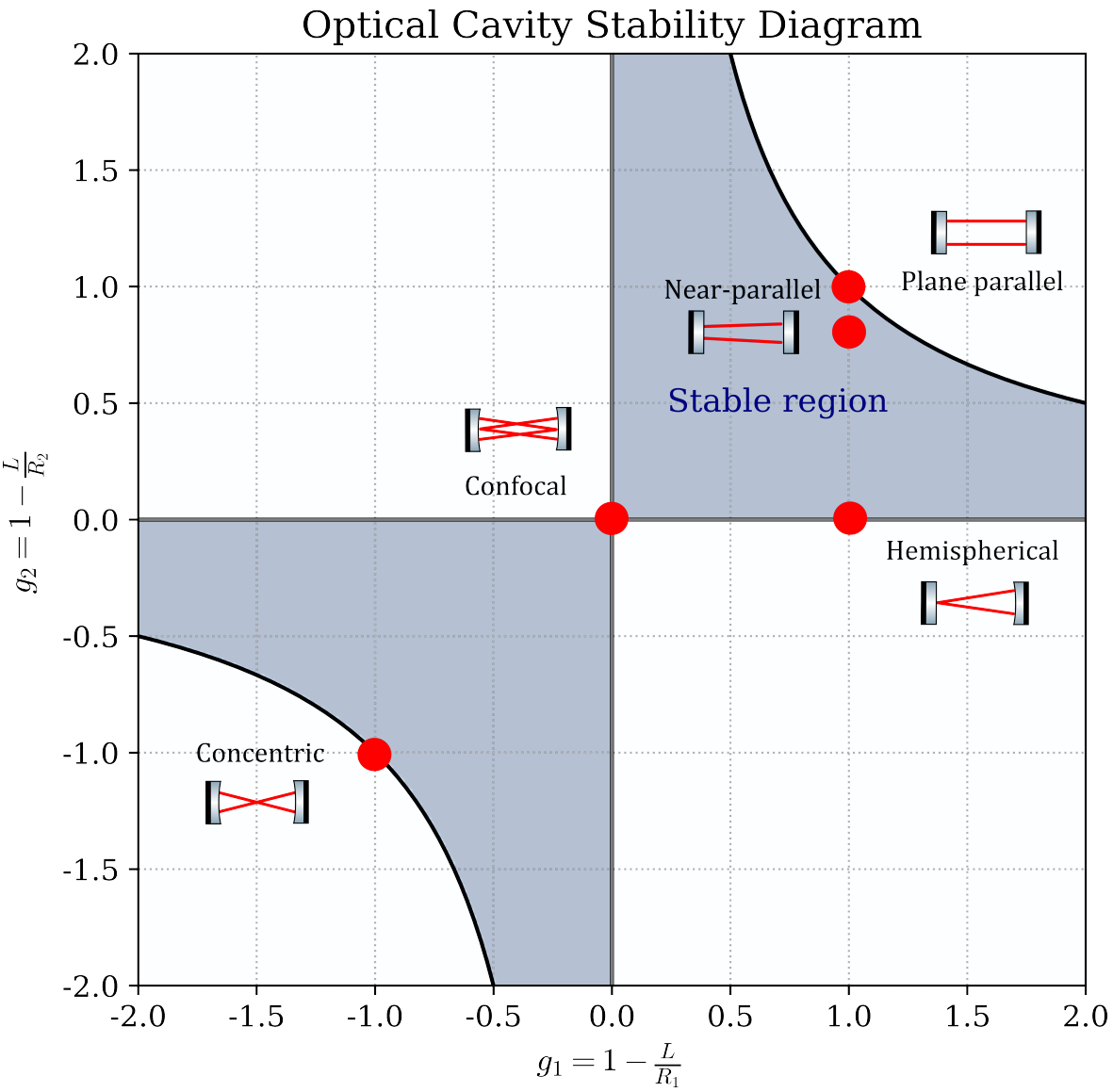

Figure 3.5: A cavity stability diagram marking out the stable region confined by the stability criterion on g_1 and g_2. The shaded area is the stable region, and several different types of cavities are marked out with circles. It can be found that the near-parallel cavity used in this experiment is within bounds of the domain. Code for the plot can be found in appendix fjkfajfeaj.

3.2.4 Transverse and longitudinal mode structure of cavity

The cavity used for stabilisation has the free spectral range given by $c/2L = 1.5$ GHz. From equation 40, it can be found that its transverse modes are given by

$$\begin{aligned} f_{qmn} &= \mathrm{FSR}\left(q + \frac{m+n+1}{\pi}\arccos(\sqrt{g_1 g_2})\right) \\ &= 1.5\mathrm{GHz}\left(q + \frac{m+n+1}{\pi}\arccos(\sqrt{0.8})\right) \\ \implies \Delta f_{\mathrm{trans}} &= 1.5\mathrm{GHz}\frac{\arccos(\sqrt{0.8})}{\pi} \approx 221\mathrm{MHz}. \end{aligned} \tag{85}$$

Another important aspect about the cavity is its *linewidth*, which is defined as FSR/$\mathcal{F}$, which

for a finesse between 20000 and 70000 puts the linewidth at between 21000-75000. For a Gaussian beam being reflected off the cavity, the detected intensity of light should drop at resonances with this spacing.

Under the assumption that the reflectivity $R = r^2$ of the mirrors is the same, equation 33 can be used to calculate R to be 0.99984 for a finesse of 20000 and 0.99995 for a finesse of 70000. Using this number, the coefficient of finesse, $F \neq \mathcal{F}$, can be estimated to be

$$F = \frac{4R}{(1-R)^2} \tag{86}$$

$$\implies 162 \cdot 10^6 < F < 1986 \cdot 10^6. \tag{87}$$

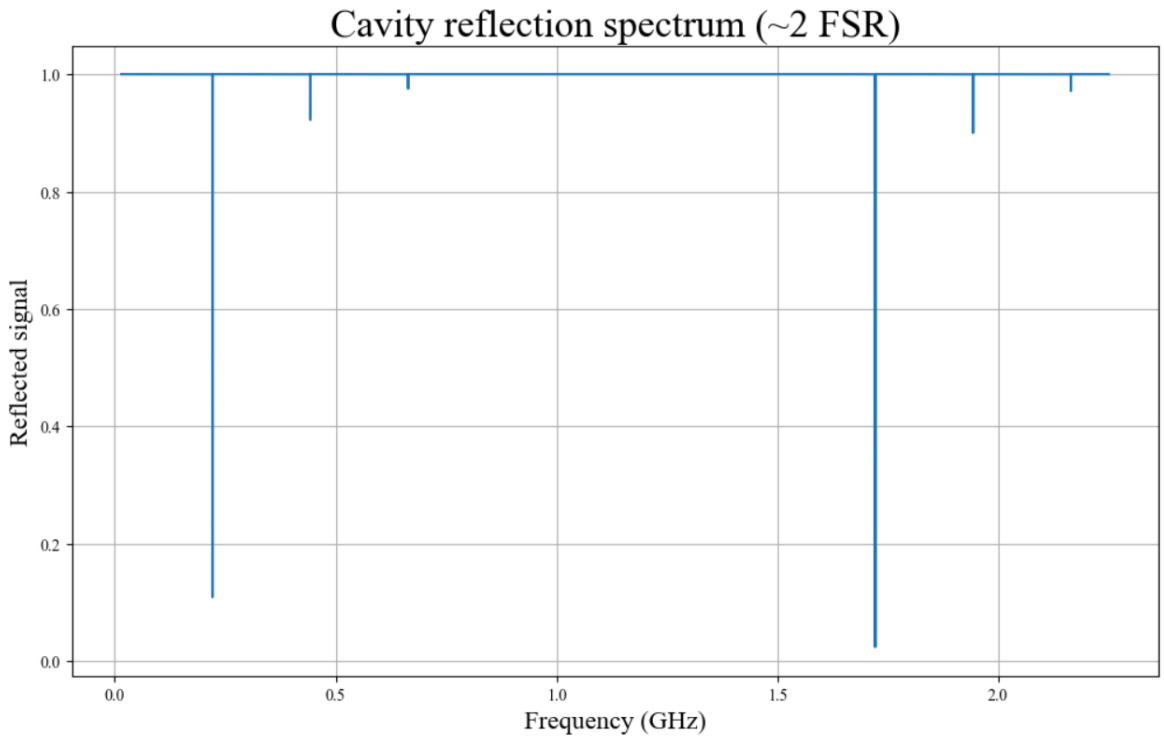

Figure 3.6: Simulated cavity reflection spectrum over circa 2 FSR. The fundamental modes are spaced one FSR apart, and between them are smaller transverse modes. For this plot, a finesse of 40000 was used. Code can be found in appendix iafiajiaf.

Using this, the Airy function describes the intensity as a function of frequency f as

$$I(f) = \frac{1}{1 + F\sin^2(4\pi L f/2c)}. \tag{88}$$

However, in practice, the intensity is more often modelled as Lorentzian as

$$I(f) \approx 1 - \frac{A}{1 + \left(\frac{2(f-f_0)}{\Delta f_{\text{FWHM}}}\right)^2}, \tag{89}$$

where A is an experimental parameter between 0 and 1 which describes how well the light couples to the mode in question. Assuming good coupling ($A = 1$) to the fundamental mode

and less coupling to the other modes ($A = 0.05$ for $m + n = 1$ and $A = 0.01$ for $m + n = 2$), the expected result should be similar to what is seen in figure 3.6 .

3.2.5 A guide to aligning a laser onto an optical cavity

The alignment of light onto a laser cavity can be divided into two steps: coarse alignment and fine alignment. After aligning collimator and mirrors approximately to the cavity, the reflected light should be visible as a spot offset from the incoming light. The mirrors are walked to overlap the reflected light with the incoming light at the collimator and at the cavity opening. Then, the photodetector (PD) on the laser side is turned on and connected to an oscilloscope. A lens with focal length 30 mm is placed before it to ensure all light is collected and directed onto the photodiode on the PD. A PD and lens pair is also placed on the other side of the cavity to measure the transmitted signal, that is much stronger than the reflected signal and may call for the use of filters on the PD.

The fine tuning comprises coupling to the fundamental mode of the light and maximising the reflection by manual turning of the mirrors. It is necessary to wait a little bit before proceeding to continue optimising the mirror angles to maximise reflection, since the oscilloscope requires some time to show the current state of the signal. For this experiment, the power of the laser was kept at 200 µW at the cavity to avoid all risks of damaging the cavity. When alignment approaches mode-matching, the modes will be clearly visible as lines as depicted in figures 3.7 and 3.8 below. The goal of the fine tuning of the alignment is to maximise the fundamental mode. This also results in a decrease in intensity for higher order modes.

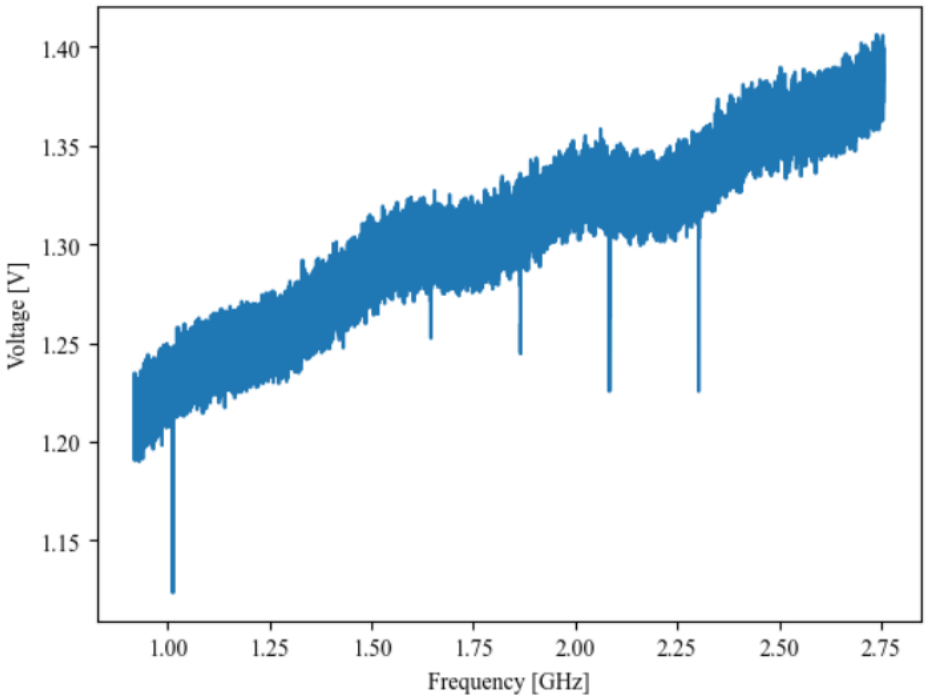

Figure 3.7: Image of the reflection spectrum when the alignment is a bit off from the cavity. The first peak on the left is the fundamental mode, but it is missing from the second FSR, where the modes of order 1-4 are clearly visible, with an indication of the fifth mode. The plot shows voltage as a function of time, where approximately 500 ms represents one FSR of 1.5 GHz.

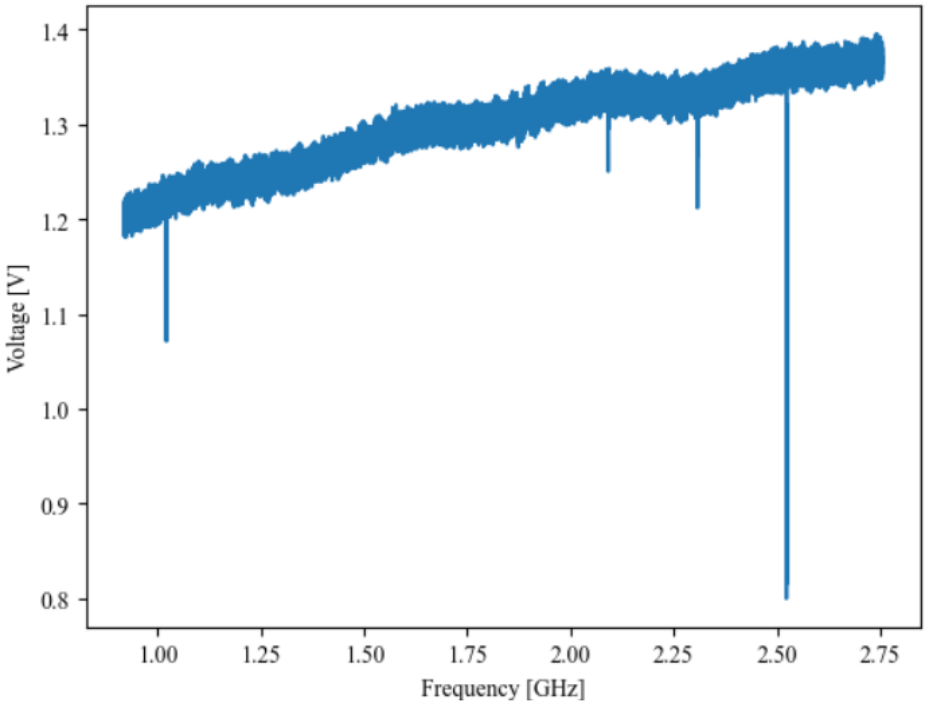

Figure 3.8: In this image, the mode matching has increased. The fundamental modes can be found represented at the first peak from the left and the last peak to the right. The first and second order modes are still visible, and there is an indication of the third order mode. Note that the first and the second fundamental modes do not have the same reflection intensity.

3.3 PDH locking

This subsection first repeats some of the theory from section 2.3.6, followed up by the expected results from a cavity of similar properties as the one used in this experiment. Lastly, the details about the connections between the PD and the EOM driver are disclosed.

3.3.1 Simulations for the reflected signal and the PDH error signal

In section 2.3.6, the reflection coefficient $F(\omega)$ was defined as

$$F(\omega) = \frac{E_r}{E_{in}} = \frac{r(e^{i\omega/\Delta f} - 1)}{1 - r^2 e^{i\omega/\Delta f}}.$$

The phase of the reflected signal is found to be the argument of this function. The argument $\arctan(\mathrm{Im}\{F\}/\mathrm{Re}\{F\})$ of this function for the experiment specific cavity can be found in figure 3.9.

The error function is given by

$$\epsilon = -P_0 \beta \, \mathrm{Im}\left[F(\omega)F^*(\omega+\omega_m) - F^*(\omega)F(\omega-\omega_m)\right],$$

which for the cavity of interest, with a supposed finesse of 40000, a mirror reflectivity of 0.999961, detuning $\beta = 0.3$ and a modulation frequency of 0.75 GHz, should yield an error signal similar to what is found in figure 3.10.

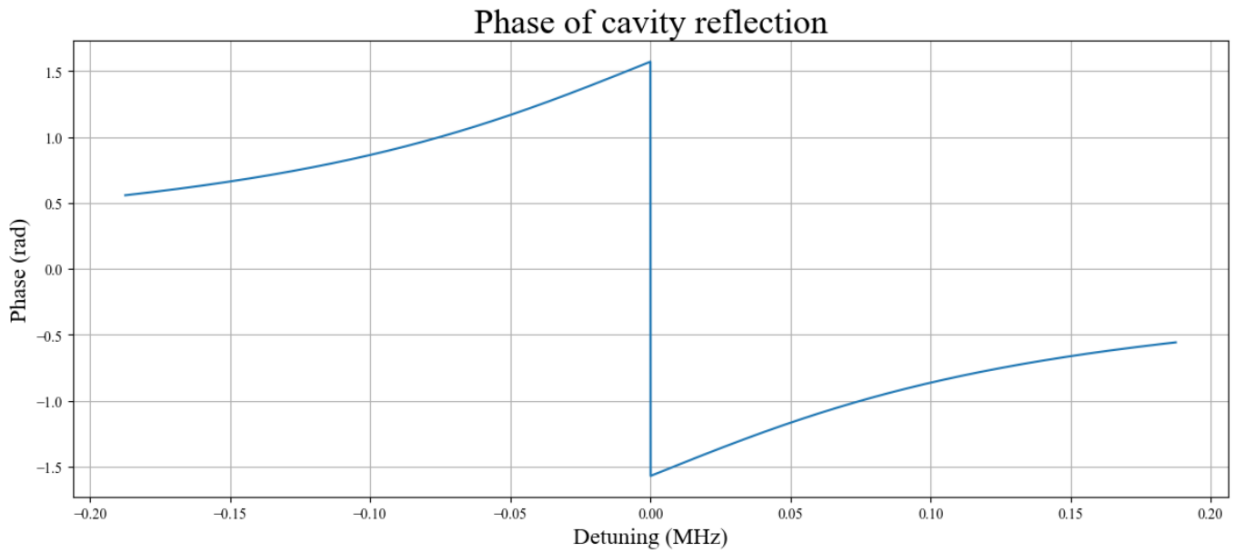

Figure 3.9: The phase of the cavity reflection is given by $\arctan(\mathrm{Im}\{F\}/\mathrm{Re}\{F\})$. At perfect resonance, the phase is discontinuous, but tends to zero the further it detunes from this frequency. The code for the plot can be found in appendix B.3.

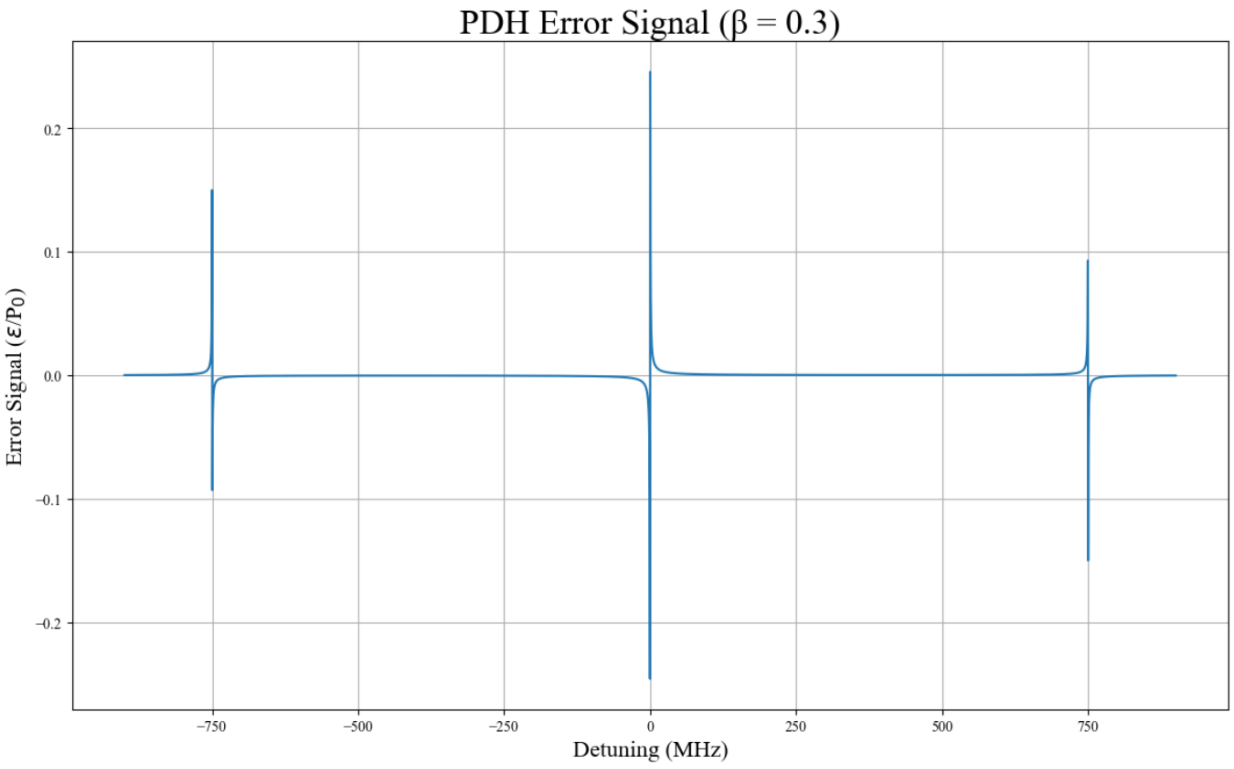

Figure 3.10: A graph depicting the expected error signal of a cavity similar to the one used for laser stabilisation in this experiment. The finesse 40000 and the modulation frequency is 0.75 GHz. Code can be found in appendix B.3.

3.3.2 Locking procedure

The locking procedure requires amplification of the PD signal in the right frequency domain. The signal goes from the photodetector to the RF+DC port on a biased tee signal splitter (ZFBT RD 4R2GW+ 0.1-4200 MHz, Mini-Circuits), the schematic of which can be found in figure 3.11.

The signal from the DC port is sent to the oscilloscope wile the signal from the RF port goes to the EOM driver. The signal from the RF port passes through a low-pass filter (BLP-25+ DC 25 MHz, Mini-Circuits) with a 50Ω impedance before it entert a low-noise amplifier (ZFL-1000LN+, Mini-Circuits). The amplified signal is sent into the PD_{in} port on the EOM driver. The signal from IF_{out} on the driver is directly connected to the oscilloscope.

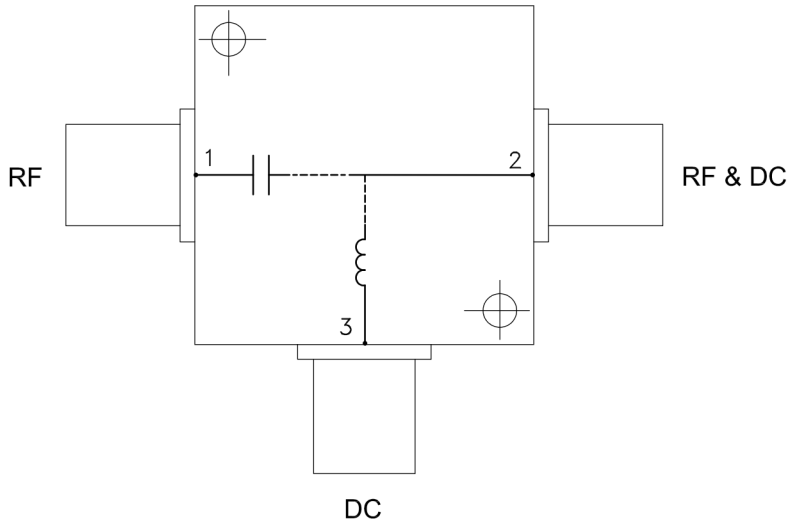

Figure 3.11: Schematic of the circuitry inside the biased tee used at the PD. Image courtesy to the Mini-Circuits manual.

4 Results

This section provides the locking results for the 707 nm laser, disclosing the approximate cavity coupling efficiency for different sweep rates. The effect of sweep rate and the laser's stability on coupling is discussed, and an attempt at estimating the cavity's finesse is made. The EOM signal is successfully generated and detected, and the results for the error signal are shown.

4.1 Alignment and cavity response

The intensity of the reflected light was detected with the PD, measured by the oscilloscope, and plotted in Python. The ratio of the fundamental peak's minimum and the intensity of the light about that peak is a measure of the coupling of the light into the cavity. The intensity of this peak can be found to fluctuate between different sweeps, even though nothing is changed between the measurements. The coupling is found to be between 30-47 per cent, but it varies largely and is affected by sweep rate, how long the laser has been on, and temperature in the lab. The fundamental peak is measured for different sweep rates, and the results are presented in figures 4.8 and 4.2 below.

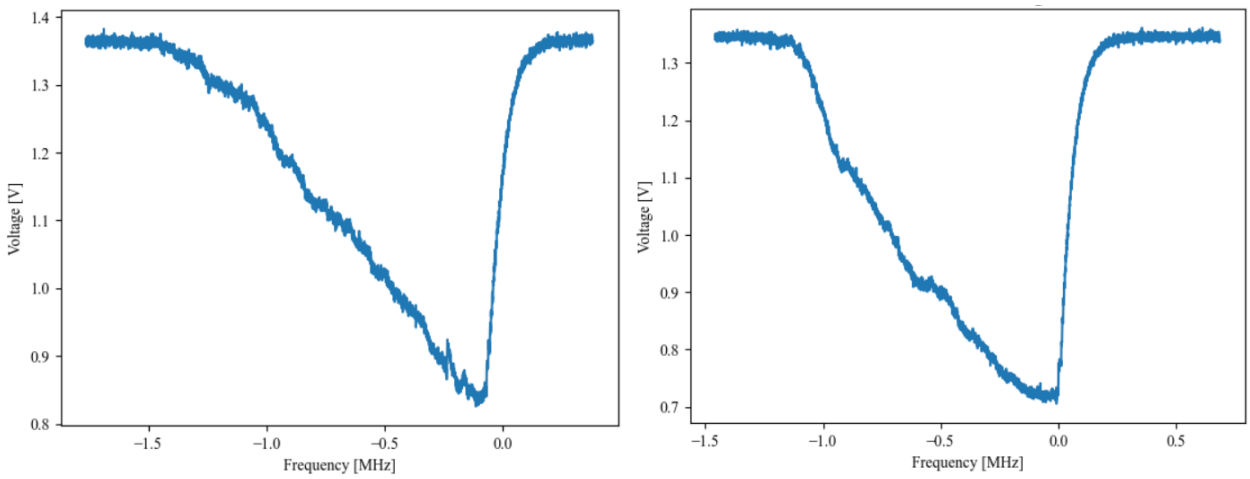

(a) Example of fundamental mode. 40% coupling.

(b) Example of fundamental mode. 48% coupling.

Figure 4.1: Two fundamental reflection dips with different coupling for a sweep rate of 3 GHz/s.

In these two figures, it is clear that the peak isn't Lorentzian or Gaussian in shape. In both of these images, the piezo voltage is increasing, causing the laser cavity to expand and the frequency to decrease. This is why the higher order modes appear before the fundamental peak as the voltage increases - the frequency is higher for a lower voltage. As the frequency approaches a resonance frequency from above, the cavity becomes more and more mode-matched. When the laser is perfectly at resonance, the absorption is complete, and a sharp dip should be observed, similar to what can be seen on the right side of these two peaks. The partial absorption before then can likely be explained by fluctuations in the laser frequency, that increasingly couple to the cavity's fundamental mode. In figure 4.8b, the left side of the peak can be found to be divided into three regions with different slopes. This could either be a defect of some kind, or some form of subtle oscillation. It could also be an feature of the high-finesse cavity, since the cavity has a much smaller linewidth than the laser.

The cavity has a finite photon lifetime

$$\tau_p = \frac{1}{2\pi\Delta f} \tag{90}$$

where Δf is the cavity linewidth, which has been calculated to be between 21000 and 75000 Hz in 32. This puts the photon lifetime at between 2.1 and 7.6 µs. However, as can be seen in figure 4.8, the peak width appears to be on the order of 400 ± 50 µs broad. For a sweep rate of 3 GHz/s, this corresponds to a resonance width of about 1.2 MHz, which is wider than the cavity's linewidth.

When the laser frequency changes faster than this, the cavity does not respond ideally, and the reflected signal becomes distorted. As the laser sweeps into resonance, the cavity field slowly builds up, but the resonance condition is crossed before there is a complete buildup of light. The field inside the cavity then interferes with the promptly reflected field as it should, but the leakage field is smaller than it might have been had the build-up been complete.

When the sweep rate is changed, the shape of the peaks change. For figures 4.8a and 4.8b, the sweep rate was approximately 3 GHz/s, that is, around six times faster than was calculated to be the highest sweep rate of the cavity (0.46 GHz/s). For those frequencies, the fundamental peak instead looks like what can be found in 4.2a and 4.2b.

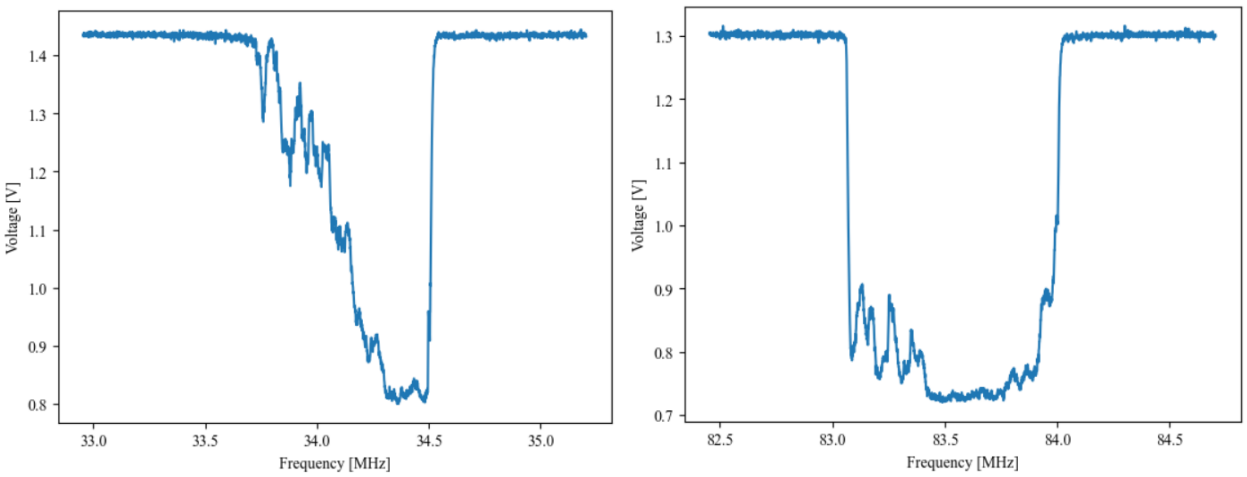

(a) Example of fundamental mode.

(b) Example of fundamental mode. This is an example of an outlier, given its lack of a jagged triangular shape.

Figure 4.2: Reflection signal for two fundamental modes with coupling around 45% for a sweep rate of 0.4 GHz/s. Frequency axes are to be treated as relative and do not correspond to a real frequency, instead serving as a measure for the length of a feature.

For an even lower sweep rate, a dip can be made to be 200 µs broad, but the noise that can be seen in 4.2a and 4.2b is more evident and appears throughout the whole feature.

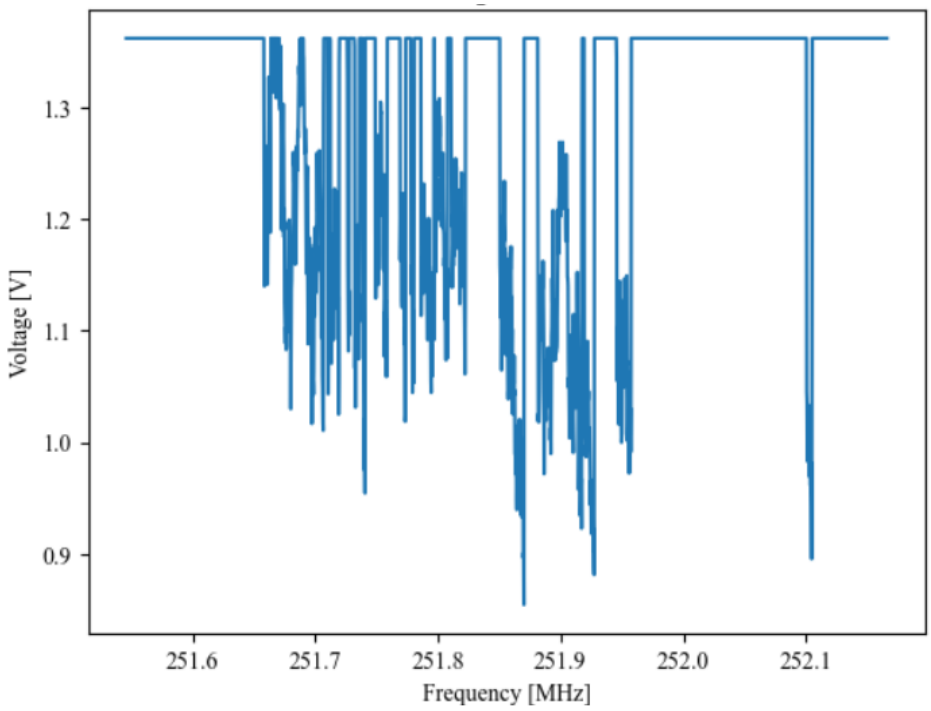

Figure 4.3: Fundamental mode with a coupling of 37% for a sweep rate of 2.5 MHz/s. The feature lasts 150 ms and is divided into many smaller intensity dips, signalling instability of the laser frequency at sweep rates this low.

The noise is thought to be from fluctuations in the laser intensity over time, which also affects the frequency, which in turn affects the coupling. The fact that the saw-tooth shape remains despite a decrease in sweep rate indicates that this is not a feature related to the sweep rate, but the system itself. It is likely connected to imperfect mode matching, but it could also be a feature of a high-finesse cavity system. To find if the mode-matching is the cause of this asymmetric behaviour, the transmission is measured and plotted, since the transmitted light does not interfere with external radiation which minimises external influences.

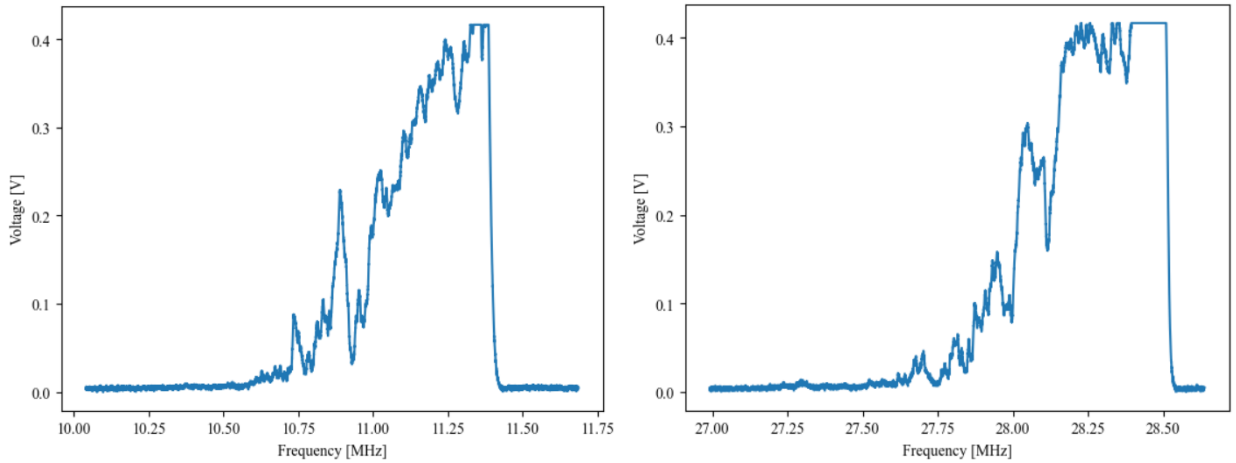

(a) Example of transmitted fundamental mode.

(b) Example of transmitted fundamental mode.

Figure 4.4: The transmission of two fundamental modes for a sweep rate of 0.4 GHz/s. Intensity crops at 0.42 V as the photodiode saturates too rapidly.

From looking at figure 4.4, it can be found that the asymmetric behaviour persists even in the transmitted signal. However, from the transmitted signal, it is less clear that the slope is unafflicted by oscillations, making this measurement more similar to a cavity ringdown measurement. However, through performing a ringdown measurement intentionally, it can be found that this behaviour does not correspond to a ringdown response but rather appears to be a consequence of laser noise that is preserved and amplified in the cavity due to the cavity's high finesse.

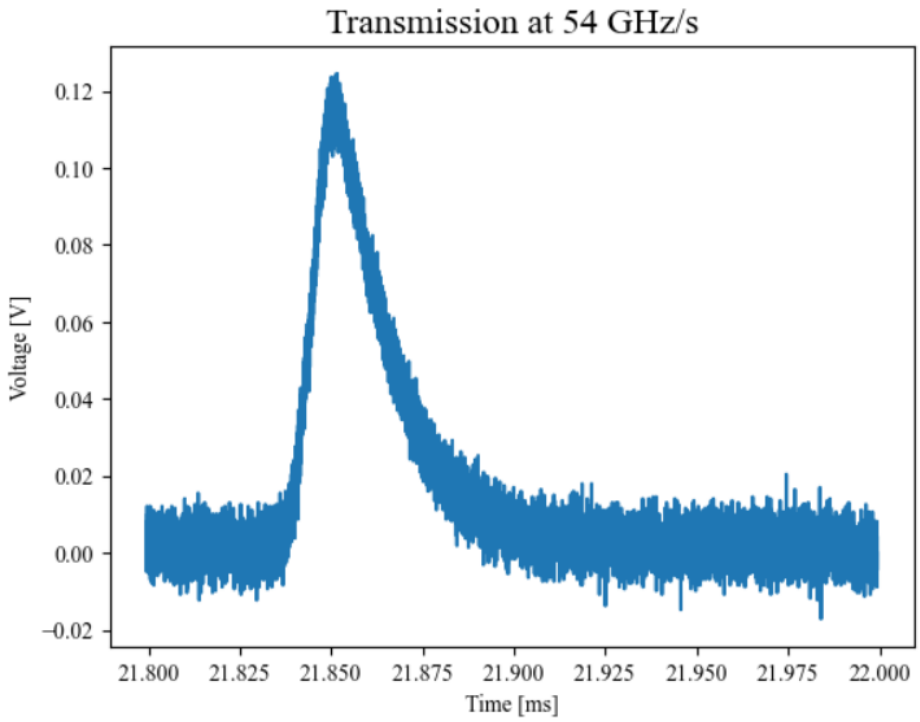

Figure 4.5: Plot over the transmission at 54GHz/s. Note the Lorentzian increase in intensity as the frequency increases, followed by the exponential decay slope. The coupling is considerably worse for higher sweep rates. There is a considerable amount of noise for intensities this low.

The general signal to noise ratio decreases as the sweep rate decreases. The noise ground floor seen in figure 4.5 is approximated by an average value of 1 mV from background radiation, with a variance of 7.5 mV.

A model simulating exponential decay of the intensity ($I(t) = I_0 \exp(-t/\tau)$) can be used on any slope whose maximum is detected (see [38]). If there is a fit, and the calculated τ agrees over multiple observations, it is likely that this is a reproducible physical phenomenon that can be used to calculate the cavity's actual finesse.

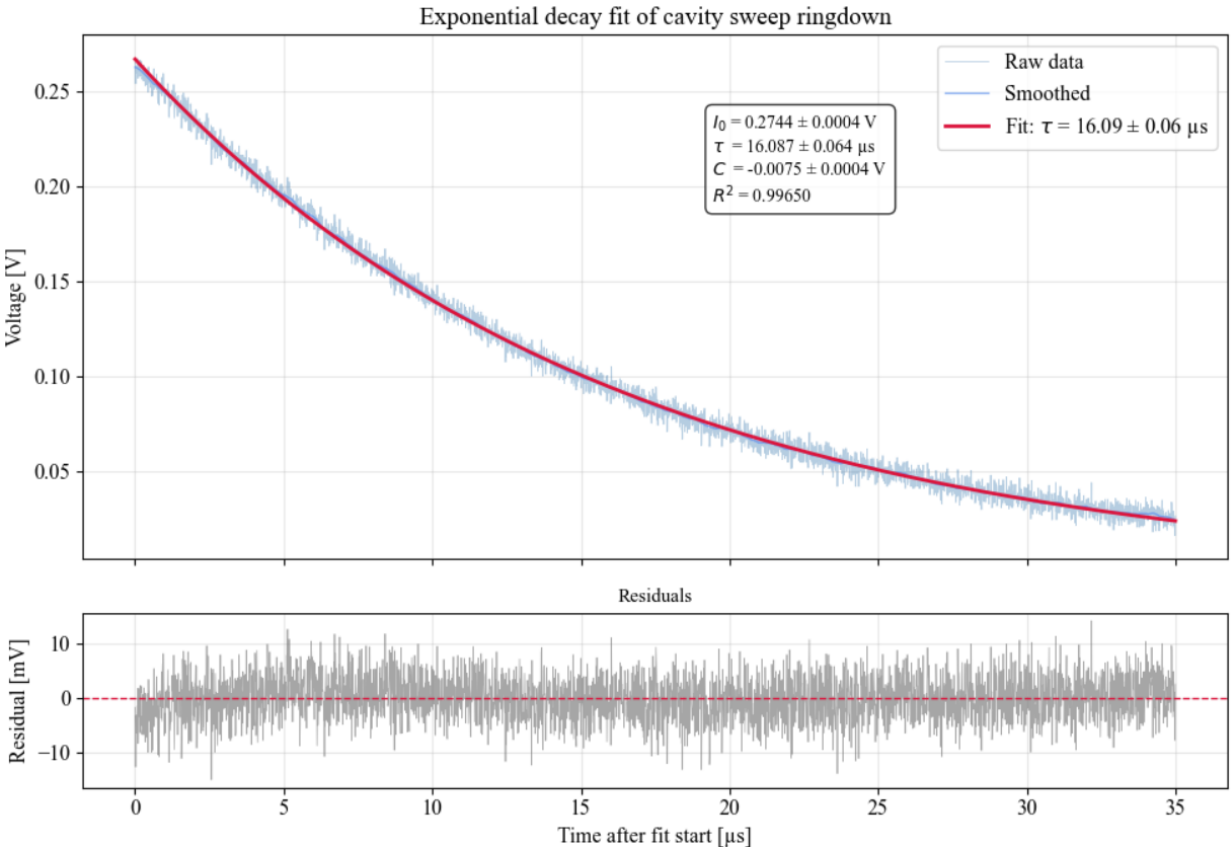

Figure 4.6: Cavity ringdown for a sweep rate of 27 GHz/s. Exponential fit using code that can be found in B.4.

This decay fit is used on several sets of data, and for a sweep rate of 54 GHz/s, the photon decay time τ is found to be between 18-20 µs, while a lower sweep rate of approximately 27 GHz/s yields a time constant between 15-18. An excerpt of typical data can be found in table 3.

Sweep rate	τ_1[µs]	τ_2[µs]	τ_3[µs]	τ_4[µs]
54 GHz/s	19.11 ± 0.21	18.20 ± 0.21	19.66 ± 0.23	19.52 ± 0.22
27 GHz/s	16.49 ± 0.08	15.58 ± 0.10	16.09 ± 0.06	15.47 ± 0.10

Table 3: A collection of calculated time constants for a selection of sweep rates. Selected data points τ are representative of the whole set. Note how the noise decreases with sweep rate.

The resulting time constants are between a factor 3-10 larger than what is expected from the cavity, which would also yield a finesse that is that much larger. This discrepancy suggests that the assumptions underlying the analysis are not fully satisfied. The imperfect fit can also be found in the slight asymmetry in the distribution of the residuals in the 0-10 and $t > 33$ µs range in figure4.6.

A potential cause for this could be the fact that this isn't a pure ringdown, and rather a sweep. The function associated with a sweep is not purely exponential, but is given by the real part of equation 91. In this equation, ω_c is the bare cavity resonance, or a resonant mode, $\omega_L(t) = \omega_0 + St$ for some unperturbed laser frequency ω_0 and sweep rate S, and κ is the half width at half maximum (HWHM) linewidth [39].

$$I(t) = \mathrm{Re}\left[\sqrt{\frac{\pi i}{2S}}\kappa f_F\left(-\sqrt{\frac{iS}{2}}\left(t - \frac{\omega_c - \omega_0 + i\kappa}{S}\right)\right)\right] \tag{91}$$

In equation 91, $f_F(x)$ is known as the Faddeeva function and is given by

$$f_F(x) = e^{-x^2}[1 - \mathrm{erf}(-ix)]. \tag{92}$$

A new model could be created using equation 91, but that was beyond the scope of the project.

4.2 Results from EOM activation

When the EOM is turned on, a peak appears at the designated location, between two fundamental peaks. Its strength is around 10±5% of the fundamental peak and is the second strongest feature of the spectrum, after the fundamental peak. The sidebands of this sideband are not visible. When the EOM is activated, the overall coupling of the cavity drops to between 30-35%.

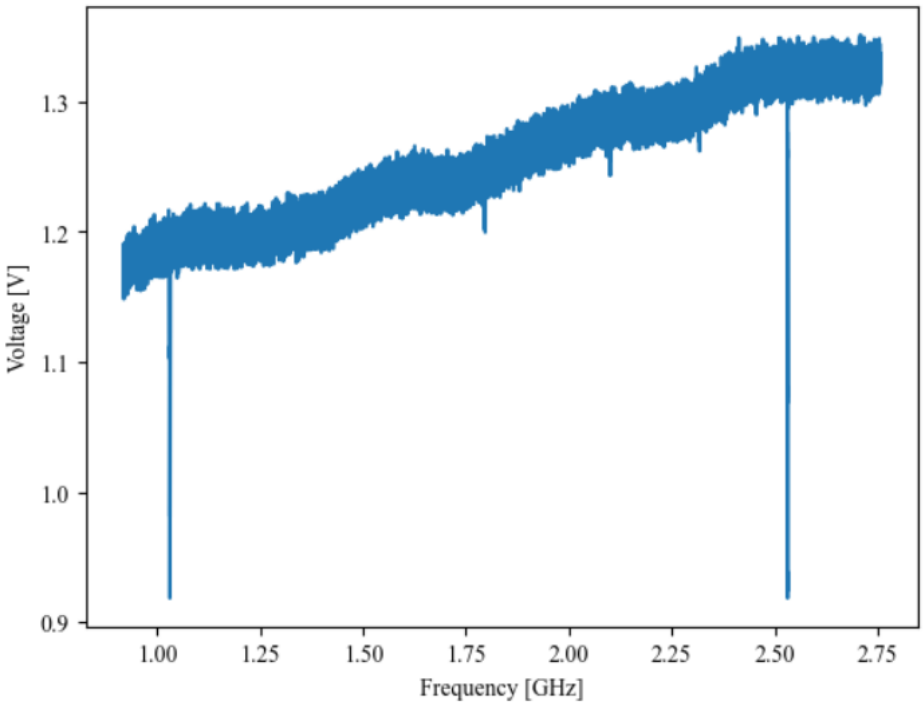

Figure 4.7: The reflected light with EOM activated, over one FSR with two neighbouring fundamental peaks to the left and the right in the graph. The modulation frequency is 75000 kHz, that is, half an FSR, resulting in the peak at the centre of the spectrum. It is of the same order of magnitude as the second transverse mode, that is larger than the first in this specific measurement. The coupling of the fundamental mode generally goes down when the EOM is activated. In this measurement, coupling is 32%.

4.3 Detection of error signal

The error signal is the signal which is detected after the reflected signal from the PD is mixed with the modulation frequency of the EOM. This error signal should have the characteristics

that can be seen in figure 3.10, and should be fed through a PID controller to control the laser frequency to ensure the laser is locked onto a resonance peak. The detected error signal is noisy and has a low intensity at this stage. Every feature in the observed spectrum has a corresponding feature in the error signal, accompanied by periodic noise from the connections.

The features detected in the error signal that have the highest intensity are from the fundamental modes, followed by the sidebands generated by the EOM, which have approximately half the intensity of the error signal corresponding to the fundamental modes.

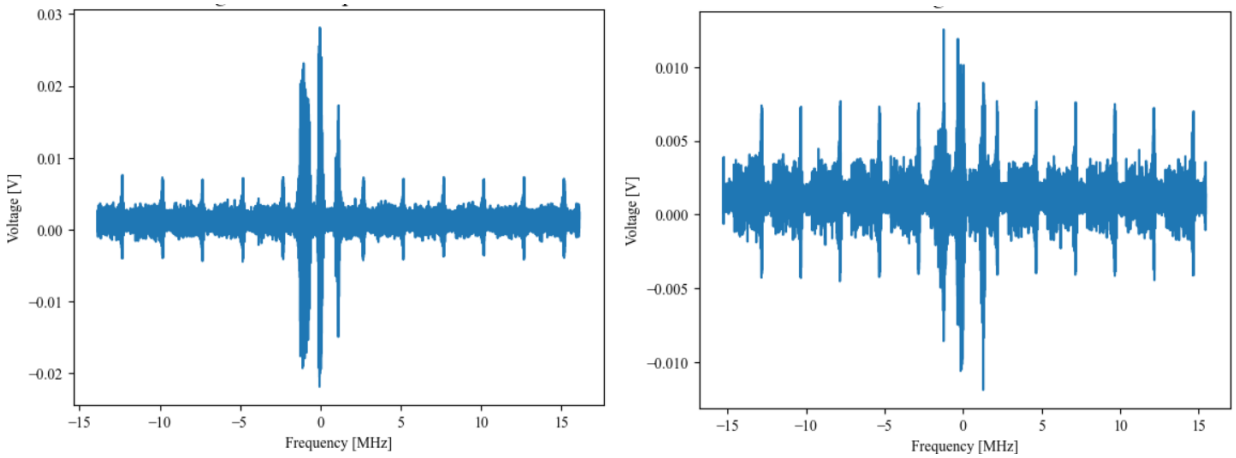

(a) Error signal aligning with the fundamental mode.

(b) Error signal aligning with the EOM signal.

Figure 4.8: The error signal detected about the fundamental mode and the EOM signal, respectively. The tendency for a signal to divide into a central signal surrounded by two satellite signals is not the norm and is a coincidence coming from laser noise, not from modulation, which is supported by the fact that the satellite signals are spaced approximately 1.5 MHz from the central peak, which doesn't correspond to any modulation in the system. The sharp signals spaced about 2.5 MHz apart come from the electronic connections.

The error signal contains noise which can be found to originate from the laser. This can be seen through matching the error signal with the directly detected signal from the PD, where minima and maxima in the reflected signal correspond to minima and maxima in the error signal. Improvements in cavity coupling alone are not expected to eliminate this contribution. No locking attempts with this signal were performed due to the subsequent loss of cavity coupling caused by misalignment.

5 Conclusions

The aim of this project went from being about implementing laser cooling to stabilisation of the two repump lasers onto an optical cavity. At the time of writing, the two lasers are aligned to the cavity, but neither of them are locked onto the cavity, since the error signal does not show anything but noise. The lasers have been found to be both elliptic and astigmatic. The laser has also been found to fluctuate in frequency when it is swept, making it difficult to attain clean, Lorentzian curves that agree with the theory and available literature; however, this is a result of having a cavity with such high finesse. An attempt was made to estimate this finesse, but the cavity sweep ringdown yielded an expected result surpassing 70000, and the uncertainties of the system and the approximation make these results unreliable. A more appropriate estimation of the cavity's finesse could be done using a model fitting a cavity sweep rather than the exponential decay model associated with a ringdown. Alternately, a real ringdown experiment, rather than a ringdown sweep, could be done by sending in a pulse of light into the cavity.

The next steps of the project are first to return the experiment to the state it was at the time of data acquisition for this thesis by ensuring the EOM, that was displaced during data collection, is properly aligned again. Once the 707 nm laser is properly aligned onto the cavity again, the error signal should be sent through a low-pass filter, and PID control will be attempted. Once the 707 nm laser is locked, work can move on to attempt the same process for the 679 nm laser.

As a general conclusion, it has been found during the course of this work that building a working laser cooling setup is a time-consuming and advanced project. It requires understanding of more theoretical subjects, such as optics and atomic physics, but also of practical skills concerning vacuum systems, dimensioning of chambers, electronics and RF signals.

References

1. Foot CJ, Brooker GA, and Hooker SM. Atomic Physics. Oxford University Press, 2005
2. McClements D and Zidonis A. How laser cutting is used in different industries. Xometry 2025. Available from: https://www.xometry.com/resources/sheet/how-is-laser-cutting-used-in-industry/
3. Lee C. Fabric laser cutting: process, benefits and optimisation. Accurl 2024. Available from: https://www.accurl.com/blog/laser-cutting-fabric/
4. Boyd MM, Zelevinsky T, Ludlow AD, Blatt S, Zanon-Willette T, Foreman SM, and Ye J. Nuclear spin effects in optical lattice clocks. Physical Review 2007; 76. DOI: http://dx.doi.org/10.1103/PhysRevA.76.022510
5. Boyd MM. High Precision Spectroscopy of Strontium in an Optical Lattice: Towards a New Standard for Frequency and Time. PhD thesis. University of Washington, 2007
6. Bakr WS, Gillen JI, Peng A, Fölling S, and Greiner M. A quantum gas microscope for detecting single atoms in a Hubbard-regime optical lattice. Nature Letters 2009; 462:74–7. DOI: https://doi.org/10.1038/nature08482
7. Greiner M, Mandel O, Esslinger T, Hänsch TW, and Bloch I. Quantum phase transition from a superfluid to a Mott insulator in a gas of ultracold atoms. Nature 2002; 415:39–44. DOI: https://doi.org/10.1038/415039a
8. Hosten O, Engelsen NJ, Krishnakumar R, and Kasevich MA. Measurement noise 100 times lower than the quantum-projection limit using entangled atoms. Nature Letters 2016; 529:505–8. DOI: http://www.nature.com/doifinder/10.1038/nature16176
9. Kim K, Chang MS, Korenblit S, Islam R, Edwards EE, Freericks JK, Lin GD, Duan LM, and Monroe C. Quantum simulation of frustrated Ising spins with trapped ions. Nature 2010; 465:590–3. DOI: https://doi.org/10.1038/nature09071
10. Jöckel A, Faber A, Kampschulte T, Korppi M, Rakher MT, and Treutlein P. Sympathetic cooling of a membrane oscillator in a hybrid mechanical-atomic system. Nature Nanotechnology 2015; 10:55–9. DOI: https://doi.org/10.1038/nnano.2014.278
11. Geraci AA and Kitching J. Ultracold mechanical resonators coupled to atoms in an optical lattice. Physical Review A 2009; 80. DOI: http://dx.doi.org/10.1103/PhysRevA.80.032317
12. Aspelmeyer M, Treutlein P, Genes C, Hammerer K, Poggio M, and Rabl P. Cavity Optomechanics. Springer-Verlag, 2014 :327–51
13. Orzel C. A Brief History of Timekeeping. BenBella Books Inc., 2022
14. Offenberg D, Zhang CB, Wellers C, Roth B, and Schiller S. Translational cooling and storage of protonated proteins in an ion trap at subkelvin temperatures. Phys. Rev. A 2008 Dec; 78(6):061401. DOI: 10.1103/PhysRevA.78.061401. Available from: https://link.aps.org/doi/10.1103/PhysRevA.78.061401
15. Chan J, Mayer Alegre TP, Safavi-Naeini AH, Hill JT, Krause A, Gröblacher S, Aspelmeyer M, and Painter O. Laser cooling of a nanomechanical oscillator into its quantum ground state. Nature 2011; 478:89–92. DOI: https://doi.org/10.1038/nature10461
16. Hunger D, Camerer S, Korppi M, Jöckel A, Hänsch TW, and Treutlein P. Coupling ultracold atoms to mechanical oscillators. Comptes Rendus Physique 2011; 12:871–87. DOI: http://dx.doi.org/10.1016/j.crhy.2011.04.015
17. Kolkowitz S, Bleszynski Jayich AC, Unterreithmeier QP, Bennett SD, Rabl P, Harris JGE, and Lukin MD. Coherent sensing of a mechnaical resonator with a single-spin qubit. Science 2012; 335. DOI: https://doi.org/10.1126/science.1216821

18. Christoph P, Wagner T, Zhong H, Wiesendanger R, Sengstock K, Schwarz A, and Becker C. Combined feedback and sympathetic cooling of a mechanical oscillator coupled to ultracold atoms. New Journal of Physics 2018 Sep; 20:093020. DOI: 10.1088/1367-2630/aadf20. Available from: http://dx.doi.org/10.1088/1367-2630/aadf20
19. Henley E and García A. Subatomic physics. World Scientific Publishing Co. Pte. Ltd., 2007
20. Metcalf HJ and Straten P. Laser cooling and trapping. Springer, 1999
21. Nordling C and Österman J. Physics Handbook for Science and Engineering. Professional Publishing House, 2014
22. Cheng DK. Fundamentals of engineering electromagnetics. Addiston-Wesley Publishing Company, 1994
23. Loudon R. The Quantum Theory of Light. Oxford University Press, 2003
24. Griffiths DJ and Schroeter DF. Introduction to Quantum Mechanics. Cambridge University Press, 2018. DOI: http://dx.doi.org/10.1017/9781316995433
25. Sakurai JJ and Napolitano J. Modern Quantum Mechanics. Camebridge University Press, 2021
26. Silfvast WT. Encyclopedia of Physical Science and Technology (Third Edition). Academic Press, 2003. DOI: https://doi.org/10.1016/B0-12-227410-5/00363-X
27. Siegman AE. Lasers. University Science Books, 1986
28. He GS, Tan LS, Zheng Q, and Prasad PN. Multiphoton Absorbing Materials: Molecular Designs, Characterizations, and Applications. Chem.Rev. 2008; 108:1245–330
29. Ready JF. Industrial Applications of Lasers. Academic Press, 1997. DOI: https://doi.org/10.1016/B978-0-12-583961-7.X5000-5
30. Corney A. Atomic and Laser Spectroscopy. Oxford University Press, 1979
31. Black ED. An introduction to Pound-Drever-Hall laser frequency stabilization. Am. J. Phys. 2000; 69:79–87. DOI: https://doi.org/10.1119/1.1286663
32. Drever RWP, Hall JL, Kowalski FV, Hough J, Ford GM, Munley AJ, and Ward H. Laser phase and frequency stabilisation using an optical resonator. Applied Physics B 1983
33. Hall JL. Frequency stabilized lasers: a parochial review. Proceedings of SPIE - The International Society for Optical Engineering 1993. DOI: 10.117/12.143668
34. Hänsch TW and Couillaud B. Laser frequency stabilisation by polarisation spectroscopy of a reflecting reference cavity. Optics communications 1980; 35:441–5
35. Aspect A, Arimondo E, Kaiser R, Vansteenkiste N, and Cohen-Tannoudji C. Laser Cooling below the One-Photon Recoil Energy by Velocity-Selective Coherent Population Trapping. Physical Review Letters 1988; 61:826–9
36. Dalibard J and Cohen-Tannoudji C. Laser cooling below the Doppler limit by polarisation gradients: simple theoretical models. Optical Society of America 1989; 6:2023–45
37. Chu S, Hollberg L, Bjorkholm JE, Cable A, and Ashkin A. Three-Dimensional Viscuous Confinement and Cooling of Atoms by Resonance Radiation Pressure. Physical Review Letters 1985; 55:48–51
38. Kallapur AG, Boyson TK, Petersen IR, and Harb CC. Nonlinear estimation of ring-down time for a Fabry-Perot optical cavity. Opt. Soc. Amer. 2011; 19:6377–86. DOI: https://doi.org/10.1364/OE.19.006377
39. Vrijsen G. Collective quantum behavior of atomic ensembles in high-finesse optical cavities. PhD thesis. Stanford University, 2011

A Supporting notes to theory

A.1 Derivation of the wave equation in free space

Starting with Maxwell's third equation, the curl of the equation is found to be

$$\nabla \times (\nabla \times \mathbf{E}) = \nabla \times \left(-\frac{\partial \mathbf{B}}{\partial t} \right). \tag{93}$$

Here, the vector identity $\nabla \times (\nabla \times \mathbf{A}) = \nabla(\nabla \cdot \mathbf{A}) - \nabla^2 \mathbf{A}$ is applied to the left hand side of the equation. The rotation of the electric field is assumed to be ρ/ε_0 in free space, given by Maxwell's first equation, and assuming the charge distribution is invariant in time, this means the gradient of the charge distribution is zero. This leaves only a term $-\nabla^2 \mathbf{E}$ on the left hand side. Continuing operations on the right hand side yields that the time derivative and curl operate on different variables, enabling the operations below.

$$\begin{aligned} -\nabla^2 \mathbf{E} &= \nabla \times \left(-\frac{\partial \mathbf{B}}{\partial t} \right) \\ &= -\nabla \times (\nabla \mathbf{B}) \\ &= -\nabla(\nabla \times \mathbf{B}) \end{aligned}$$

The curl of the magnetic field density is given by Maxwell's fourth and last equation, which can be inserted into the equation above.

$$\begin{aligned} -\nabla^2 \mathbf{E} &= -\nabla \left(\varepsilon_0 \mu_0 \frac{\partial \mathbf{E}}{\partial t} + \mu_0 \mathbf{J} \right) \\ &= -\varepsilon_0 \mu_0 \nabla \left(\frac{\partial \mathbf{E}}{\partial t} \right) \\ &= -\varepsilon_0 \mu_0 \frac{\partial^2 \mathbf{E}}{\partial t^2} \end{aligned}$$

As shown, Maxwell's equations lead to a second order partial differential equation describing a wave. In the simplest case, this wave is both plane and monochromatic, which means that the electric field solving the wave equation comes on the form $\mathbf{E}(\mathbf{r}, t) = \mathbf{E_0} \exp(i(\mathbf{k} \cdot \mathbf{r} - \omega t))$ where $\mathbf{r}$ is the position in three-dimensional space, $\mathbf{k}$ is the wave vector, and ω is the frequency of the wave.

A.2 Einstein A and B coefficients

Assuming an atom has two energy levels E_1 and E_2, each energy level might have more than one energy state, or a *degeneracy*, represented by g_1 and g_2. When this atom interacts with radiation that has an energy density $\rho(\omega)$ per unit frequency interval, the radiation will induce transitions from the lower to the upper level of the atom at a rate which is proportional to $\rho(\omega_{12})$ with a proportionality constant B_{12}. It can be observed that at a frequency $\omega_{12} = (E_2 - E_1)/\hbar$, the atom interacts most strongly with the incoming radiation. This is the atom's *resonant frequency*. By symmetry, it is also assumed that the radiation will cause transitions from the upper level to the lower level with some proportionality constant B_{21}. By

introducing A_{21}, a coefficient representing the rate of the transition frequency, it is possible to formulate a *rate equation* as seen in equation 94 below.

$$\frac{dN_2}{dt} = N_1 B_{12}\rho(\omega_{12}) - N_2 B_{21}\rho(\omega_{12}) - N_2 A_{21} \tag{94}$$

Here, N_1 and N_2 are the number of atoms residing on the first and second energy level, respectively. By assuming that there are only two levels, it can also be inferred that $N_1 + N_2$ must always remain constant, which in turn leads to equality 95.

$$\frac{dN_1}{dt} = -\frac{dN_2}{dt} \tag{95}$$

A relationship between the A and B coefficients can be found by knowing the energy density $\rho(\omega)$ of the radiation. In many cases, this density is set to be governed by *Planck's law*, yielding a Planck distribution as seen in 96.

$$\rho(\omega) = \frac{\hbar\omega^3}{\pi^2 c^3}\frac{1}{e^{\frac{\hbar\omega}{k_B T}} - 1} \tag{96}$$

This particular distribution at equilibrium yields that $A_{21} = (\hbar\omega^3/\pi^2 c^3)B_{21}$ and $B_{12} = (g_2/g_1)B_{21}$.

A.3 Derivation of the angular momentum selection rules

Consider the angular momentum $\mathbf{L} = [\hat{L}_x, \hat{L}_y, \hat{L}_z]$ and the angular momentum squared $\mathbf{L}^2 = \hat{L}_x^2 + \hat{L}_y^2 + \hat{L}_z^2$. The commutative relationship between two orthogonal components of $\mathbf{L}$ is e.g. $[\hat{L}_x, \hat{L}_y] = \hat{L}_x\hat{L}_y - \hat{L}_y\hat{L}_x = i\hbar\hat{L}_z$. The axis of interest can then be seen to fulfil the eigenvalue problem for some wavefunction ψ_{lm}, or, alternately, some state $|l, m\rangle$, as seen in equation 97.

$$\hat{L}_z|l, m\rangle = m\hbar|l, m\rangle \tag{97}$$

By defining step operators $\hat{L}_\pm = \hat{L}_x \pm i\hat{L}_y$, it is possible to apply for example $\hat{L}_+$ to the axis of interest, that is, the z-axis. This will yield the useful relationship $[\hat{L}_z, \hat{L}_+] = \hbar\hat{L}_+$, which is derived in 98.

$$\begin{aligned}
[\hat{L}_z, \hat{L}_+] &= \hat{L}_z\hat{L}_+ - \hat{L}_+\hat{L}_z \\
&= \hat{L}_z(\hat{L}_x + i\hat{L}_y) - (\hat{L}_x + i\hat{L}_y)\hat{L}_z \\
&= \hat{L}_z\hat{L}_x - \hat{L}_x\hat{L}_z + i(\hat{L}_z\hat{L}_y - \hat{L}_y\hat{L}_z) \\
&= [\hat{L}_z, \hat{L}_x] + i[\hat{L}_z, \hat{L}_y] \\
&= i\hbar\hat{L}_y - i^2\hbar\hat{L}_x \\
&= \hbar\hat{L}_+
\end{aligned} \tag{98}$$

With a state $|\psi_{lm}\rangle = \hat{L}_+|l, m\rangle$, using the definition of m from $\hat{L}_z|l, m\rangle = m\hbar|l, m\rangle$, it is possible to derive the value of $\hat{L}_z|\psi_{lm}\rangle$. This derivation is found in 99.

$$
\begin{aligned}
\hat{L}_z|\psi_{lm}\rangle &= \hat{L}_z\hat{L}_+|l,m\rangle \\
&= ([\hat{L}_z,\hat{L}_+]+\hat{L}_+\hat{L}_z)|l,m\rangle \\
&= [\hat{L}_z,\hat{L}_+]|l,m\rangle + \hat{L}_+\hat{L}_z|l,m\rangle \\
&= \hbar\hat{L}_+|l,m\rangle + \hat{L}_+\hat{L}_z|l,m\rangle \\
&= \hbar\hat{L}_+|l,m\rangle + \hat{L}_+\hbar m|l,m\rangle \\
&= \hbar(m+1)\hat{L}_+|l,m\rangle \\
&= \hbar(m+1)|\psi_{lm}\rangle
\end{aligned}
\tag{99}
$$

In words, this means that $\hat{L}_+|l,m\rangle$ is an eigenstate of $\hat{L}_z$ with the eigenvalue $\hbar(m+1)$. This defines $\hat{L}_+|l,m\rangle$ as a $|l,m+1\rangle$ state up to some normalisation constant. Therefore, it can be concluded that $\hat{L}_+|l,m\rangle \propto |l,m+1\rangle$.

The square of the angular momentum is $\mathbf{L}^2 = \hat{L}_x^2+\hat{L}_y^2+\hat{L}_z^2$. Using the step operators from before, this can be rewritten as

$$
\mathbf{L}^2 = \hat{L}_-\hat{L}_+ + \hat{L}_z^2 + \hbar\hat{L}_z. \tag{100}
$$

In a physical system, it is reasonable to assume that there exists some state $|l,m_{\max}\rangle$ which fulfils $\hat{L}_+|l,m_{\max}\rangle = 0$. If this is not assumed, the spectrum would be infinite, which is physically impossible. Applying 100 to this state yields the system seen in

$$
\begin{aligned}
\mathbf{L}^2|l,m_{\max}\rangle &= (\hat{L}_-\hat{L}_+ + \hat{L}_z^2 + \hbar\hat{L}_z)|l,m_{\max}\rangle \\
&= \hat{L}_-\hat{L}_+|l,m_{\max}\rangle + \hat{L}_z^2|l,m_{\max}\rangle + \hbar\hat{L}_z|l,m_{\max}\rangle \\
&= 0 + m_{\max}^2\hbar^2|l,m_{\max}\rangle + m_{\max}\hbar^2|l,m_{\max}\rangle \\
&= \hbar^2(m_{\max}^2+m_{\max})|l,m_{\max}\rangle
\end{aligned}
\tag{101}
$$

Seeing m as a projection of the angular momentum along a chosen axis, it follows that the maximum value of a vector of length l projected onto an axis is l. Thus, it is clear that $m_{\max} = l$, yielding the familiar relation $\mathbf{L}^2 = l(l+1)\hbar^2$.

A.4 Force on atoms

In a quantum mechanical system, the force that acts upon a particle is often defined as the expectation value of a quantum mechanical force operator, as is found in equation 102.

$$
\vec{F} = \langle\hat{F}\rangle = \frac{d}{dt}\langle\hat{p}\rangle \tag{102}
$$

Here, $\hat{p}$ is supposed to be equal to $-i\hbar\partial/\partial z$, that is, acting along only the z-axis. This $\hat{p}$ forms the commutative relationship with the Hamiltonian $\hat{H}$ as $[\hat{H},\hat{p}] = i\hbar\partial\hat{H}/\partial z$. The force on an atom can therefore be rewritten as

$$
\vec{F} = -\langle\frac{\partial\hat{H}}{\partial z}\rangle. \tag{103}
$$

A.5 ABCD-matrices

The ABCD matrix method assumes that any optical system can be described by an initial input vector and a propagation matrix specific to the system. The idea can be seen in equation 104.

$$\begin{bmatrix} z_f \\ \theta_f \end{bmatrix} = \begin{bmatrix} A & B \\ C & D \end{bmatrix} \begin{bmatrix} z_i \\ \theta_i \end{bmatrix} \tag{104}$$

In an optical system, each component - free space, lenses, mirrors - have their own specific propagation matrix. A model for an optical system can be modelled in its entirety through lining different propagation matrices up and multiplying them right to left, in the order the beam propagates through the system.

The propagation matrix for light through free space of length L is

$$\begin{bmatrix} 1 & L \\ 0 & 1 \end{bmatrix}, \tag{105}$$

for a thin lens of focal length f it is

$$\begin{bmatrix} 1 & 0 \\ -\frac{1}{f} & 1 \end{bmatrix}, \tag{106}$$

and when the light is reflected at a mirror of radius R, the propagation matrix is given by

$$\begin{bmatrix} 1 & 0 \\ -\frac{2}{R} & 1 \end{bmatrix}. \tag{107}$$

The thin lens approximation is only valid when the lens thickness is much smaller than the focal length, and the angles fulfil the paraxial criterion. In the case that a lens is thick, it can be divided into smaller components with their own transmission properties. This also holds true for lenses that have different shape on their two sides, as is the case with plano/concave lenses.

A.6 Lasers

A.6.1 Population inversion

Population inversion is a phenomenon which occurs when the number N_i of atoms in an excited state $|i\rangle$ is larger than the number N_j of atoms in a lower energy state $|j\rangle$. When this occurs, the intensity of the laser beam will grow with distance through the media. To illustrate this, consider two excited states $|1\rangle$ and $|2\rangle$ and a ground state $|0\rangle$. The number N of atoms in this ensemble is assumed to be constant and all atoms are assumed to be in one of the three introduced states. This yields the three rate equations found in 108-110, expressed in terms of the Einstein coefficients A and B, the pumping rate R from the ground state to $|2\rangle$ and the mean energy density $\langle W \rangle$.

$$\frac{dN_2}{dt} = N_0 R - N_2 A_{21} - N_2 A_{20} - (N_2 - N_1) B_{21} \langle W \rangle \tag{108}$$

$$\frac{dN_1}{dt} = N_2 A_{21} - N_1 A_{10} - (N_2 - N_1) B_{21} \langle W \rangle \tag{109}$$

$$\frac{dN_0}{dt} = -N_0 R + N_1 A_{10} + N_2 A_{20} \tag{110}$$

The sum of these three rate equations is zero, since $N_0 + N_1 + N_2 = N$ is a constant. For lasers, it is often useful to consider beam strength in terms of intensity density rather than energy density. The two densities are related by a scaling with the velocity of light according to

$$\langle I \rangle = c \langle W \rangle. \tag{111}$$

The time-dependence of $\langle W \rangle$ is given by

$$\frac{\partial \langle W \rangle}{\partial t} = \frac{N_2 - N_1}{V} F(\omega) B_{21} \langle W \rangle \hbar \omega, \tag{112}$$

where V is the sample volume and $F(\omega)$ is the so called *lineshape function*, which is a distribution in frequency space. Common lineshape functions are the Gaussian and Lorenzian functions. Equation 112 describes the net rate of change of the beam energy density at position z, and through solving for $N_2 - N_1$ from equations 108-110 under steady-state conditions, the expression

$$N_2 - N_1 = \frac{N_0 R (A_{10} - A_{21})}{A_{10}(A_{20} + A_{21}) + (A_{10} + A_{20}) B_{21} \langle W \rangle} \tag{113}$$

is found. For physical systems, N_0 can be substituted for N due to the small probability of excitation of the higher energy levels. The *gain coefficient* $G(\omega)$ at frequency ω is defined as equation 114 which can also be expressed as the expression found in 118.

$$G(\omega) = \frac{1}{\langle I \rangle} \left(1 + \frac{\langle I \rangle}{I_s} \right) \frac{\partial \langle I \rangle}{\partial z} \tag{114}$$

$$= \frac{1}{c\langle W \rangle} \left(1 + \frac{c\langle W \rangle}{\frac{cA_{10}(A_{20}+A_{21})}{(A_{10}+A_{20})B_{21}}} \right) \frac{\partial \langle I \rangle}{\partial \langle W \rangle} \frac{\partial t}{\partial z} \frac{\partial \langle W \rangle}{\partial t} \tag{115}$$

$$= \frac{1}{c\langle W \rangle} \left(1 + \frac{c\langle W \rangle}{\frac{cA_{10}(A_{20}+A_{21})}{(A_{10}+A_{20})B_{21}}} \right) \frac{\partial \langle I \rangle}{\partial \langle W \rangle} \frac{\partial t}{\partial z} \frac{N_2 - N_1}{V} F(\omega) B_{21} \langle W \rangle \hbar \omega \tag{116}$$

$$= \left(1 + \frac{c\langle W \rangle}{\frac{cA_{10}(A_{20}+A_{21})}{(A_{10}+A_{20})B_{21}}} \right) \frac{1}{\langle W \rangle} \frac{\frac{N_0 R(A_{10}-A_{21})}{A_{10}(A_{20}+A_{21})+(A_{10}+A_{20})B_{21}\langle W \rangle}}{Vc} F(\omega) B_{21} \hbar \omega \tag{117}$$

$$= \frac{R(A_{10} - A_{21})}{A_{10}(A_{20} + A_{21})} \frac{N_0 F(\omega) B_{21} \hbar \omega}{Vc} \tag{118}$$

A.7 Modulation of laser beam

In this subsection, the mathematical gymnastics behind the electric fields used to control the frequency of the laser can be found. First, the expression for the incoming electric field will be expanded using Bessel functions, upon which it can be shown that it is reasonable to approximate the signal as consisting of a signal at a carrier frequency ω with sidebands at $\omega \pm \Omega$.

Bessel functions are solutions to the ordinary differential equation found in 119.

$$x^2 \frac{d^2 f(x)}{dx^2} + x \frac{df(x)}{dx} + (x^2 - \alpha^2) f(x) = 0 \tag{119}$$

It is possible to define the solution to this equation with a Bessel function J of order n.

$$J_n(x) = \frac{1}{\pi} = \int_0^\pi \cos(nt - x\sin t)\,dt = \frac{1}{\pi}\mathrm{Re}\left[\int_0^\pi e^{i(nt - x\sin t)}\,dt\right] \tag{120}$$

B Code to plots

The code used to plot the figures in the main text was written mostly by the author, ChatGPT, and Claude. Contributions will be made clear in the individual cases. The code applies the formulae introduced in the theory section for a specific system. To ensure that everyone can reproduce the plots, the code is presented in its original state here.

B.1 Cavity stability diagram

The cavity stability criterion is presented in section ref, and demands that $0 \leq g_1 g_2 \leq 1$ for the stability parameters g_1 and g_2. Different types of cavities place themselves in different places on the stability diagram. Their location can be easily calculated or found in reference texts, such as in Siegman's *Lasers* (1986) [27]. This code was made by ChatGPT.

```
import matplotlib.pyplot as plt
import matplotlib as mpl

mpl.rcParams['font.family'] = 'sans-serif'
mpl.rcParams['font.sans-serif'] = ['Times New Roman']  # or another font you prefer
mpl.rcParams['mathtext.fontset'] = 'stixsans'
mpl.rcParams['axes.unicode_minus'] = False  # fixes minus sign rendering

import numpy as np
import matplotlib.pyplot as plt

# Define grid
g1 = np.linspace(-2, 2, 400)
g2 = np.linspace(-2, 2, 400)
G1, G2 = np.meshgrid(g1, g2)

# Stability condition: 0 < g1*g2 < 1
stability = (G1 * G2 > 0) & (G1 * G2 < 1)

# Plot
plt.figure(figsize=(6, 6))
```

```
plt.contour(G1, G2, G1*G2, levels=[0, 1], colors='k', linewidths=1.5)
plt.imshow(stability, extent=[-2, 2, -2, 2],
           origin='lower', cmap='Blues', alpha=0.3)

# Labels and formatting
plt.xlabel(r'$g_1 = 1 - L/R_1$')
plt.ylabel(r'$g_2 = 1 - L/R_2$')
plt.title('Optical Cavity Stability Diagram')
plt.xlim(-2, 2)
plt.ylim(-2, 2)
plt.grid(True)
plt.axhline(0, color='gray', lw=1)
plt.axvline(0, color='gray', lw=1)

# Annotate stable region
plt.text(0.5, 0.5, 'Stable region', color='navy', fontsize=12, ha='center
    ')

plt.show()
```

B.2 Expected mode structure of near-planar optical cavity

The expected mode structure is found in figure 3.6 and plots an example of how the reflection spectrum for a near-planar Fabry-Pérot-like cavity with a finesse of 40000 is expected to look. The two large peaks are the axial modes, spaced by 1 FSR= 1.5 GHz, and two smaller peaks are seen to the side of these peaks, spaced by the smaller transverse mode spacing of approximately 221 MHz. It is important to note that arbitrary mode weights have been added to the spectrum to yield this plot, and the basis for adding these weights is because higher order modes are expected to have more losses due to the nature of the cavity and the increasing size of the modes [27].

```
import numpy as np
import matplotlib.pyplot as plt


# Constants
c = 3e8
L = 0.1
FSR = c / (2 * L)

# Cavity parameters
g1 = 1.0
g2 = 0.8
theta = np.arccos(np.sqrt(g1 * g2))

# Transverse spacing
delta_f_trans = FSR * theta / np.pi

# Finesse and linewidth
Finesse = 40000
linewidth = FSR / Finesse

# Frequency axis (~1.2 FSR)
f = np.linspace(0.01*FSR, 1.5*FSR, 100000)

# Lorentzian dip
```

```
def lorentzian(f, f0, gamma, amplitude):
    return amplitude / (1 + ((f - f0)/(gamma/2))**2)

# Mode weights (adjust for alignment quality)
mode_weights = {
    (0,0): 1.0,
    (1,0): 0.05,
    (0,1): 0.05,
    (2,0): 0.01,
    (1,1): 0.01,
    (0,2): 0.01,
}

# Build spectrum
signal = np.ones_like(f)

# Include longitudinal orders around 0
q_range = range(-1, 2)

for q in q_range:
    base_freq = q * FSR

    for (m,n), weight in mode_weights.items():
        mode_shift = (m + n + 1) * delta_f_trans
        f_mode = base_freq + mode_shift

        signal -= lorentzian(f, f_mode, linewidth, weight)

plt.rcParams.update({'font.family': 'Times New Roman', 'text.usetex':
    False})
# Plot
plt.figure(figsize=(12,7))
plt.plot(f / 1e9, signal)
plt.xlabel("Frequency (GHz)",fontsize=16)
plt.ylabel("Reflected signal",fontsize=16)
plt.title("Cavity reflection spectrum (~2 FSR)",fontsize=24)
plt.grid()
plt.show()
```

B.3 Simulated error signals and cavity reflection phase

During PDH locking, it is important to keep track of the phase of the reflected light from the optical cavity, as this allows for an evaluation of the laser frequency's proximity to resonance. The basis for this is the *reflection coefficient*, which is a function of frequency. It is defined as

$$F(\omega) = \frac{E_r}{E_{in}} = \frac{r(e^{i\omega/\Delta f} - 1)}{1 - r^2 e^{i\omega/\Delta f}},$$

where Δf is the free spectral range and r is the amplitude reflection coefficient of the mirrors, which is assumed to be the same for both mirrors. While the intensity is symmetric about resonance, the phase is anti-symmetric and can be found through taking the argument of as $F(\omega) = \arctan(\mathrm{Im}(F)/\mathrm{Re}(F))$. The unknown coefficient, r can be calculated using equation 33, which for a finesse of 40000 yields a value of r as 0.99961. This means that the expression for $F(\omega)$ can be evaluated in an arbitrary range of frequencies. This code was made by the author.

```
import numpy as np
import matplotlib.pyplot as plt
from scipy.special import jv  # Bessel functions

# Parameters
FSR = 1.5e9
finesse = 40000
r = 0.999961 # follows from finesse through F = pi*r/(1-r^2)
gamma = FSR / finesse
f_mod = 0.75e9
beta = 0.3  # modulation depth (try 0.1  1  .0)

def F(omega):
    return r*(np.exp(1j*omega/FSR)-1)/(1-r**2*np.exp(1j*omega/FSR))

def phase_plot(omega):
    Im = np.imag(F(omega))
    Re = np.real(F(omega))
    return np.arctan(Im/Re)

# Frequency axis
detuning = np.linspace(-5*gamma, 5*gamma, 4000)

# Total reflected field
E_reflected = np.zeros_like(detuning, dtype=complex)

# Phase of carrier reflection
phase = phase_plot(detuning)

# Plot
plt.rcParams.update({'font.family': 'Times New Roman', 'text.usetex':
    False})

plt.figure(figsize=(12,10))

#plt.subplot(2,1,1)
#plt.plot(detuning/1e6, error_signal)
#plt.title(f"PDH Error Signal (   = {beta})",fontsize=24)
#plt.xlabel("Detuning (MHz)",fontsize=16)
#plt.ylabel("Error Signal (arb.)",fontsize=16)
#plt.grid()

plt.subplot(2,1,2)
plt.plot(detuning/1e6, phase)
plt.title("Phase of cavity reflection",fontsize=24)
plt.xlabel("Detuning (MHz)",fontsize=16)
plt.ylabel("Phase (rad)",fontsize=16)
plt.grid()

plt.tight_layout()
plt.show()
```

The next step is to consider what the sidebands generated by the EOM do to this signal. The incoming electromagnetic field changes as

$$E_{in} = E_0[J_0(\beta)e^{i\omega t} + J_1(\beta)e^{i(\omega+\Omega)t} - J_1(\beta)e^{i(\omega-\Omega)t}],$$

and the reflected signal becomes

$$E_{ref} = E_0[F(\omega)J_0(\beta)e^{i\omega t} + F(\omega+\Omega)J_1(\beta)e^{i(\omega+\Omega)t} - F(\omega-\Omega)J_1(\beta)e^{i(\omega-\Omega)t}].$$

The power detected is the absolute square of E_{ref}. The signal from this is mixed with the signal also fed to the EOM, and when $\Omega \gg \text{FSR}/\mathcal{F}$, the error signal ϵ becomes

$$\epsilon = -P_0\beta \,\text{Im}\left[F(\omega)F^*(\omega+\Omega) - F^*(\omega)F(\omega-\Omega)\right]. \tag{121}$$

Plotting this for a finesse of 40000, a modulation depth $\beta = 0.3$, a power $P_0 = 1$, and a modulation frequency $\Omega = 0.75$ GHz yields the plot for the figure found in figure 3.10. The code below was made by the author.

```
import numpy as np
import matplotlib.pyplot as plt
from scipy.special import jv  # Bessel functions

# Parameters
FSR = 1.5e9
finesse = 40000
gamma = FSR / finesse
f_mod = 0.75e9
beta = 0.3  # modulation depth (try 0.1  1  .0)
P_0 = 1
r = 0.999961 # follows from finesse through F = pi*r/(1-r^2)

# Frequency axis
detuning = np.linspace(-0.6*FSR, 0.6*FSR, 4000)

def F(omega):
    return r*(np.exp(1j*omega/FSR)-1)/(1-r**2*np.exp(1j*omega/FSR))

def F_conj(omega):
    return np.conj(F(omega))

error_signal=-beta*np.imag(F(detuning)*F_conj(detuning+f_mod)-F_conj(
    detuning)*F(detuning-f_mod))

# Plot
plt.rcParams.update({'font.family': 'Times New Roman', 'text.usetex':
    False})

plt.figure(figsize=(12,14))
plt.subplot(2,1,1)
plt.plot(detuning/1e6, error_signal)
plt.title(f"PDH Error Signal (   = {beta})",fontsize=24)
plt.xlabel("Detuning (MHz)",fontsize=16)
plt.ylabel("Error Signal ($\epsilon$/P$_0$)",fontsize=16)
plt.grid()

plt.tight_layout()
plt.show()
```

Did this not stick? *An introduction to Pound–Drever–Hall laser frequency stabilization* by Black (2001) is an excellent walkthrough to PDH locking.

B.4 Exponential decay fit

This exponential decay model takes in data from the transmitted signal of the cavity when the cavity is swept at a comparatively high sweep rate. The data comes directly from the photodiode placed immediately after the cavity housing. The peak is found through plotting this normally in Python.

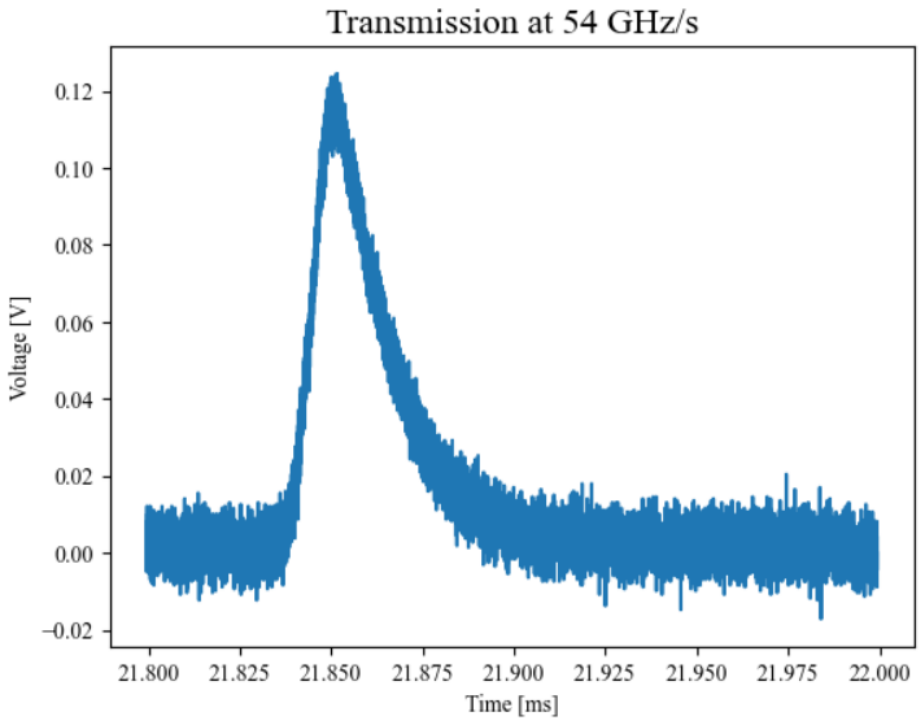

Figure B.1: The initial data as plotted in Python.

From this, it is evident that the peak is initially Lorentzian in shape, but that it trails off in an exponential decay-like manner. To find this exponential behaviour, the first issue is to handle the noise that can be seen in this graph, and the Lorentzian must also be handled. The noise is handled using something called a Savitzky-Golay filter, which isn't a filter in the electronical sense, but rather a digital signal processing technique that smoothens the noisy data by fitting nearby data points to a low-degree polynomial (in this case, a polynomial of order 3).

Once this smoothened curve has been found, the exponential decay is fitted to this by assuming the slope is described by the model $I(t) = I_0 \cdot \exp(-t/\tau)$, although a constant C is added to compensate for a noise floor in the data, that could be from leakage radiation from the cavity or from other light sources in the room. The parameter τ is found through finding the value of τ in a range of values which minimises the error function of the model. The programming for this was left entirely to the AI *Claude*, and it produced the following code.

```
    """
Cavity Ringdown Spectroscopy - Exponential Decay Fitting
============================================================
Fits I(t) = I0 * exp(-t/tau) + C to the post-peak decay region
of a cavity ringdown signal from an R&S MXO44 oscilloscope CSV.

Author: (your name)
Date:   2026-05-19
"""
```

```
10
11 import numpy as np
12 import pandas as pd
13 import matplotlib.pyplot as plt
14 from scipy.optimize import curve_fit
15 from scipy.signal import savgol_filter
16
17 #        0. CONFIG


18
19 FILE = r"Z:\HQL\Users\The other Alex\Thesis data\T10Hz_2026-05-19
       _2_135042.csv"
20
21 # Row window that contains your fundamental peak (from your original
       script)
22 LB = 180_000
23 HB = 200_000
24
25 # How many points after the peak maximum to skip before starting the fit.
26 # Skipping a small number of points avoids the Lorentzian rise
       contaminating
27 # the exponential fit.  Tune this if the fit looks off.
28 SKIP_AFTER_PEAK = 100          # ~1  s  at 10 ns/sample
29
30 # How many points after the peak to include in the fit window.
31 # The signal reaches noise floor (~0.002 V) around 50  s      5000
       samples.
32 # Setting this slightly shorter keeps us in the clean exponential region.
33 FIT_WINDOW = 3500              # ~35  s
34
35 # Optional: smooth the raw data before fitting to help curve_fit converge
       .
36 # Uses Savitzky-Golay.  Set SMOOTH = False to fit raw data directly.
37 SMOOTH        = True
38 SG_WINDOW_LEN = 101           # must be odd; ~1  s  at 10 ns/sample
39 SG_POLYORDER  = 3
40
41 #        1. LOAD DATA


42
43 # The MXO44 CSV has 37 header rows before the TIME,C3 column names
44 df = pd.read_csv(FILE, skiprows=37, header=0, low_memory=False)
45 df.columns = ["TIME", "V"]
46 df = df.apply(pd.to_numeric, errors="coerce").dropna()
47
48 # Slice to the peak window (same logic as your original script)
49 subset = df.iloc[LB:HB].reset_index(drop=True)
50 t_raw = subset["TIME"].values        # seconds
51 v_raw = subset["V"].values
52
53 #        2. FIND PEAK AND BUILD FIT ARRAYS


54
55 peak_idx = int(np.argmax(v_raw))
56 print(f"Peak found at local index {peak_idx}")
```

```
print(f"  Time  : {t_raw[peak_idx]*1e3:.6f} ms")
print(f"  Voltage: {v_raw[peak_idx]:.4f} V")

# Fit region starts SKIP_AFTER_PEAK samples past the peak
fit_start = peak_idx + SKIP_AFTER_PEAK
fit_end   = fit_start + FIT_WINDOW

t_fit = t_raw[fit_start:fit_end]
v_fit = v_raw[fit_start:fit_end]

# Shift time axis so t=0 is the start of the fit window.
# This makes I0 directly interpretable as the signal at fit-start,
# and avoids numerical issues with large absolute time values.
t0    = t_fit[0]
t_rel = t_fit - t0                    # seconds, starting at 0

# Optionally smooth for initial parameter estimation / cleaner plot
if SMOOTH:
    v_smooth = savgol_filter(v_fit, window_length=SG_WINDOW_LEN,
                             polyorder=SG_POLYORDER)
else:
    v_smooth = v_fit

#        3. ESTIMATE INITIAL PARAMETERS


# Good initial guesses are critical for curve_fit.
# I0  : value at the start of the fit window (from smoothed signal)
# tau : rough estimate from where the signal drops to 1/e of its peak
# C   : noise floor = mean of the last 500 samples in the fit window

noise_floor = np.mean(v_fit[-500:])
I0_guess    = v_smooth[0] - noise_floor

# Find the index where smoothed signal first drops below I0/e + C
target = I0_guess / np.e + noise_floor
crossings = np.where(v_smooth < target)[0]
tau_guess = t_rel[crossings[0]] if len(crossings) > 0 else 10e-6

print(f"\nInitial parameter guesses:")
print(f"  I0  : {I0_guess:.4f} V")
print(f"  tau : {tau_guess*1e6:.2f}  s ")
print(f"  C   : {noise_floor:.4f} V  (noise floor)")

#        4. DEFINE MODEL AND FIT



def ringdown_model(t, I0, tau, C):
    """Exponential decay with baseline offset: I(t) = I0*exp(-t/tau) + C
    """
    return I0 * np.exp(-t / tau) + C

# Bounds keep parameters physically sensible:
#   I0  > 0 (positive signal)
#   tau in [10 ns, 1 ms]  (nanoseconds to milliseconds)
#   C   can be small positive or slightly negative (baseline uncertainty)
lower_bounds = [0,      10e-9,  -0.05]
```

```
upper_bounds = [10,     1e-3,    0.05]

popt, pcov = curve_fit(
    ringdown_model,
    t_rel,
    v_fit,                              # fit to raw (noisy) data
    p0=[I0_guess, tau_guess, noise_floor],
    bounds=(lower_bounds, upper_bounds),
    maxfev=10_000,
)

I0_fit, tau_fit, C_fit = popt
perr = np.sqrt(np.diag(pcov))        # 1-sigma uncertainties
I0_err, tau_err, C_err = perr

print(f"\nFit results:")
print(f"  I0  = {I0_fit:.5f}    {I0_err:.5f} V")
print(f"  tau = {tau_fit*1e6:.4f}    {tau_err*1e6:.4f}  s ")
print(f"  C   = {C_fit:.5f}    {C_err:.5f} V")

#         5. RESIDUALS AND GOODNESS-OF-FIT



v_pred    = ringdown_model(t_rel, *popt)
residuals = v_fit - v_pred
ss_res    = np.sum(residuals**2)
ss_tot    = np.sum((v_fit - np.mean(v_fit))**2)
r_squared = 1 - ss_res / ss_tot
rmse      = np.sqrt(np.mean(residuals**2))

print(f"\nGoodness of fit:")
print(f"  R     = {r_squared:.6f}")
print(f"  RMSE = {rmse*1e3:.4f} mV")

#         6. PLOT



plt.rcParams.update({
    "font.family": "Times New Roman",
    "text.usetex": False,
    "font.size": 12,
})

fig, axes = plt.subplots(
    2, 1,
    figsize=(10, 7),
    gridspec_kw={"height_ratios": [3, 1]},
    sharex=True,
)

# --- Top panel: data + fit ---
ax = axes[0]
t_plot_ms = (t_fit - t0) * 1e6          #  s  for plotting

ax.plot(t_plot_ms, v_fit,
        color="steelblue", alpha=0.4, linewidth=0.6, label="Raw data")
```

```
164 if SMOOTH:
165     ax.plot(t_plot_ms, v_smooth,
166             color="cornflowerblue", linewidth=1.0, alpha=0.8, label="
    Smoothed")
167 ax.plot(t_plot_ms, v_pred,
168         color="crimson", linewidth=2.0,
169         label=rf"Fit: $\tau$ = {tau_fit*1e6:.2f}    {tau_err*1e6:.2f}  s
    ")
170
171 ax.set_ylabel("Voltage [V]")
172 ax.set_title("Cavity Ringdown     Exponential Decay Fit", fontsize=14)
173 ax.legend(loc="upper right")
174 ax.grid(True, alpha=0.3)
175
176 # Annotate fit parameters on plot
177 textstr = (
178     rf"$I_0$ = {I0_fit:.4f}    {I0_err:.4f} V"
179     "\n"
180     rf"$\tau$  = {tau_fit*1e6:.3f}    {tau_err*1e6:.3f}  s "
181     "\n"
182     rf"$C$  = {C_fit:.4f}    {C_err:.4f} V"
183     "\n"
184     rf"$R^2$ = {r_squared:.5f}"
185 )
186 ax.text(0.55, 0.85, textstr, transform=ax.transAxes,
187         fontsize=10, verticalalignment="top",
188         bbox=dict(boxstyle="round,pad=0.4", facecolor="white", alpha=0.8)
    )
189
190 # --- Bottom panel: residuals ---
191 ax2 = axes[1]
192 ax2.plot(t_plot_ms, residuals * 1e3,
193          color="gray", linewidth=0.5, alpha=0.7)
194 ax2.axhline(0, color="crimson", linewidth=1.0, linestyle="--")
195 ax2.set_xlabel("Time after fit start [ s ]")
196 ax2.set_ylabel("Residual [mV]")
197 ax2.set_title("Residuals", fontsize=11)
198 ax2.grid(True, alpha=0.3)
199
200 plt.tight_layout()
201 plt.savefig("ringdown_fit.png", dpi=150, bbox_inches="tight")
202 plt.show()
203 print("\nPlot saved to ringdown_fit.png")
```